DEVELOPMENT OF EARTHQUAKE-RESISTANT ULTIMATE STRENGTH DESIGN METHOD FOR CONCRETE-FILLED STEEL STRUCTURES

Hanbin GE

DEVELOPMENT OF EARTHQUAKE-RESISTANT ULTIMATE STRENGTH DESIGN METHOD FOR CONCRETE-FILLED STEEL STRUCTURES

by

Hanbin GE

A thesis submitted for the degree of Doctor of Engineering
at the Department of Civil Engineering,
Nagoya University

Nagoya, JAPAN

December, 1993

ACKNOWLEDGEMENTS

The author wishes to express the most sincere thanks and appreciation to his advisor, Professor Tsutomu Usami for his continuous guidance, encouragement and invaluable support throughout the course of this work.

Deep acknowledgements are expressed to Professor Tada-aki Tanabe and Professor Kentaro Yamada for serving on the examining jury committee and making many invaluable suggestions.

Thanks are also due to Associate Professor Yoshihito Itoh and Associate Professor Eiji Mizuno for their constructive discussions and invaluable advice. Acknowledgement is also extended to Associate Professor Junichiro Niwa for his useful suggestions.

The author would like to express the most sincere gratitude to Professor Tetsuhiko Aoki of Aichi Institute of Technology for the invaluable advice and great assistance.

The author extends his gratitude to Professor Yu Hu and Professor Hai-Long Ma of Huazhong University of Science and Technology, China, who encouraged the author continuously to accomplish the work in the past 5 years. Acknowledgement is also due to the authorities and the staff of Huazhong University of Science and Technology, China, where the author has been employed, for their assistance and for recommending him to take up the Special Program in Nagoya University.

The author expresses his gratitude to Research Associate Hirotaka Oda for his continuous assistance.

Thanks also go to Miss. Noriko Ito and Miss. Kimiko Kamigaito for their help and support.

Provided the supporting scholarship from MONBUSHO (Ministry of Education, Science and Culture of the Japanese Government) is also deeply appreciated.

Finally, the author would like to express his deepest sense of gratitude to his wife, Ying Cai, for her patience, understanding and continuous moral support during this research work, and his parents for preparing him intellectually and spiritually for this important stage of his life.

TABLE OF CONTENTS

1 INTRODUCTION

1.1 General Remarks

Seismic design is an attempt to assure that strength and deformation capacities of structures exceed the demands imposed by severe earthquakes with an adequate margin of safety. Accordingly, strength and ductility are two of the most important considerations in the design of a structure. **Fig. 1.1** shows two types of typical load-displacement behavior (hysteretic curves) of structures under cyclic loading. It is apparent that a structure showing the behavior of type 2 [**Fig. 1.1(b)**] is suitable in the event of a severe earthquake, because it has a large deformation capacity, and dissipates a considerable amount of energy.

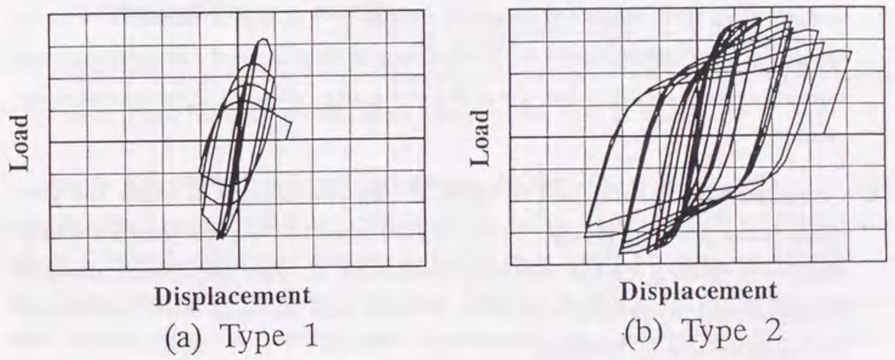

Fig. 1.1 Load-Displacement Hysteretic Curves

A large number of steel bridge piers have been designed and constructed in Japan. With the rapid development of urban highway and bridge constructions, the use of such structures will be more and more popular. Steel bridge piers are normally designed as cantilever columns or planar rigid frames. Cross sectional shapes are mostly thin-walled box sections or pipe sections. It has been recognized that seismic design of steel piers is very important for total life-line system. Hence, they must be able to withstand the severe earthquakes without collapsing.

Good earthquake-resistance design requires a deep knowledge of structures' behav-

ior under earthquake loading. For the purpose, a great number of investigations have been made on the inelastic behavior of steel box columns with and without stiffeners under cyclic loading in recent years [Fukumoto and Kusamu, 1985; Watanabe et al. 1988; Sakurai et al. 1988; Kawashima et al. 1989; Watanabe et al. 1990; Usami et al. 1991, 1992, 1993]. Some of the most important findings observed in the experiments are as follows.

1. Strength degradation of the test specimens are initiated by local buckling on the flange panels near the column base;

2. Strength degradation, ductility and energy-absorption capacity are largely affected by both width-thickness ratio of flange plates and compressive axial load;

3. Much improved behavior can be obtained by increasing the stiffener rigidity (γ_l) to more than three times the optimum rigidity (γ^*) that is obtained from linear elastic buckling theory. However, the increase in ductility and energy-absorption capacity is very limited when the stiffener rigidity ratio (γ_l/γ^*) is increased beyond 3;

4. Compared with the standard columns, the hybrid columns in which the yield stress of the stiffeners is larger than the yield stress of the plate panels are more effective in undergoing the inelastic deformation. In this case, special attention should be paid to distinguishing of two different steel materials when the columns are manufactured by workers;

5. Some improvement in strength and ductility can also be expected by providing extra numbers of transverse stiffeners, daphragms as well as longitudinal stiffeners;

6. In some cases, e.g., for the columns having large width-thickness ratio and slenderness ratio, the improvement in strength and ductility due to the provided stiffeners seems still insufficient to assure the integrity of the columns during severe earthquakes.

On the other hand, the use of concrete-filled steel structures has become increasingly popular in civil and architectural engineering structures. This is because of their

excellent earthquake-resistant properties, namely high stiffness, high strength, high ductility, and large energy-absorption capacity. In the concrete-filled columns, there is a mutual enhancement of ductility, because the steel plate provides confinement for the concrete, which in turn prevents the inward buckling of the plate. Moreover, this form of composite column offers additional advantages such as high impact resistance.

Accordingly, the use of concrete filled steel box sections can be expected to further improve the inelastic behavior of the steel columns, especially for those with large width-thickness ratio and slenderness ratio. The advantages of the concrete-filled steel sections are:

1. Local buckling of plate panels can be delayed or prevented due to the presence of the filled-in concrete;

2. Ductility and strength capacity can be significantly improved;

3. Reduction in use of steel makes design more economical than standard steel bridge piers, since the cost of concrete is cheaper than that of steel.

Due to the above mentioned advantages the application of concrete-filled steel columns has been extended to bridge piers in Japan since the 1980's. First application of concrete-filled steel columns to bridge piers was in an annex construction to the Osaka-Ikeda Highway Line (Nakai and Yoshikawa, 1984). On the other hand, in some already constructed bridge piers, the concrete was placed inside up to a certain height to provide extra protection if a vehicle collides into them. **Fig. 1.2** shows such steel bridge piers constructed in the Nagoya Urban Highway. Another example, shown in **Fig. 1.3**, is a partially concrete-filled composite bridge pier of the Kansai International Airport Connection Bridge. In this project, the use of partially concrete-filled bridge piers was also aimed at reducing the weight of the pier itself. Obviously, the use of the filled-in concrete in such structures is passive and not economical unless the resulting extra strength and ductility are taken into consideration for earthquake resistance. In order to ensure that these structures are able to withstand the severe earthquakes without collapsing, partially concrete-filled steel section wherein the effect of filled-in concrete is taken into account in the design would be the most effective and hence economical structures for bridge piers.

Fig. 1.2 Partially Concrete-Filled Steel Bridge Piers

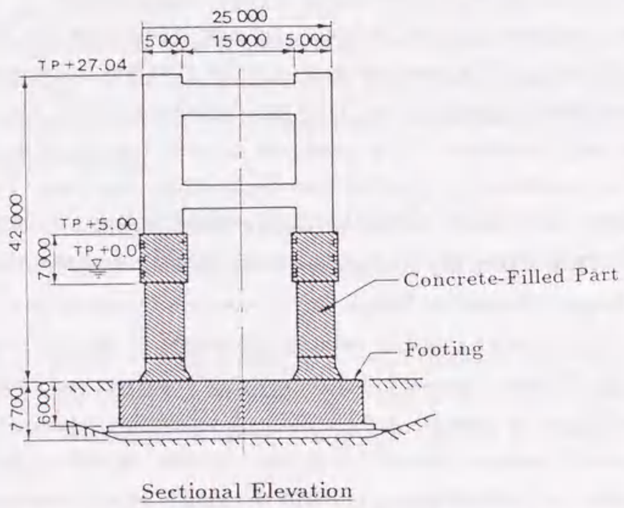

Sectional Elevation

Fig. 1.3 Bridge Piers of Kansai International Airport Connection Bridge

A series of extensive studies have been carried out in Osaka City University and Hanshin Expressway Highway Public Cooperation (Nakai and Yoshikawa, 1984; Nakai et al. 1985 and 1986; Kitada et al. 1989; Kitada and Nakai, 1991). The inelastic behavior of concrete-filled steel columns was investigated under monotonic loading. As a result, a draft recommendation for design and construction of steel bridge piers with composite columns (concrete-filled structures) was first proposed in Japan in 1986. After that, a task committee chaired by Prof. Ikeda of Yokohama National University summarized the research achievements in this field in *Guidelines for Design of Steel-Concrete Composite Constructions* (1989). In spite of the increasing popularity of concrete-filled steel bridge piers, very little research has been done on the inelastic behavior under cyclic loading to date.

1.2 Contents of Present Study

This research was undertaken to develop a rational earthquake-resistant ultimate-strength design method for concrete-filled steel box columns. For this purpose, the elasto-plastic behavior of such members was investigated experimentally and theoretically. In the experimental work, the effects of main parameters such as width-thickness ratio parameter, slenderness ratio parameter, axial force and length of the filled-in concrete on the column behavior were studied. In view of the situation that a diaphragm was not provided over the filled-in concrete in some constructed bridge piers, the effect of the diaphragm on the structural performance of the member was also examined. In the theoretical work, a simple analytical method was developed to obtain the ultimate strengths and deformations of concrete-filled steel box columns. In the end, a design recommendation was proposed for design of this type of composite columns.

The thesis consists of nine chapters. In the present chapter, a brief introduction is presented.

Chapter 2 describes experimental studies undertaken on the cyclic behavior of concrete-filled steel box stub-columns in compression. For comparison, hollow steel box column specimens were also loaded to failure. The ultimate strength, deformation and collapse behavior of two types of columns were compared. In the comparison, the effect of plate width-thickness ratio and stiffener rigidity on the behavior of columns was examined. The test results showed that high strength and high ductility can be

expected from the concrete-filled steel columns. In the case of concrete-filled composite columns, an empirical reduction factor that accounts for the effect of the size of the filled-in concrete prism and the concrete strength class was introduced in evaluating the compressive strength of the concrete, and the local buckling strength of the plate panel was then compared with available empirical design formulas for a thin-walled steel member in compression.

Chapter 3 presents an elasto-plastic finite displacement analysis of the concrete-filled thin-walled steel stub-columns of box shape. In order to describe rationally the inelastic behavior of concrete, a hardening-softening model developed by Wu and Tanabe (1990) is extended in the analysis of such composite columns. A comparison was made between the analytical results and test data. Furthermore, a parametric study was conducted to investigate the effects of the parameters such as plate aspect ratio, plate width-thickness, initial plate out-of-flatness and concrete strength. Finally, a local buckling strength formula was proposed for design of concrete-filled box stub columns in compression.

Chapter 4 is devoted to a discussion of the experimental results of partially concrete-filled steel box columns modeling steel bridge piers. These experiments were conducted under a constant axial load and a cyclic lateral loading. The width-thickness ratio parameter, slenderness ratio parameter, axial force and length of the filled-in concrete were chosen as main test parameters. The test results were then discussed in the light of ductility and energy-absorption capacity of steel bridge piers.

Chapter 5 forms a sequel to the previous chapter and focuses on the experiments of partially concrete-filled steel columns with small slenderness ratios. Besides those parameters considered in the previous experiment, the effect of a diaphragm over the filled-in concrete on the column behavior was investigated.

Chapter 6 addresses the development of the analytical models in order to obtain the moment-curvature relations for hollow steel box column segments and concrete-filled steel column segments subjected to compression combined with a uniaxial bending moment. A set of formulas were found to closely approximate the moment-curvature curve of locally buckled steel box column segments under uniform moment. To take into account the effect of moment gradient, a modification factor was introduced in the ultimate strength formula under pure bending. Moreover, approximate expressions

ignoring local buckling for the moment-curvature relation of steel box column segments were also proposed. Furthermore, for the concrete-filled steel section, the moment-curvature relation was computed by a simplified numerical calculation method in which buckling is not included, and predicted by the proposed approximate expressions.

Chapter 7 is concerned with the development of an efficient computation method for determining the ultimate strength and deformation of concrete-filled steel box columns in a simple way. For this purpose, the moment-curvature relations without considering local buckling presented in Chapter 6 are integrated along the column axis by using the finite element technique. Based on the experimental observations, a criterion was introduced to rationally define failure of the member. In order to examine the capability of the developed computation method, a comparison of the computed results and experimental data was made. Furthermore, a parametric study was carried out to provide design charts for determining the ultimate strength and deformation of concrete-filled columns. Finally, a recommendation for determining the optimum length of the filled-in concrete was proposed.

Chapter 8 gives recommendations for practical design of concrete-filled steel box columns on the basis of both theoretical and experimental investigations. It is hoped that the proposed design method will be of great use for obtaining a rational earthquake-resistant ultimate-strength design.

Finally, the conclusions of the study are given in Chapter 9, and scope for future work on this topic is discussed.

2 EXPERIMENTAL INVESTIGATION ON THE STRENGTH OF CONCRETE-FILLED THIN-WALLED STEEL BOX STUB-COLUMNS IN COMPRESSION

2.1 General Remarks

Design codes such as *BS 5400* Part 5 (1979), ACI-318-83 ("Building" 1983) and "DIN 18806 Teil 1" (1981) have been proposed for designing composite columns. In Japan, a draft recommendation for bridge piers concerning composite columns with box cross sections was prepared by the Hanshin Expressway Highway Public Cooperation (*Recommendation* 1986). However, large discrepancies exist among the design codes, even though the same design methodology and experimental data base are used.

Extensive research on the strength of steel box columns with and without stiffeners has been carried out (e.g., Usami 1982; Usami and Fukumoto 1982; Usami 1984; Usami and Fukumoto 1989; Usami 1990). Research on concrete-filled thin-walled steel box columns has also been conducted, but most of these works focused on columns with small plate width-thickness ratios, so that no local buckling occurred (Narayanan 1988; Kitada et al. 1989). Very few experimental studies (Tomii 1977; Nakai et al. 1986) on concrete-filled thin-walled steel box columns with large width-thickness ratios are available and so understanding of the behavior of such columns is insufficient.

This chapter presents an experimental study on the strength and deformation of concrete-filled steel box stub columns. Six specimens of concrete-filled square box stub columns with and without longitudinal stiffeners were tested under concentric compressive load. For comparison, four specimens of steel square box stub columns were also loaded to failure. The ultimate strength, ductility, and collapse behavior of the two types of columns were compared. In the comparison, the effect of width-thickness ratio and stiffener rigidity on the behavior of the columns was examined.

2.2 Outline of Experiment

2.2.1 Test Specimen

Ten specimens (six concrete-filled steel box columns and four steel box columns) were tested to failure under concentric compression. Details of the test specimens are

shown in **Fig. 2.1**; and the measured dimensions of all the test specimens are listed in **Tables 2.1** and **2.2**. In **Tables 2.1** and **2.2**, specimen designations starting with a U refer to columns without stiffeners, and those starting with an S refer to columns with stiffeners. The numerals following the U or S are related to the value of equivalent width-thickness ratio R [**Eq. (2.1)**]. In each test specimen, the last character, S or C, represents steel square box columns or concrete-filled square box columns, respectively. In addition, HC means that the concrete used was high strength concrete, called high-performance concrete (Ozawa et al. 1989), instead of ordinary concrete. For the columns with stiffeners, the figure within parentheses represents the ratio of relative

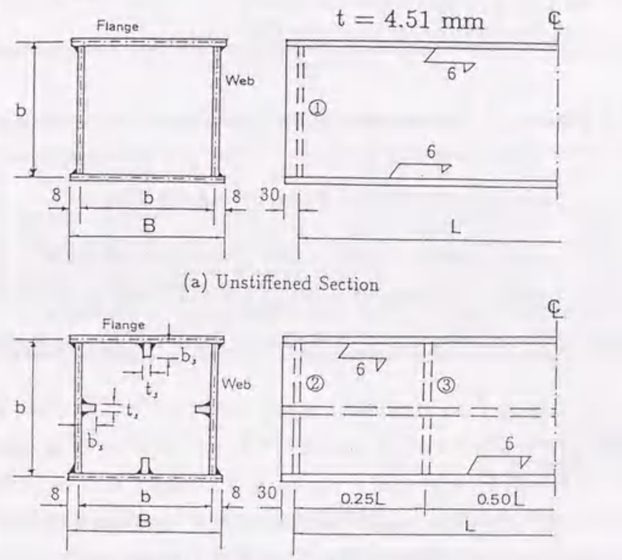

Fig. 2.1 Test Specimens

flexural rigidity, γ_l, of one longitudinal stiffener to its optimum value, γ^*, obtained from linear buckling theory ("DIN 4114" 1953; *JRA 90* 1990). The rigidities of longitudinal stiffeners used in this study were decided by coinciding γ_l with γ^*, as well as with $0.35\gamma^*$. The width-thickness ratio parameter R is defined as follows:

Table 2.1 Measured Dimensions of Test Specimens without Stiffeners

Specimen	b (mm)	B (mm)	A_s (mm^2)	A_c (mm^2)	L (mm)	r (mm)	b/t	R with k=4.0
U9-S	197	213	3654	—	592	81.0	43.7	0.844
U9-C	196	213	3654	37100	592	29.5	43.7	0.839
U12-S	263	279	4842	—	789	108.	58.3	1.126
U12-C	263	279	4842	66800	790	36.2	58.3	1.126
U12-HC	263	279	4842	66800	789	36.2	58.3	1.126
U15-S	329	345	6030	—	988	118.	73.0	1.409
U15-C	329	345	6030	105300	988	39.8	73.0	1.409

Notes: B = Total Width of Flange Plates; b = Width of Flange Plates;
A_s = Cross Sectional Area of Steel; A_c = Cross Sectional Area of Concrete;
L = Total Length of Specimen; r = Radius of Gyration of Cross Section;
R = Width-thickness Ratio Parameter [**Eq. (2.1)**].

Table 2.2 Measured Dimensions of Test Specimens with Stiffeners

Specimen	b (mm)	B (mm)	b_s (mm)	t_s (mm)	A_s (mm^2)	A_c (mm^2)	r (mm)	$\frac{\gamma_l}{\gamma^*}$	R with k=16.0
S75-S(1)	328	344	38.1	4.36	6714	—	132.	1.11	0.702
S75-C(1)	328	345	38.0	4.36	6714	104616	43.3	1.11	0.702
S75-C(0.35)	329	344	25.1	4.34	6480	104850	43.1	0.35	0.705

Notes: b_s = Width of Stiffener; t_s = Thickness of Stiffener; L = 1316 mm;
γ_l = Relative Flexural Rigidity; γ^* = Optimum Relative Flexural Rigidity.

$$R = \frac{b}{t}\sqrt{\frac{12(1-\nu^2)}{\pi^2 k}}\sqrt{\frac{\sigma_y}{E}} \tag{2.1}$$

where b = flange or web width; t = plate thickness; k = buckling coefficient with the value of $4n^2$; σ_y = nominal yield stress of the plate; E = Young's modulus; ν = Poison's ratio; and n = number of subpanels in each plate panel (e.g., n = 1 for unstiffened plate, and n = 2 for stiffened plate).

The diaphragms were designed to form the stiffened plate with the aspect ratio a/b = 3.0 for columns without stiffeners, and a/b = 2.0 for columns with stiffeners. The rigidities of diaphragms were designed such that the nodes of buckling waves occur at these locations. A fillet weld with 6 mm leg length was used for the flange-web junctions throughout. A circular opening with a diameter of 100 mm, 150 mm, or 200 mm was made so as to pour concrete. The concrete surface at each end of the

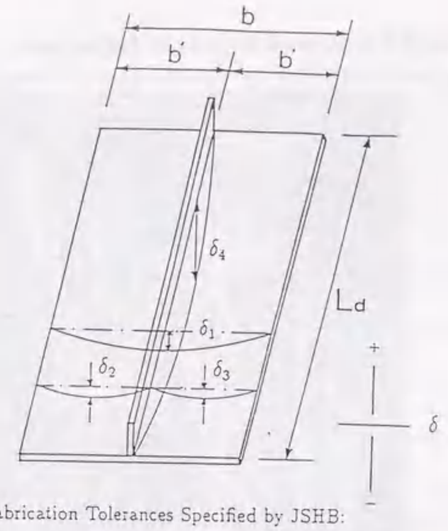

Fabrication Tolerances Specified by JSHB:
δ_1=b/150, δ_2=δ_3=b'/150 and δ_4=L_d/1000

Fig. 2.2 Measurement of Initial Imperfections

concrete-filled column was roughened by chipping and then capped with a thin layer of neat cement paste so that the steel and concrete could be loaded uniformly.

2.2.2 Initial Out-of-Flatness

The initial plate deflections of two flange surfaces of each specimen were measured using a dial gage with an accuracy of 0.002 mm. **Fig. 2.2** shows the measurement of initial imperfections; and **Table 2.3** gives the ratio of the measured maximum initial imperfections to b, b', or L_d. The measured values were less than the fabrication tolerances ($\delta_1/b = 1/150$; $\delta_2/b' = \delta_3/b' = 1/150$; and $\delta_4/L_d = 1/1{,}000$) of the *JRA 90* code (1990), with a few exceptions, such as in specimens S75-S(1) and S75-C(0.35).

2.2.3 Residual Stress

The measurements of the residual stress distribution in steel plate panels due to welding were not conducted, since a similar study had already been done (Usami et al. 1991). In that study, the residual stress was of the typical rectangular shape distribution (Dwight 1969). The maximum tensile residual stresses were about the yield stress σ_y, while the compressive residual stresses were about $0.5\sigma_y$.

Table 2.3 Measured Results of Initial Imperfections

Specimen	Surface	δ_1/b ×10^{-3}		δ_2/b' ×10^{-3}		δ_3/b' ×10^{-3}		δ_4/L_d ×10^{-3}	
		+	−	+	−	+	−	+	−
U9-S	A	4.58	1.65	—	—	—	—	—	—
	B	3.11	1.82	—	—	—	—	—	—
U9-C	A	4.09	0.58	—	—	—	—	—	—
	B	4.80	—	—	—	—	—	—	—
U12-S	A	3.06	0.43	—	—	—	—	—	—
	B	3.60	—	—	—	—	—	—	—
U12-C	A	3.15	0.28	—	—	—	—	—	—
	B	2.18	0.46	—	—	—	—	—	—
U12-HC	A	3.24	0.15	—	—	—	—	—	—
	B	4.21	—	—	—	—	—	—	—
U15-S	A	0.83	0.32	—	—	—	—	—	—
	B	2.43	—	—	—	—	—	—	—
U15-C	A	0.44	0.97	—	—	—	—	—	—
	B	2.33	—	—	—	—	—	—	—
S75-S(1)	A	0.30	3.43	1.06	1.01	1.13	0.27	—	1.72
	B	0.07	2.82	0.65	1.07	0.58	—	0.11	0.71
S75-C(1)	A	—	2.19	0.95	2.17	0.50	1.89	—	0.50
	B	0.56	0.75	0.97	1.44	1.54	0.91	0.05	0.18
S75-C(0.35)	A	1.04	1.62	1.97	0.36	1.16	0.48	0.57	1.24
	B	1.27	3.63	1.33	0.75	1.63	0.75	1.47	0.47

For Notations, refer to Fig. 2.2.

2.2.4 Loading Method

Fig. 2.3 shows the test setup. Tests were carried out under cyclic loading in a 5.88 MN (600 tonf) testing machine. To assure uniform compression, preliminary tests within the elastic range were conducted by adjusting the loading plate, based on the measurements of eight strain gages attached at each end (top and bottom) of the test specimens. The measured strain at each of the eight gages was compared to the average of the eight measured strains at each end. Adjustment of the loading plate was terminated when the difference between the measured strain and the average value was not more than 5%.

The axial shortening between the diaphragms was measured using four displacement transducers (see **Fig. 2.3**) in each loading stage. The average axial strain of each

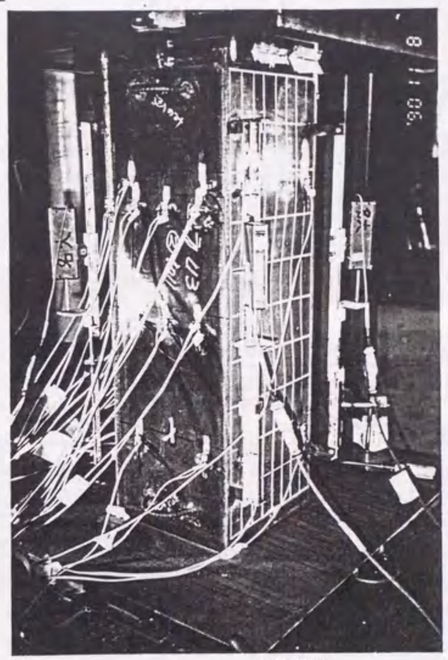

Fig. 2.3 Test Setup

specimen, $\overline{\varepsilon}$, is calculated as follows:

$$\overline{\varepsilon} = \frac{1}{4}\sum_{i=1}^{4}\frac{\triangle_i}{L_i} \tag{2.2}$$

where $\triangle_i$, L_i = axial shortening measured with the displacement transducer and the corresponding distance of each dial gage. Moreover, the strains at specified points were measured using 16 strain gages.

The loading process was conducted at two phases as shown in **Fig. 2.4**. At the initial phase, a load-controlled type of loading using an increment of 0.1 times the estimated maximum load, P_{max}, was adopted until $P_{max}/2$ was reached. Then a displacement-controlled loading was applied. The displacement increment used in this

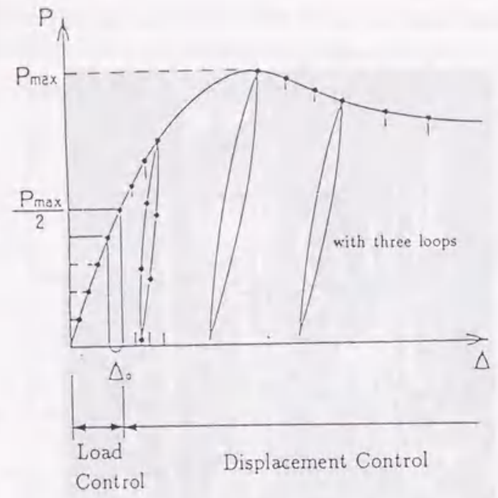

Fig. 2.4 Loading Method

phase is the increment observed from dial gages at the last step of the load-controlled phase. This increment was increased appropriately after the peak. A cyclic loading with three loops was carried out up to failure.

2.3 Results and Discussions

2.3.1 Material Properties

The steel used was mild steel of grade SS400 (nominal yield stress $\sigma_y = 235$ MPa), and the nominal thickness of each test specimen was 4.5 mm. The mechanical properties were determined by using tensile-coupon tests. The results are given in **Table 2.4** as the average values of three test pieces in each series.

The concrete used had a water/cement ratio of 55.2% (by weight) for ordinary concrete, made with ordinary portland cement; and 31.6% (by weight) for high-performance concrete (Ozawa et al. 1989), made with low-heat cement. The aggregate was well graded with a maximum size of 20 mm. To determine the compressive strength of concrete, 12 cylinders (10cm diameter $\times$ 20cm height) were cast from the same concrete used inside the concrete-filled column. The cylinders were cured until the column specimens were tested. The mechanical properties were determined by using compressive-coupon tests. The average values obtained from three cylinders are listed in **Table 2.5**.

Table 2.4 Material Properties of Steel

Series	E (GPa)	ν	σ_y (MPa)	ε_y $(\times 10^{-3})$	E_{st} (GPa)	ε_{st} $(\times 10^{-2})$	Remarks
Plate	197	0.269	266	1.34	9.40	1.53	—
Stiffener-38	198	0.248	309	1.55	8.13	2.20	$b_s = 38\ mm$
Stiffener-25	199	0.279	301	1.48	6.67	1.62	$b_s = 25\ mm$

Notes: E = Young's Modulus, σ_y = Yield Stress, ε_y = Yield Strain, ν = Poisson's Ratio, E_{st} = Strain-hardening Modulus, ε_{st} = Strain at Onset of Strain-hardening

Table 2.5 Material Properties of Filled-Concrete

Series	Days	E_c (GPa)	μ	f_c (MPa)	Test Column
C	37	27.9	0.165	39.2	U9-C
	47	28.3	0.157	40.4	U12-C, S75-C(0.35)
	53	30.7	0.168	40.6	U15-C, S75-C(1)
H	35	31.5	0.184	48.3	U12-HC

Notes: f_c = Uniaxial Compressive Cylinder Strength of Concrete,
C = Ordinary Concrete, H = High-performance Concrete

2.3.2 Failure Modes

Typical failure modes of the test specimens are shown in **Fig. 2.5**. In the case of steel box columns, it was observed during the experiment that local buckling failure of the plate panels occurred before the maximum load was reached. The steel panels buckled at the central part of the specimens. At the two opposite faces of the columns, buckling occurred inward; at the other two perpendicular faces, buckling occurred outward. It could be concluded that each steel box column demonstrates a very symmetric buckling mode about the axes of the cross section.

In the case of concrete-filled columns, the following important phenomena were observed: (1) Local plate buckling occurred initially in one of the plates of the columns just before the maximum load was reached, and other buckling deformations took place in the other plates after the peak. (2) The steel plates buckled at different locations,

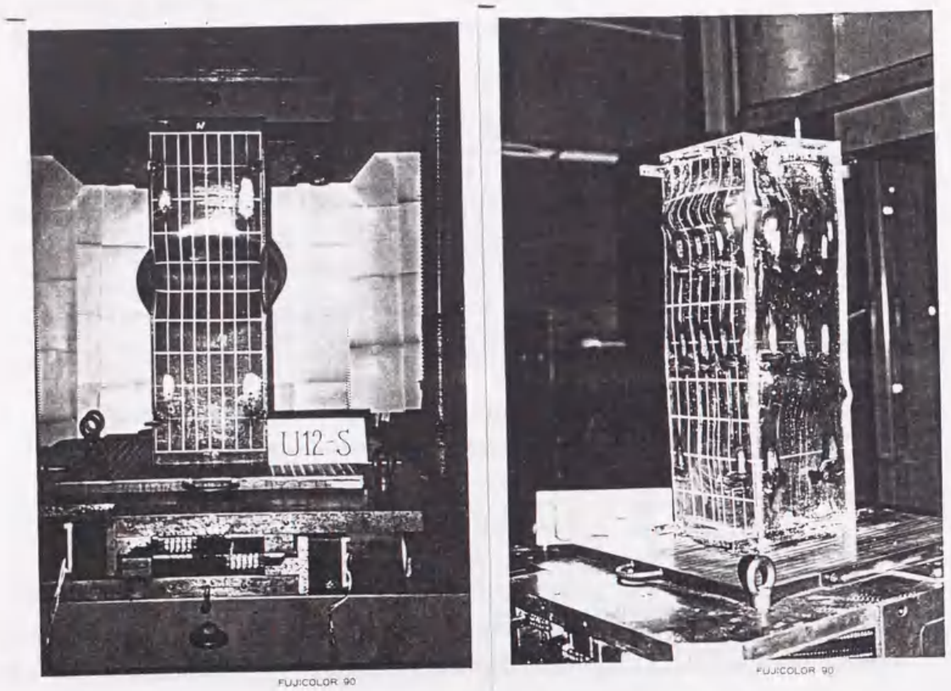

Fig. 2.5 Typical Failure Appearances of Test Specimens

including at the central portion. (3) The steel plates buckled outward in all faces. (4) The increase in deformation became faster after local buckling, and cracks in the weld occurred in some of concrete-filled columns [such as specimens U9-C, U12-HC, U15-C, and S75-C(1)] when the axial strain of the specimen became relatively large (e.g., at about 1.2% in the case of specimen U9-C).

Usually, the fracture of a concrete prism subjected to concentric compression load is produced by generating cracks through splitting or sliding, as shown in **Fig. 2.6(a)** and **(b)**. Hence, the failure of the concrete-filled box columns may intuitively be assumed to take the pattern as shown in **Fig. 2.6(c)**. Once the web plates of all the concrete-filled steel columns were removed after failure by gas-cutting (**Fig. 2.7**), it was observed that the concrete behind the portions of plates that buckled was seriously crushed, while no damage was observed in the other parts. Thus, it can be concluded that local

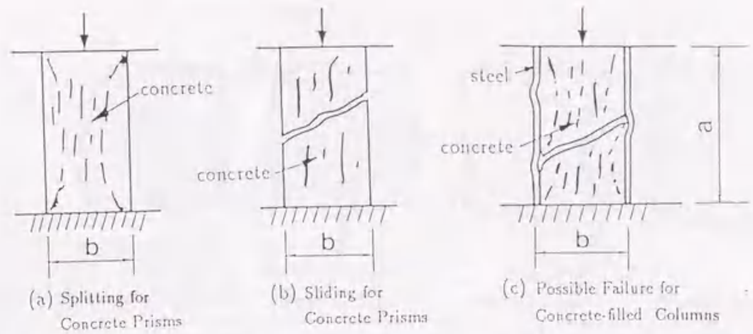

Fig. 2.6 Failure Patterns for Concrete Prisms and Concrete-Filled Columns: (a) Sliptting for Concrete Prisms; (b) Sliding for Concrete Prisms; (c) Possible Failure for Concrete-Filled Columns

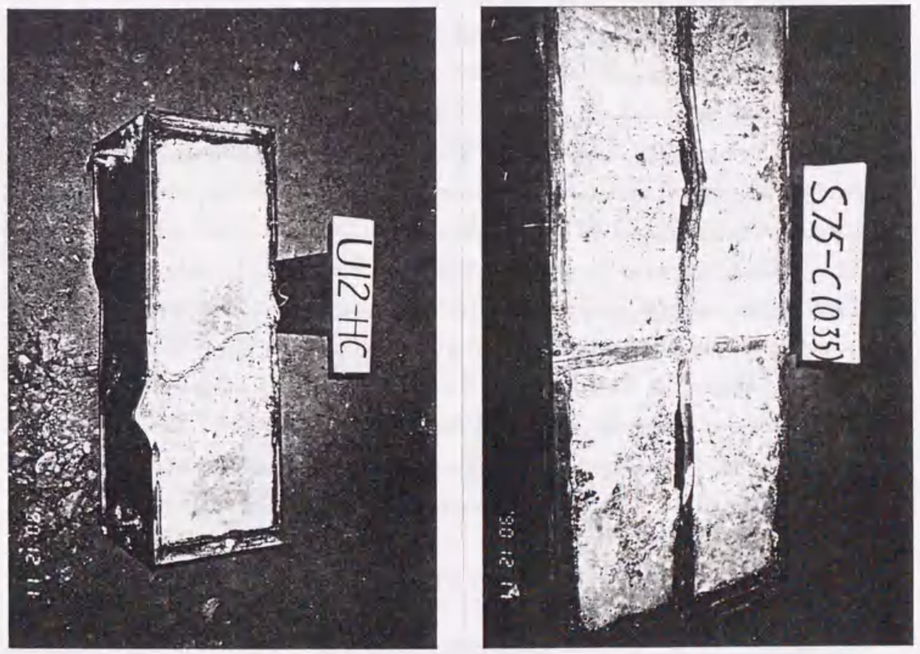

Fig. 2.7 Typical Failure Appearances of Filled-in Concrete

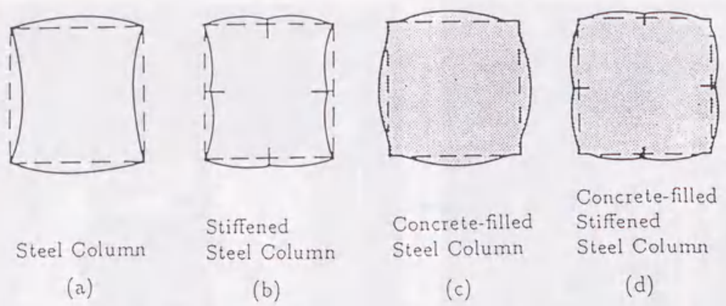

Fig. 2.8 Failure Modes of Test Specimens: (a) Steel Column; (b) Stiffened Steel Column; (c) Concrete-Filled Steel Column; (d) Concrete-Filled Stiffened Steel Column

plate buckling was induced after concrete was damaged. It was also observed that the steel plates were separated from the filled-in concrete in the places where buckling occurred, and the crushing of concrete followed the pattern in **Fig. 2.6(c)**.

The buckling modes of the plate panel after collapse of each specimen could be classified in four groups, as shown in **Fig. 2.8**. For the unstiffened steel column, the steel plates buckled alternately in convex and concave surfaces, with the nodes at the corners of columns; and for the stiffened steel column, the steel plates buckled in roughly the same form as in the unstiffened steel column, but nodes did not occur at the stiffeners. In the case of the concrete-filled column, all the steel panels buckled outward. The buckling of steel plates toward the interior direction must have been prevented by the filled-in concrete. It must be noted that for the buckling modes of two stiffened composite columns, the stiffeners contributed to a great extent to the overall shape of the buckling of columns even when stiffener rigidities were small, because the local buckling of longitudinal stiffeners was prevented by the filled-in concrete.

2.3.3 Load versus Average Strain Hysteretic Curves

Examples of the load-average strain hysteretic curves are shown in **Fig. 2.9**. The hysteretic loops in the steel column [**Fig. 2.9(a)**] were very narrow even after the peak. On the other hand, the hysteretic loops in the concrete-filled columns [**Fig.**

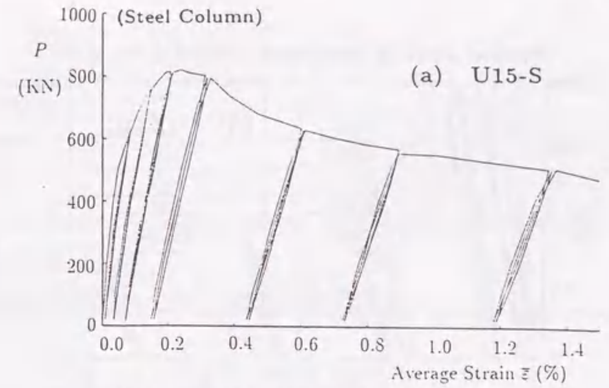

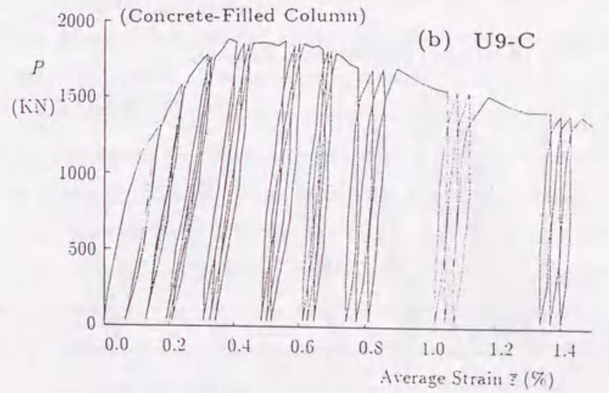

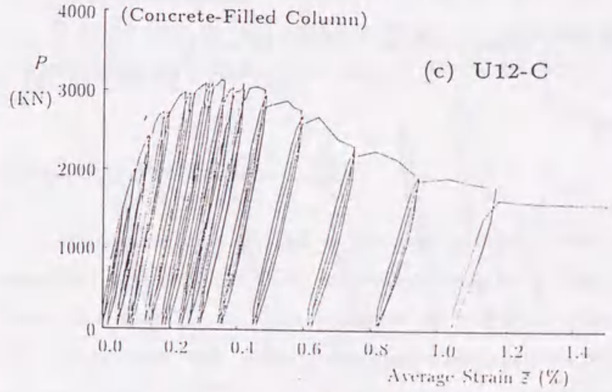

Fig. 2.9 Examples of Load versus Average Strain Curves under Cyclic Compression Load (to be continued)

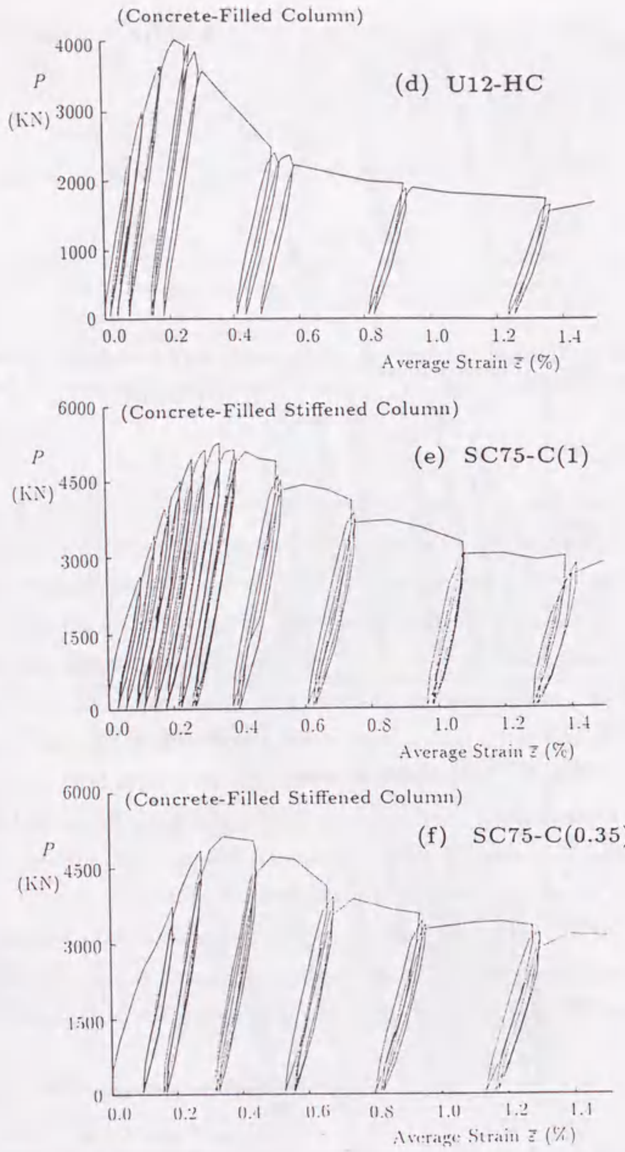

Fig. 2.9 Examples of Load versus Average Strain Curves under Cyclic Compression Load (continued)

Table 2.6 Ultimate Strengths of Steel Columns

Specimen	P_u (KN)	σ_u / σ_y	
		Test	Prediction (Usami)
U9-S	821	0.846	0.829
U12-S	803	0.624	0.622
U15-S	805	0.503	0.497
S75-S(1)	1598	0.882	0.861

P_u = Maximum Load;
σ_u = Average Ultimate Stress of the Plate Panel.

2.9(b) to **(f)**] were relatively narrow in the early cycles, and then became wider at the later cycles. This phenomenon implied that the filled-in concrete had been damaged more or less before the peak. The hysteretic curves of concrete-filled columns also showed that the hysteretic loops just after the peak become apparently wide, implying that more serious damage in the filled-in concrete has occurred. This phenomenon was very obvious in specimen U12-HC [**Fig. 2.9(d)**]. It was observed that the increase of deformation was very difficult to control just after the peak, although the load was made constant at a certain loading level. Accordingly, the stiffness decreased rapidly in this concrete-filled column. On the other hand, a comparison between the load versus average strain hysteretic curve of the specimen U9-C and that of the other concrete-filled columns showed that the degree of damage of the filled concrete in U9-C is larger than the others. It could thus be said that the hysteretic curve is significant when investigating the structural performance of composite structures such as concrete-filled columns.

2.3.4 Ultimate Strength of Steel Columns

Fig. 2.10 shows comparisons of load versus average strain envelope curves for three unstiffened steel box columns. The maximum loads of all the steel columns are given in **Table 2.6** together with the predicted ultimate strengths proposed by Usami (1990). The maximum loads and post buckling strengths were almost the same in steel box columns U9-S, U12-S and U15-S although the cross-sectional areas were different. On the other hand, the stiffened steel box column specimen S75-S(1) had a higher compression capacity than these unstiffened steel box columns (see **Table**

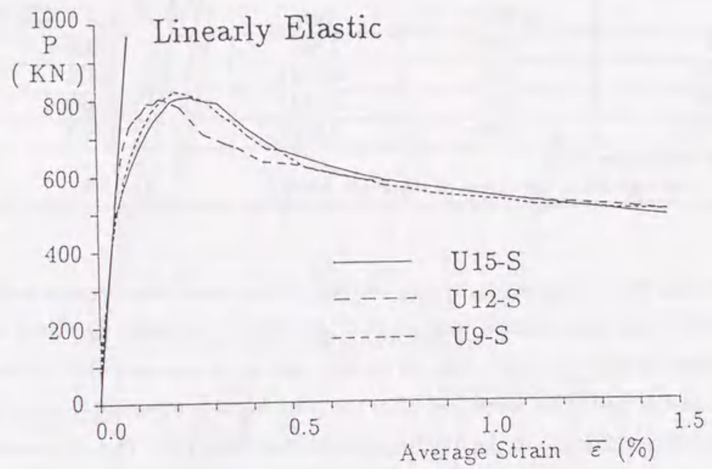

Fig. 2.10 Load versus Average Strain Envelope Curves of Unstiffened Steel Box Columns

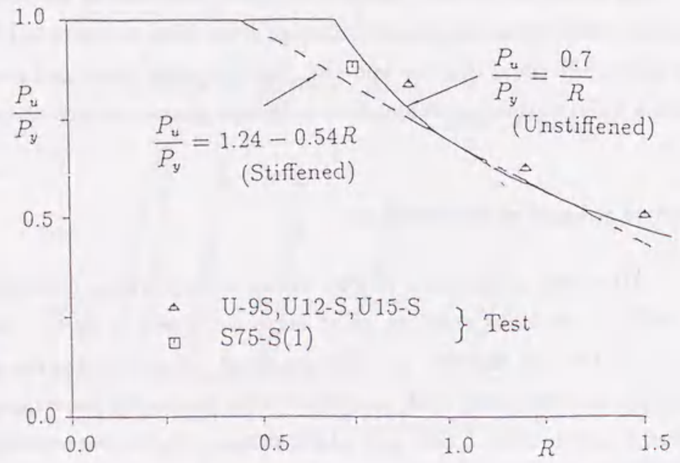

Fig. 2.11 Comparisons of Predicted and Experimental Ultimate Strength of Steel Columns

2.6). It is noted that the cross-sectional areas of the specimens S75-S(1) and U15-S were nearly the same, but the former had twice the capacity of the latter. This means that longitudinal stiffeners are very effective against the local buckling of the plate panel. The ultimate strengths of steel columns are plotted against the width-thickness ratio parameter R in **Fig. 2.11**. The strength of the steel box column is reduced as the plate width-thickness parameter R is increased. **Fig. 2.11** also shows that the experimental results agree well with predictions according to the strength formulas proposed by Usami (1990). These proposed empirical formulas are

$$\frac{P_u}{P_y} = \frac{0.7}{R} \leq 1.0 \tag{2.3}$$

for unstiffened plate; and

$$\frac{P_u}{P_y} = 1.24 - 0.54R \leq 1.0 \tag{2.4}$$

for stiffened plate.

2.3.5 Ultimate Strength of Concrete-filled Columns

Experimental load-average strain envelope curves of the concrete-filled box columns are presented in **Fig. 2.12**, and the maximum loads are given in **Table 2.7**. The ultimate strength increased with the plate width-thickness ratio R due to the net increase of the concrete cross-sectional area. However, specimen U15-C showed relatively lower strength than expected. This may be due to a sudden crushing of the filled concrete during the test. It was found after removing the steel plates of specimen U15-C by gas-cutting that the concrete mix was not well-distributed; that is, the upper filled concrete had less coarse aggregate. This was due to improper pouring of the concrete.

A so-called high-performance concrete with a superflowing property, for which a high-early-strength low-heat cement was used, was poured in the specimen U12-HC. High-performance concrete, defined as a high-level construction material based on the durability design of concrete structures, was developed by Ozawa et al. (1989). This type of concrete can be filled into all corners of formwork without using a vibrator, since it has a high filling capacity. The high-performance concrete has less coarse aggregate and more powder materials than conventional air-entrained (AE) concrete (Ozawa et al. 1989). **Fig. 2.12** showed that although a higher ultimate strength was reached,

a higher post buckling strength was not obtained; and this specimen lost its stiffness sharply, unlike in the columns filled with the ordinary concrete. It should be noted that the high-performance concrete mix was very pulpy, and its slump flow was 57 cm (the slump of the ordinary concrete mix was 12 cm).

For some empirical strength design formulas the comparison of the local buckling strength of steel plates in the concrete-filled column requires a knowledge of the characteristic strength of the concrete, f_{ck}. This is very important for evaluating the ultimate strength of concrete-filled box columns. To determine the compressive strength of the concrete inside the steel box, three kinds of concrete specimens have been used in past studies: (1) cylinder (Nakai et al. 1986; Tomii et al. 1977); (2) cube (Shakirkhalil 1991); and (3) prism with the same size as the filled-in concrete in the concrete-filled composite column (Kitada et al. 1989). In any structural analysis carried out for plain, reinforced, or prestressed concrete members, stressed by a centric compressive load or an eccentric compressive load of small eccentricity, the value of prismatic strength determined on prisms loaded with centric compressive stresses is used. The prismatic strength, f_{cp}, is a function of the ratio of height a to side b of the cross section, as well as the concrete class. As pointed out by Avram et al. (1981), the prismatic strength drops with increasing a/b, and with increasing the concrete class even for the same slenderness a/b. The value of the ratio f_{cp}/f_{cc} is supposed to be about 0.9 for a prism with $a/b = 3.0$ and 0.6 for a prism with the concrete class C40 ($f_{cc} = 40$ N/mm^2). On the other hand, the following relation is suggested by Avram (1981) for the conversion coefficient between the cubic compressive strength f_{cc} and the cylindrical compressive strength f_c:

$$\frac{f_c}{f_{cc}} = 0.8 \tag{2.5}$$

Therefore, the value of the ratio $f_{cp}/f_c = 0.9 \times 0.6 \,/\, 0.8 = 0.675$ in this case. It should be noted that the ratio f_{cp}/f_c depends on many factors, and thus it should not be constant. Based on these considerations, an empirical reduction factor is introduced to account for the difference in strength between the cylindrical strength f_c and the prismatic strength f_{cp} of the concrete member

$$f_{ck} = f_{cp} = \beta f_c \tag{2.6}$$

The value of β is taken to be 0.7 in this study, based on the foregoing considerations.

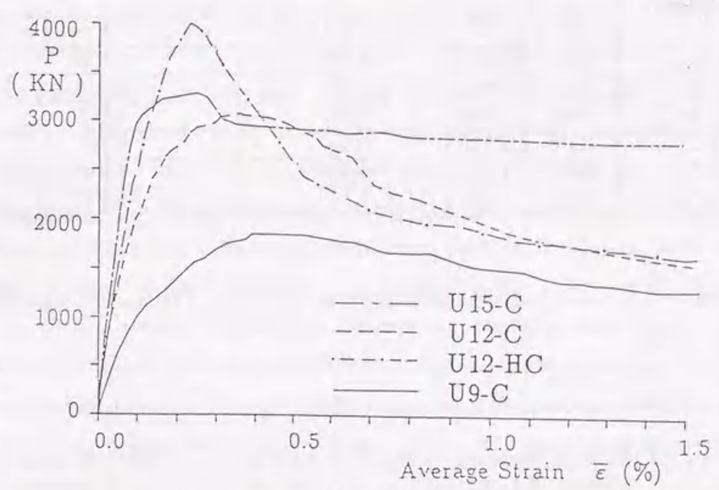

Fig. 2.12 Load versus Average Strain Envelope Curves of Concrete-Filled Unstiffened Steel Box Columns

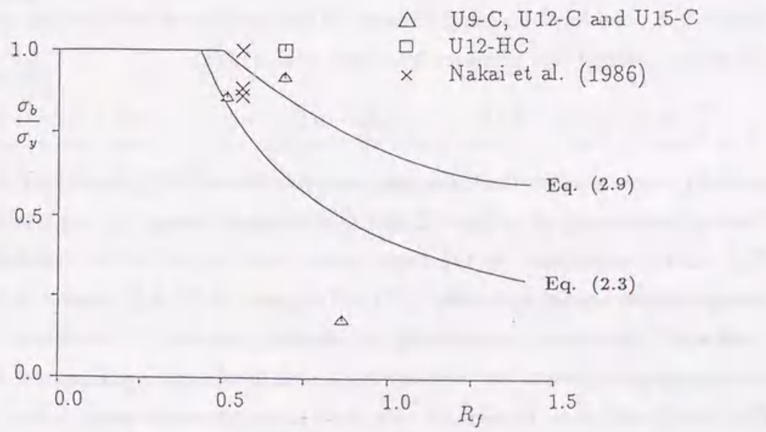

Fig. 2.13 Comparisons of Predicted and Experimental Ultimate Strength of Steel Plates in Concrete-Filled Columns

Table 2.7 Ultimate Strengths of Concrete-Filled Columns

Specimen	P_u (KN)	σ_b / σ_y		
		Test	Prediction (Usami)	Prediction (Kitada et al.)
U9-C	1845	0.855	0.834	0.988
U12-C	3070	0.916	0.622	0.858
U12-HC	3999	1.000	0.622	0.858
U15-C	3275	0.175	0.497	0.755
S75-C(1)	5030	1.000	0.861	0.920
S75-C(0.35)	5158	1.000	0.859	0.770

In the case of concrete-filled steel box columns, therefore, the squash load P_y can be predicted as follows:

$$P_y = \sigma_y A_s + f_{ck} A_c \tag{2.7}$$

To evaluate the local buckling strength of steel plates in concrete-filled columns, the strengths (σ_b/σ_y) are predicted by using the following equation:

$$\frac{\sigma_b}{\sigma_y} = \frac{P_u - f_{ck}A_c}{A_s\sigma_y} = \frac{P_u - \beta f_c A_c}{A_s \sigma_y} \tag{2.8}$$

in which, P_u = maximum test load of each concrete-filled column. The computed values, σ_b/σ_y, of steel plate component in all the concrete-filled columns are listed in **Table 2.7**. The local buckling strength of the unstiffened compression plate with all the edges clamped was proposed by Nakai et al. (1985)

$$\frac{\sigma_b}{\sigma_y} = 0.433(R_f - 0.5)^2 - 0.831(R_f - 0.5) + 1.0, \qquad (0.5 < R_f < 1.3) \tag{2.9}$$

where R_f = plate width-thickness parameter, with $k = 10.67$ (plate with fixed loading—fixed unloading edges) in **Eq. (2.1)**. This ultimate strength curve is also plotted in **Fig. 2.13**, together with the experimental data and with the predicted ultimate strength curve expressed by **Eq. (2.3)** (R is replaced by R_f). Moreover, three experimental data by Nakai et al. (1986) are also shown in **Fig. 2.13**. It can be seen that the experimental points are above the predicted local buckling strength curve given by **Eq. (2.3)**, with $R = R_f$ in most cases, and some points are even above the predicted curve for a clamped plate [**Eq. (2.9)**]. It can also be seen that one point (U15-C) is below the curve of **Eq. (2.3)**. In the case of stiffened composite columns, the local

buckling strength of the stiffened plate is predicted by using a simplified calculation method proposed by Nakai et al. (1985). As shown in **Table 2.7**, this method gives relatively smaller predictions than the experimental ones, because the bond and/or frictional forces between steel plates and filled-in concrete are neglected.

As mentioned previously, two sorts of cross sections of the stiffener were designed in this study. Although the relative rigidities of both specimens are different, their ultimate strengths and post buckling behavior are nearly the same, as shown in **Fig. 2.14**. It was found from **Table 2.7** that a considerable increase in the ultimate strength was obtained in these two stiffened concrete-filled columns, compared with those of the unstiffened concrete-filled columns. This means that the stiffening effect tends to increase due to the bonding between the stiffener and concrete, although the relative rigidity γ_l is smaller than the required minimum value γ_{req} in the specimen S75-C(0.35).

Comparisons of the strength and ductility behavior of the concrete-filled box column and the steel box column are given in **Fig. 2.15**. The maximum strengths were obtained at about $\bar{\varepsilon} = 0.2\%$ in the steel box columns; and at about $\bar{\varepsilon} = 0.4\%$ in the concrete-filled box columns. Obviously, the maximum strengths of the concrete-filled columns were much larger than those of the steel columns due to a contribution of the filled concrete component. It is thus concluded that the concrete-filled column shows good structural performance, for example higher strength and higher ductility, than the steel column.

2.4 Summary

An experimental study on the strength and deformation of steel columns and concrete-filled columns was conducted. The comparative study between two types of columns showed that high ductility as well as high strength can be expected from concrete-filled columns. For the buckling of steel panels in concrete-filled columns, the test results showed somewhat lower strength than the calculated values obtained from **Eq. (2.9)**, or somewhat higher strength than the calculated values obtained from **Eq. (2.3)** in some cases. Thus, further study on the strength characteristic is necessary to formulate practical equations for design. It was also found that the significant stiffening effects of longitudinal stiffeners on the strength can be expected in both the steel column and concrete-filled column, although the stiffening effects against the

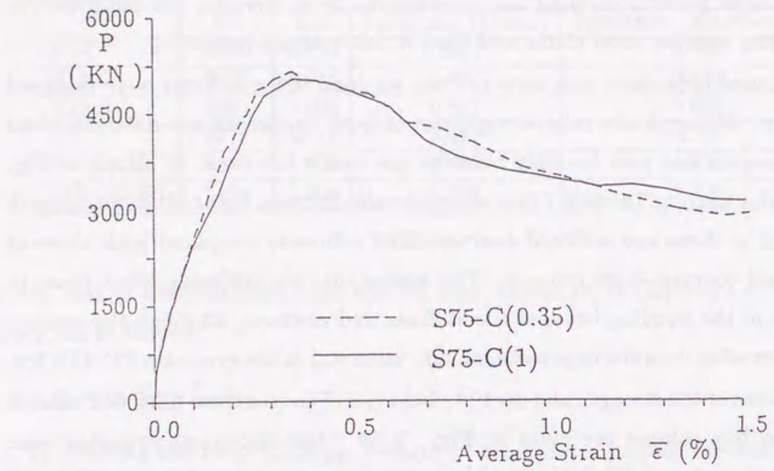

Fig. 2.14 Load versus Average Strain Envelope Curves of Stiffened Steel Box Columns: Influences of Stiffener Rigidity

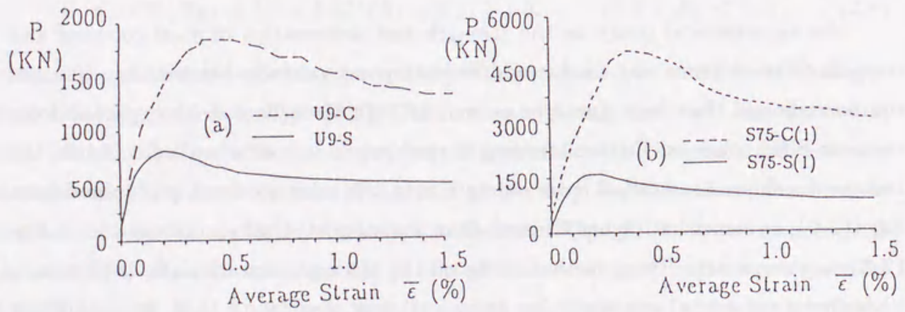

Fig. 2.15 Comparisons of Structural Performances of Concrete-Filled Columns with those of Steel Columns

buckling mode of the plate panels are not as much expected when the relative rigidity of the stiffener is small. All the steel panels in the concrete-filled column buckled outward because buckling toward the interior was prevented by the filled-in concrete. The fracture of the concrete-filled column depends to a great extent on the fracture of the filled concrete member, and thus special care must be given to the casting of the concrete.

3 NUMERICAL STUDY ON THE STRENGTH OF CONCRETE-FILLED THIN-WALLED STEEL BOX STUB-COLUMNS IN COMPRESSION

3.1 General Remarks

In chapter 2, an experimental study on the structural performances of concrete-filled thin-walled steel box stub-columns was presented. Compared to the available experimental work, almost no theoretical work on elasto-plastic finite displacement analysis of concrete-filled columns is available.

This chapter presents an elasto-plastic finite displacement analysis on the concrete-filled thin-walled steel stub-columns of box shape. In the analysis, a hardening-softening model developed by Wu and Tanabe (1990) is utilized to describe the elasto-plastic behavior of concrete. The contact element for interface combined with the bilinear constrained shell element for the plate and the three-dimensional arbitrarily distorted cubic element for concrete are employed. Both initial geometrical imperfections and residual stresses are considered in the plate elements. Analytical results are compared with prior experimental results. Furthermore, a parametric study is conducted to investigate the effects of various parameters such as plate aspect ratio, plate width-thickness ratio, and concrete strength. Finally, a design formula is proposed for concrete-filled box stub-columns in compression.

3.2 Outline of Analysis

To compute the load-deformation characteristics of steel and concrete-filled steel columns of box shape, the MARC research program (1988) was used.

3.2.1 Analytical Model

Concrete is assumed to be filled in between two rigid diaphragms equipped at the column ends. Thus, one eighth of the part between two diaphragms of the column, shown in **Fig. 3.1**, is taken for the analysis because of symmetry. Since the existence of both the diaphragm and the filled-in concrete, the loaded edges are assumed to be fixed. Finite element mesh for the steel plate panel and for the concrete member is also shown in **Fig. 3.1**.

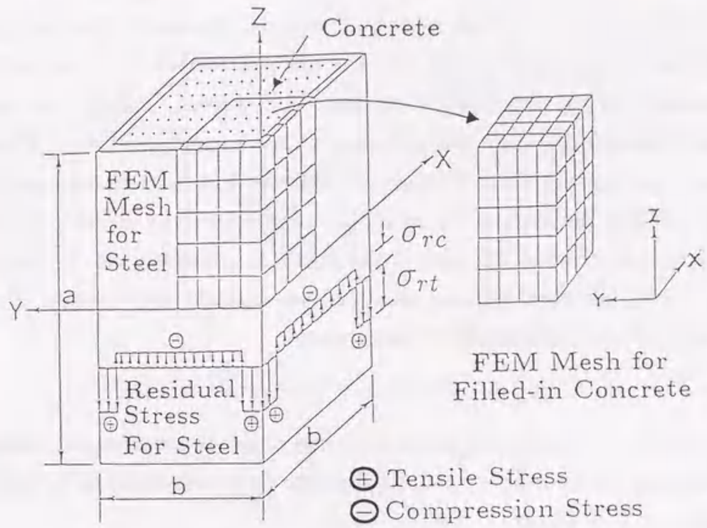

Fig. 3.1 Analytical Model

3.2.2 Element Type

Three element types were considered: (1) An eight-node thin shell element (discrete Kirchhoff element) was employed for the steel plate element [**Fig. 3.2(a)**]. This kind of element has four corner nodes with three degree-of-freedom at each node and four mid-side nodes with only one degree-of-freedom (rotation of edge about itself) at each node. The element has been found to give good results for the analysis of complicated plate structures since the absence of local higher order degrees of freedom will allow for direct connections between folded plates without tying requirements along the folds (MARC 1988; Usami at al. 1991). (2) An eight-node isoparametric element with three global degree-of-freedom per node was used to model the concrete element [**Fig. 3.2(b)**]. (3) In addition, to account for the interaction between steel and concrete, a contact element (MARC 1988) was employed between any two nodes of the

interface. This element has four nodes, two of which are physical or external nodes and two are internal to accommodate the lagrangian multipliers [**Fig. 3.2(c)**]. The degree-of-freedom of the external nodes depends on the element types with which these nodes are associated (e.g., the node associated with the element for the steel plate has three cartesian (x,y,z) displacements, and the node associated with the element for the concrete member has also three global degree-of-freedom). The first internal node has only one degree-of-freedom, corresponding to the normal gap force. The second internal node has a maximum of three degree-of-freedom, two frictional force and the frictional slip. Since the friction characteristic is too difficult to define quantitatively for the structure in question, the true distance gap, in which the two end-points will be at least a given minimum distance apart, is then assumed in this study. Therefore, the constraint enforced by this true distance gap is

$$|\vec{X}_4 - \vec{X}_1| \geq d \tag{3.1}$$

where, $\vec{X}_1$ and $\vec{X}_4$ are coordinate vectors of the first node and fourth node, respectively, d is the minimum distance between the end-points (d is considered to be half of the plate thickness in this study).

3.2.3 Initial Out-of-Flatness

For the analysis of columns tested, the measured values of the initial out-of-flatness are used in the flange plates and the same form of the initial out-of-flatness in the web plates. For the analysis of columns considered in the parametric study, the initial plate deflections are assumed to be the form as follows (see **Fig. 3.3**):

$$\delta = -\frac{\delta_{max}}{4}[1 - \cos\frac{2\pi}{a}(Z - a/2)][1 - \cos\frac{2\pi}{b}Y] \quad \text{in } Y - Z \text{ plane} \tag{3.2}$$

$$\delta = -\frac{\delta_{max}}{4}[1 - \cos\frac{2\pi}{a}(Z - a/2)][1 - \cos\frac{2\pi}{b}X] \quad \text{in } X - Z \text{ plane} \tag{3.3}$$

where, δ_{max} is the maximum plate deflection, δ is the outward displacement at coordinate (Y,Z) or (X,Z) in the coordinate system shown in **Fig. 3.1**.

3.2.4 Residual Stress

The residual stresses of the plate panel due to welding are considered as shown in **Figs. 3.1** and **3.3**. The tensile and compressive residual stresses are the yield stress, σ_y, and 0.3 times of yield stress, respectively, i.e.,

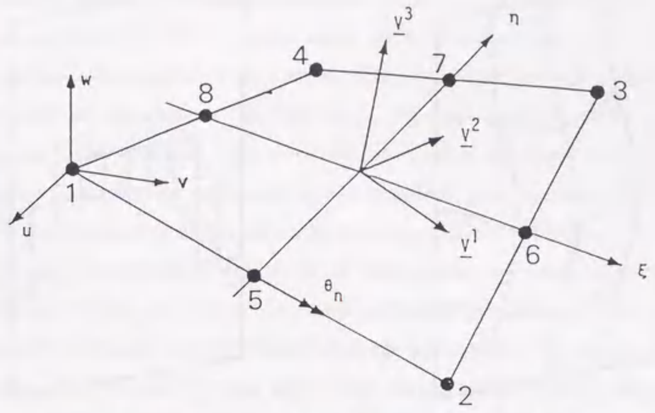

(a) Bilinear Constrained Shell Element for Steel Plate

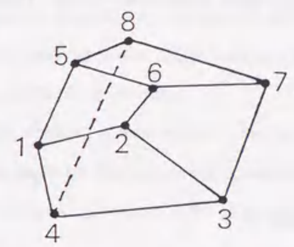

(b) Arbitrarily Distorted Cube Element for Concrete

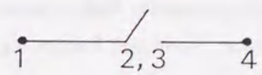

4 nodes
2 physical or external nodes (1, 4)
2 internal nodes (2, 3)

(c) Contact Element for Interface

Fig. 3.2 Element Types

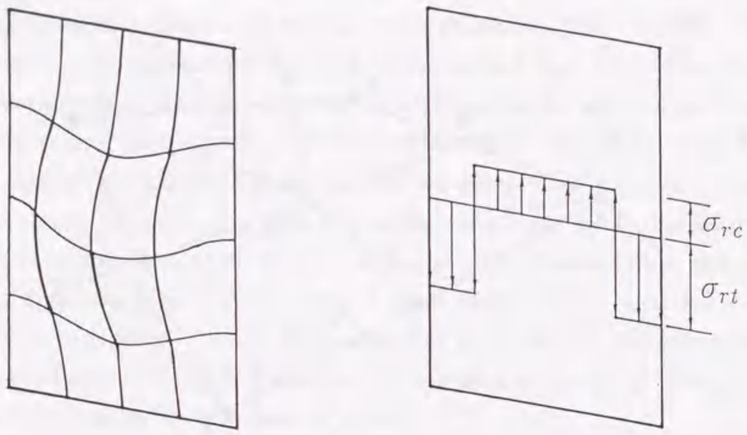

Initial Deflections Residual Stresses

Fig. 3.3 Initial Deflection Shape and Residual Stress Distribution for Each Plate

$$\sigma_{rt} = \sigma_y, \qquad \sigma_{rc} = 0.3\sigma_y \tag{3.4}$$

are assumed in the analysis.

3.3 Material Nonlinearities

3.3.1 Steel Material

The von Mises yield criterion with normality flow rule is adopted to account for the material nonlinearity of the steel plate. No strain hardening is considered.

3.3.2 Concrete Material

A large number of material models using the classical plastic theory with a well-pronounced yield plateau have been developed referring to metals (Chen 1982). However, it may be inappropriate to concrete. In order to find satisfactory hardening rules and formulations of the inelastic dilatancy, of the hydrostatic pressure sensitivity, of the strain-softening tendency and of microcracking etc., extended and appropriate investigations will become available. The endochronic theory of inelasticity has been

extended to concrete by Bazant et al. (1976). This model characterizes the accumulation of inelastic strain by a scalar parameter function of strain increments and the resulting law seems to be able to model some of the essential features of concrete behavior. However, unfortunately it is comparatively complex for practical application, since it has a lot of parameters. In this study, An elasto-plastic model proposed by Wu and Tanabe (1990) is used. This constitutive model is proposed for concrete under compressive loading referring especially to the classical work-hardening plasticity theory, in which compression is either strain hardening or strain softening. The non-linear behavior such as microcracking etc. is dealt with a damage parameter accumulated and a subsequent loading surface in the stress surface is defined depending on the plastic strain history through the introduced damage parameter. In the implementation of the problem, the Drucker-Prager type yield surface relating with the well-known Mohr-Coulomb criterion, where the mobilized friction angle and mobilized cohesion are introduced, is adopted with the associative flow rule. The main characteristics of this model are: (1) both strain hardening behavior and strain softening behavior can be modeled, (2) it is easy to use because only four material parameters are needed to determine the response of concrete behavior.

In this model, the failure surface is assumed to be varying with a damage parameter in the stress space. The damage of the concrete material accumulated due to the progressive growth of the microcracks is taken into account through a damage parameter, ω, the quantity is defined by

$$\omega = \frac{\eta}{\sigma_e \varepsilon_0} \int dW^p \tag{3.5}$$

in which σ_e is the effective stress, dW^p is the incremental plastic work, η is a material constant and

$$\varepsilon_0 = \frac{f_c}{E_c} \tag{3.6}$$

Here, E_c denotes the modulus of elasticity of concrete, and f_c is the uniaxial compressive strength. An effective plastic strain increment $d\varepsilon_p$ is generally defined in relation with the incremental plastic work dW_p (Chen 1982):

$$dW^p = \sigma_{ij} d\varepsilon_{ij}^p = \sigma_e d\varepsilon_p \tag{3.7}$$

in which, σ_{ij} is the stress tensor, $d\varepsilon_{ij}^p$ is the plastic strain increment. Substituting **Eq. (3.7)** into **Eq. (3.5)** yields

$$\omega = \eta \int d\varepsilon_p/\varepsilon_0 \tag{3.8}$$

The following Drucker-Prager type yield criterion is employed

$$f = \alpha_f I_1 + \sqrt{J_2} - \kappa_f = 0 \tag{3.9}$$

Introducing the concept of the effective stress, it can be expressed as

$$\sigma_e = \frac{\kappa_f}{\sqrt{1/3} - \alpha_f} = \frac{\alpha_f I_1 + \sqrt{J_2}}{\sqrt{1/3} - \alpha_f} \tag{3.10}$$

Where, I_1=σ_{kk} and J_2=$\frac{1}{2}s_{ij}s_{ij}$ are the first invariant of the stress tensor σ_{ij} and second invariant of deviatoric stress tensor s_{ij} respectively, and α_f and κ_f are material constants. These two material constants are related to Mohr-Coulomb constants by

$$\alpha_f = \frac{2\sin\phi^*}{\sqrt{3}(3-\sin\phi^*)}, \qquad \kappa_f = \frac{6c^*\cos\phi^*}{\sqrt{3}(3-\sin\phi^*)} \tag{3.11}$$

in which c^*, ϕ^* are defined as the mobilized cohesion and friction. These parameters are considered to be not constant, and dependent on the the plastic strain history through the damage parameter ω. The relation proposed by Wu and Tanabe (1990) is used and defined as follows:

$$c^* = c\ \exp[-(M\omega)^2] \tag{3.12}$$

$$\phi^* = \begin{cases} \phi\sqrt{2\omega - \omega^2} & \omega \le 1 \\ \phi & \omega > 1 \end{cases} \tag{3.13}$$

where M is a material constant, c the cohesion and ϕ the internal-friction angle of the concrete.

The relationship between the effective stress, σ_e, and the effective plastic strain, ε_p, has the form

$$\sigma_e = \sigma_e(\varepsilon_p) \tag{3.14}$$

Differentiation gives the increment relation

$$d\sigma_e = H(\sigma_e)d\varepsilon_p \tag{3.15}$$

where $H(\sigma_e)$ is a plasticity modulus associated with the rate of expansion of the yield or loading surface

$$H = \frac{d\sigma_e}{d\varepsilon_p} \tag{3.16}$$

H being the slope of the uniaxial stress-plastic strain curve at the current value of σ_e. Such a parameter H is considered to be the work-hardening coefficient, and its expression can be written as

$$\begin{aligned} H &= \frac{d\sigma_e}{d\varepsilon_p} \\ &= \frac{\partial\sigma_e}{\partial\alpha_f}\frac{\partial\alpha_f}{\partial\varepsilon_p} + \frac{\partial\sigma_e}{\partial\kappa_f}\frac{\partial\kappa_f}{\partial\varepsilon_p} \\ &= \frac{\partial\sigma_e}{\partial\alpha_f}\frac{\partial\alpha_f}{\partial\omega}\frac{\partial\omega}{\partial\varepsilon_p} + \frac{\partial\sigma_e}{\partial\kappa_f}\frac{\partial\kappa_f}{\partial\omega}\frac{\partial\omega}{\partial\varepsilon_p} \end{aligned} \tag{3.17}$$

Here,

$$\frac{\partial\sigma_e}{\partial\alpha_f} = \frac{\kappa_f}{(\sqrt{1/3} - \alpha_f)^2}, \quad \frac{\partial\sigma_e}{\partial\kappa_f} = \frac{1}{(\sqrt{1/3} - \alpha_f)}, \quad \frac{\partial\omega}{\partial\varepsilon_p} = \frac{\eta}{\varepsilon_0} \tag{3.18}$$

$$\frac{\partial\alpha_f}{\partial\omega} = \frac{2\sqrt{3}\cos\phi^*}{(3-\sin\phi^*)^2}\frac{\partial\phi^*}{\partial\omega} \tag{3.19}$$

$$\frac{\partial\kappa_f}{\partial\omega} = \frac{6c^*(1-3\sin\phi^*)}{\sqrt{3}(3-\sin\phi^*)^2}\frac{\partial\phi^*}{\partial\omega} - \frac{12\ c\ M^2\omega}{\sqrt{3}(3-\sin\phi^*)}\exp[-(M\omega)^2]\cos\phi^* \tag{3.20}$$

$$\frac{\partial\phi^*}{\partial\omega} = \begin{cases} \frac{1-\omega}{\sqrt{2\omega-\omega^2}}\phi & \omega \le 1 \\ 0 & \omega > 1 \end{cases} \tag{3.21}$$

As usual, the flow rule is of the form

$$d\varepsilon_{ij}^p = \lambda\frac{\partial f}{\partial\sigma_{ij}} \tag{3.22}$$

it can also be redefined in the following form

$$d\varepsilon_{ij}^p = d\varepsilon_p\frac{\partial\sigma_e}{\partial\sigma_{ij}} \tag{3.23}$$

where $d\varepsilon_p$ and $\partial\sigma_e/\partial\sigma_{ij}$ are equivalent plastic strain increment and nondimensional flow direction, respectively. It can be obtained from **Eq. (3.10)** that

$$\frac{\partial\sigma_e}{\partial\sigma_{ij}} = \frac{\alpha_f\delta_{ij}}{\sqrt{1/3} - \alpha_f} + \frac{1}{\sqrt{1/3} - \alpha_f}\frac{s_{ij}}{2\sqrt{J_2}} \tag{3.24}$$

Here, δ_{ij} is the Kronecker delta.

Accordingly, with the work-hardening coefficient H [**Eq. (3.16)**] and the flow rule [**Eq. (3.23)**], the constitutive relation that describes the incremental stress-strain relation for an elastic-plastic material such as concrete can be easily obtained using the conventional method (Chen 1982, MARC 1988) on the basis of the discussions previously. To use this model in simulating the concrete behavior, there are four material parameters except for three material properties (E_c, f_c and μ) needed to be determined by experiment: η, M, c and ϕ. Following Wu and Tanabe, a value of 2.0 is used for the constant M.

3.4 Numerical Results

3.4.1 Prediction of Concrete Behavior

To determine material parameters from test data, a computer program to analyze concrete behavior in compression has been written based on the foregoing numerical algorithm. First, the values of material parameters are arbitrarily varied to study the effect of each parameter. For instance, it is found that the softening behavior varies with the different values of η, and the softening compliance increases with that parameter. Next, by trial-and-error approach, the values of material parameters are found by fitting the Kupfer's experimental data of concrete in uniaxial compression (1969). Shown in **Fig. 3.4** is a comparison ofuniaxial test data and predictions. The solid lines in the figure are predicted uniaxial compressive stress-strain curves obtained using three different values of the softening parameter, η. As is seen, the hardening and softening behavior of concrete may be rationally predicted using $\eta = 0.27$. Values of this parameter and the other three parameters used are listed in **Table 3.1**. Then, predictions of stress-strain response for biaxial and triaxial tests are conducted using the same parameters as in the uniaxial case. **Fig. 3.5** is the fitting of biaxial test data (Kupfer 1969). Fits of nonproportional triaxial tests (Schickert et al. 1977) are as shown in **Fig. 3.6**. Reasonable agreement is seen in the comparisons for different loading paths.

Table 3.1 Parameters Used in the Simulation and Parametric Analysis

Parameter	M	η	c	ϕ
Simulation	2.0	0.15, 0.20, 0.27	$f_c/2.4$	30°
Analysis	2.0	0.27	$f_c/2.4$	30°

3.4.2 Comparison with Test Results of Concrete-Filled Stub-Column in Compression

In chapter 2, concentric compression tests were conducted on four steel square box stub-columns and six concrete-filled square box stub-columns under cyclic loads. The plate width-thickness ratio parameter R was changed to investigate its influence on the strength of box stub-columns. Besides ordinary concrete, the so-called high-performance concrete (Ozawa et al. 1989) was also used as the filled-in concrete in that experimental study. This kind of concrete is made with a high-early-strength low heat cement, and is of super-flowing property.

In this section, the numerical results of elasto-plastic finite displacement analyses on one steel column and two concrete-filled columns are presented and discussed. Although the tests were made under cyclic loading as explained in chapter 2, only the envelope curves of the load-deformation characteristics are discussed here.

Steel Columns

As an example, the analytical result of one steel column tested is presented. The geometrical and material properties of this specimen are given in chapter 2. The measured initial plate out-of-flatness and residual stress are considered. The computed average stress-strain curve is compared with experimental results as shown in **Fig. 3.7**. In the figure, P_y is the squash load ($\sigma_y A_s$), and $\bar{\varepsilon}$ is the average strain (column shortening / column length). It is seen from **Fig. 3.7** that the analytical result is in good agreement with the experiment. The experimental curve seems to be deviating slightly from the linear behavior as early at starting of loading. This may be due to the friction between two L-type anchors used to fix displacement transducers (see **Fig. 2.3**).

Concrete-filled Columns

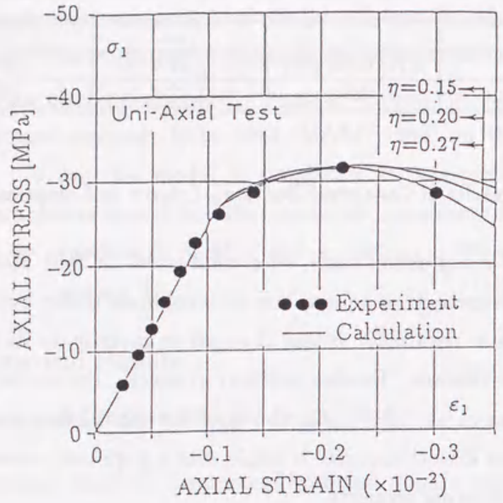

Kupfer, Hilsdorf, and Rusch (1969)
E=24900.0MPa
f_c=32.1MPa
μ=0.18
c=13.4MPa
ϕ=30°
M=2.0

Fig. 3.4 Fit of Uniaxial Test Data of Concrete

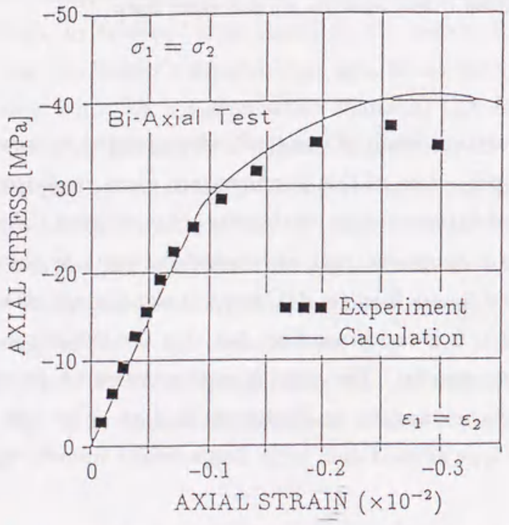

Kupfer, Hilsdorf, and Rusch (1969)
E=24900.0MPa
f_c=32.1MPa
c=13.4MPa
μ=0.18
ϕ=30°
M=2.0
η=0.27

Fig. 3.5 Fit of Biaxial Test Data of Concrete

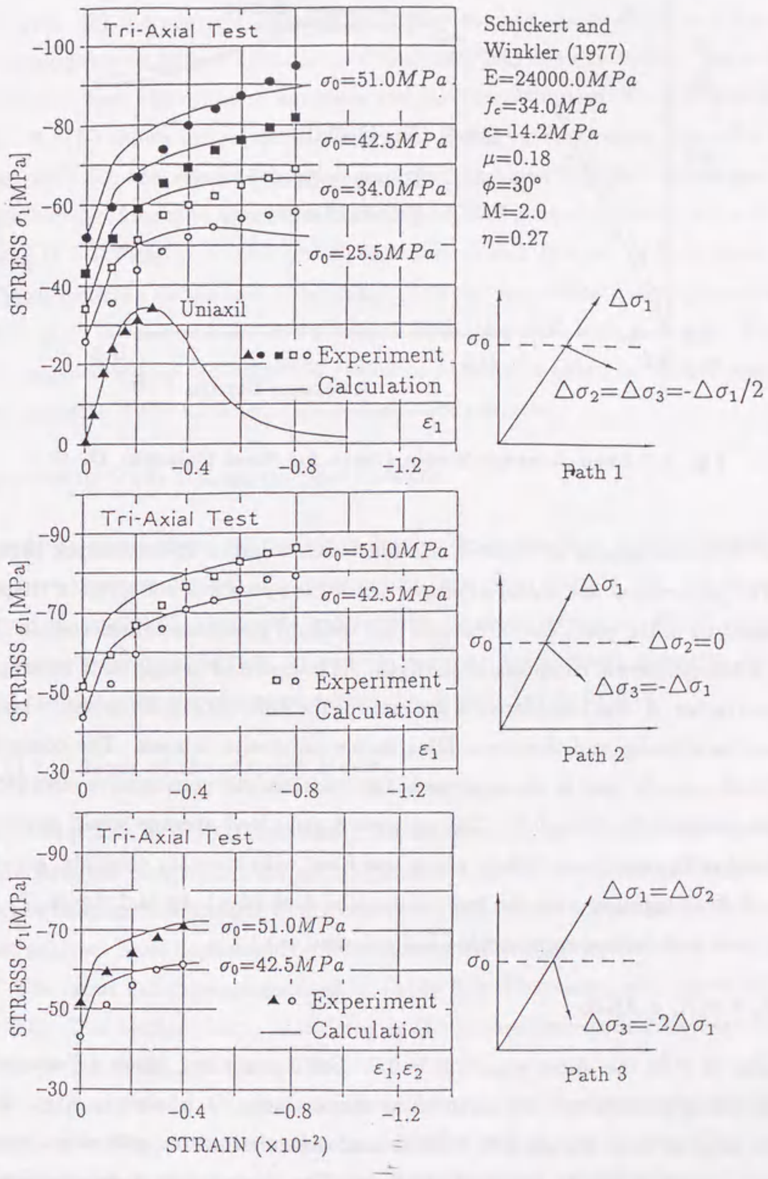

Schickert and Winkler (1977)
E=24000.0MPa
f_c=34.0MPa
c=14.2MPa
μ=0.18
ϕ=30°
M=2.0
η=0.27

Fig. 3.6 Fit of Triaxial Test Data of Concrete

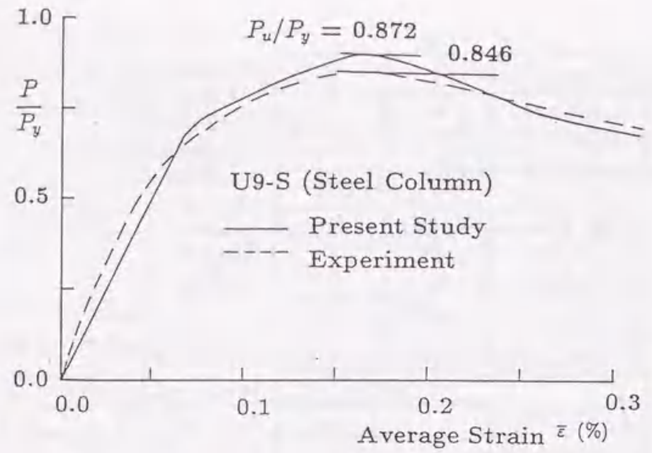

Fig. 3.7 Load-Average Strain Curve for Steel Column: U9-S

The computed results of two concrete-filled stub-columns specimens are presented here. The geometrical and material properties of the specimens are given in chapter 2. The measured initial plate out-of-flatness and residual stress are considered. In **Table 2.5**, f_c is the cylindrical compressive strength. As interpreted in chapter 2, an empirical reduction factor, β, was considered to account for the difference in compressive strength between the cylinder and the prism filled in the composite column. The compressive strength of concrete used in the analysis is the characteristic compressive strength, f_{ck}, with the value of βf_c ($\beta = 0.7$). The computed axial load-average strain curves (the solid lines) of the specimen U12-C, which was filled with ordinary concrete, are shown in **Fig. 3.8(a)** together with the test results (the dash lines). In each figure, P_y is the squash load, and defined in concrete-filled columns as:

$$P_y = \sigma_y A_s + \beta f_c A_c \tag{3.25}$$

The value of β in the above equation is 0.7. For comparison, three different values of η (softening parameter) are assumed in the analysis. It is seen in **Fig. 3.8(a)** that the analysis may not predict well the load-deformation characteristics, however, the ultimate strengths are not much different. The discrepancy of deformation may be attributed to: (1) the tests were made under cyclic loading instead of monotonic

loading, so the response of concrete-filled columns tested show somewhat different with the analysis. (2) the concrete material properties used in the analysis were obtained from the compression tests of cylinders and there may be some difference in the material properties between the cylinder test-piece and the concrete prism filled in columns.

Fig. 3.8(b) shows the computed axial load-average strain curves (the solid lines) together with the test results (the dash lines) for specimen U12-HC, which was filled with the high-performance concrete. In the figure, two computed curves are obtained by taking $\beta = 0.7$ and $\beta = 0.85$, but P_y is obtained with $\beta = 0.7$ in both cases. It is found that, contrary to the case of ordinary concrete, the ultimate strength computed with $\beta = 0.85$ is closer to the experimental ones than that with $\beta = 0.7$. Thus, it may be reasonable that the empirical reduction factor β is taken to be 0.85 when the filled-in concrete is the so-called high-performance concrete.

3.4.3 Parametric Study of Concrete-Filled Columns

In order to obtain some information to develop design formula, a series of parametric studies have been conducted. The parameters taken into account are: (1) steel plate aspect ratio, α=a/b; (2) steel plate width-thickness ratio parameter, R; (3) steel plate initial geometrical imperfection, δ; and (4) concrete compressive strength, f_c. The value of the softening parameter of concrete, η, is assumed to be 0.27.

Case (1): Effects of the Aspect Ratio

For steel plates in pure compression, the aspect ratio, α, that provides the lowest ultimate strength ranges from 0.7 to 1.0 (Bradfield 1982). To investigate the effect of the aspect ratio on the strength of the concrete-filled stub-column, elasto-plastic finite element analyses have been made on four concrete-filled columns with different aspect ratios. The input data are summarized in **Table 3.2**. The values of α are varied from 1.0 to 3.0. The section shape sonsidered is the square box-section having identical thickness in the flange and web plates.

The computed load, P, versus average strain (column shortening/column length), $\bar{\varepsilon}$, are shown in **Fig. 3.9**. It is seen from **Fig. 3.9** that the concrete-filled column with smaller aspect ratios of the component plates shows generally better structural performances such as higher strength and higher ductility than those with higher aspect

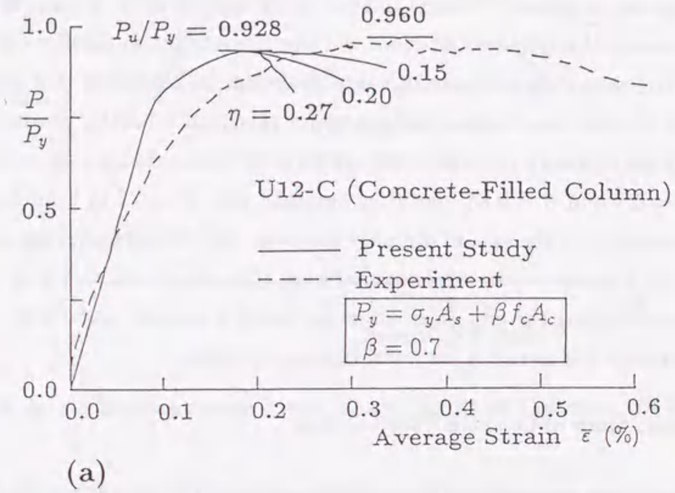

(a)

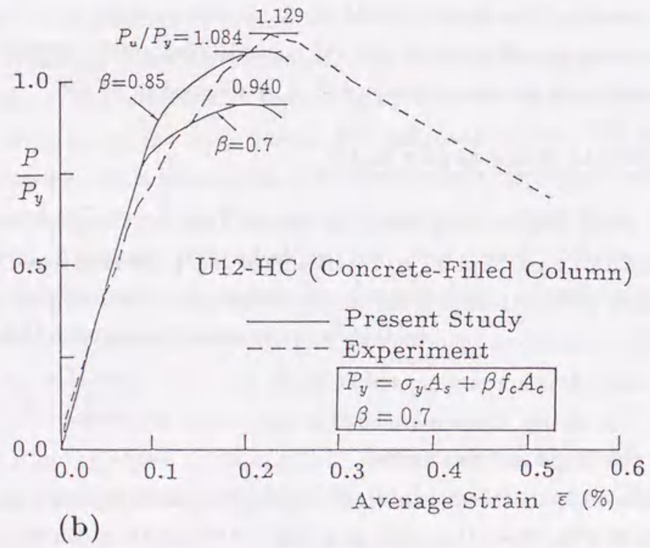

(b)

Fig. 3.8 Load-Average Strain Curves for Concrete-Filled Steel Columns

Table 3.2 Input Data for Concrete-Filled Stub-Column Analysis in Figure 3.9

Property or Parameter		Value
(a) Steel		
Young's modulus	$E(GPa)$	206
Yield stress	$\sigma_y(MPa)$	314
Poisson's ratio	ν	0.3
Plate thickness	$t(mm)$	20
Aspect ratio	α=a/b	1.0, 1.5, 2.0 and 3.0
Width-thickness ratio parameter	R	0.9
Residual stress	σ_{rc}/σ_y	0.3
Initial plate deflection	δ_{max}/b	1/500
(b) Concrete		
Compressive strength	$f_c(MPa)$	23.5
Elastic modulus	$E_c(GPa)$	24.5
Poisson's ratio	μ	0.18

ratios of the component plates. This may be due to the confined extent of the filled-in concrete. Therefore, it is advisable that the number of the diaphragms should be increased to obtain smaller aspect ratios for the component plates in practical design.

The computed ultimate loads, P_u/P_y, are plotted against the aspect ratios, α, of the component plates in **Fig. 3.10**. The ultimate strength is decreased as the aspect ratio α is increased from 1.0 to 2.0, and then increased slightly as the aspect ratio α is increased from 2.0 to 3.0. Therefore, the lowest ultimate strength is given at about α=2.0.

Very interesting plots obtained from the analysis are three-dimensional deformed geometry plots shown in **Figs. 3.11** to **3.13**. The deformed plots are configurations of the analyzed part (one-eighth of the concrete-filled column) at about $\bar{\varepsilon} = 0.1\%$, 0.2% and 0.3%, showing how the interface between the component plate panel and component concrete deforms during the process of loading. As can be seen form the figures, the component plate panels and component concrete have been separated at the mid-surface, even at $\bar{\varepsilon} = 0.1\%$. This is because Poison's ratio of steel is larger than that of concrete. As the average strain of the column increases, i.e., $\bar{\varepsilon} = 0.2\%$, the plate panels are separated more obviously from the filled-in concrete because of local plate buckling of the steel plates. It is also noted that only one buckling wave forms in both two plate panels for cases where $\alpha = 1.0$ (**Fig. 3.11**) and $\alpha = 2.0$ (**Fig. 3.12**), while

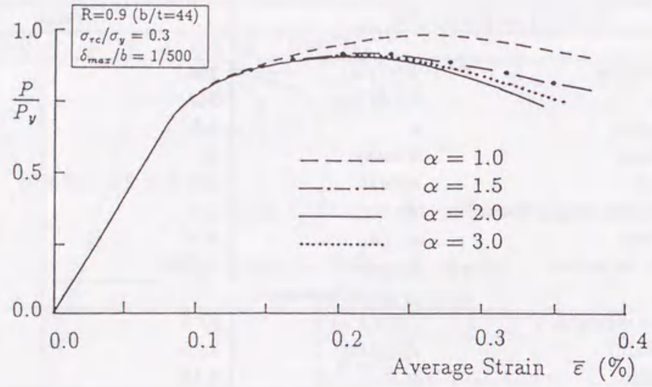

Fig. 3.9 Computed Load-Average Strain Curves: Effect of Aspect Ratio α

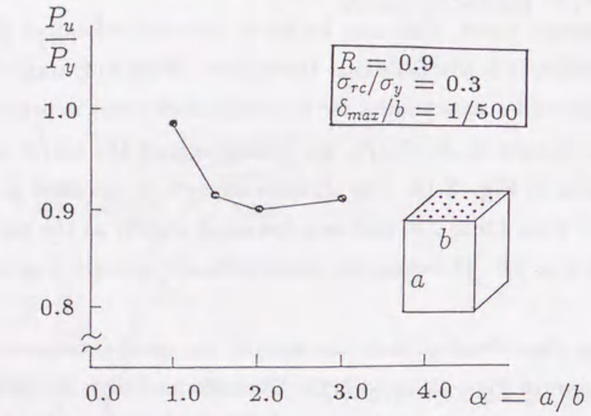

Fig. 3.10 Effect of Plate Aspect Ratio on Ultimate Strength of Concrete-Filled Steel Columns

one buckling wave forms in one of two panels and three buckling waves in another panel where $\alpha = 3.0$ (**Fig. 3.13**). The latter is evident from a prior experimental study.

Case (2): Effects of the Width-thickness Ratio Parameter

For concrete filled rectangular hollow profiles, the limit value of the plate width-thickness ratio proposed in Eurocode 4 (1990) is

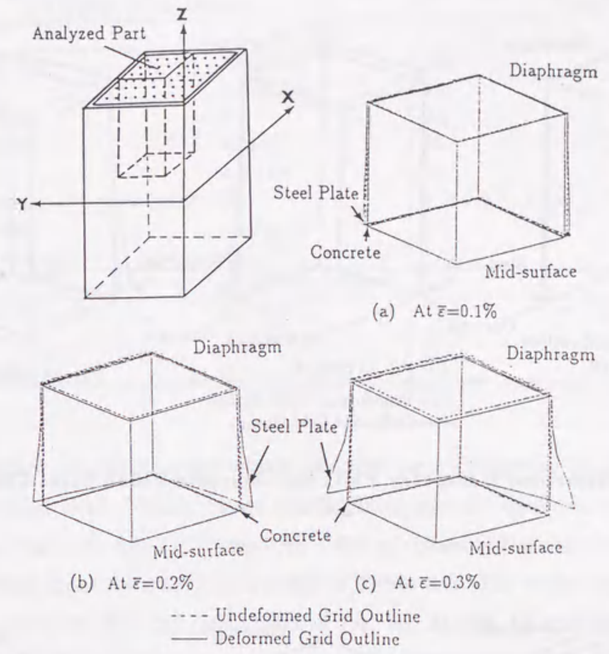

Fig. 3.11 3-D Deformed Geometry Plots for Concrete-Filled Steel Column: α = 1.0

$$\frac{b}{t} \leq 52\epsilon \tag{3.26}$$

Here, the factor ϵ accounts for different yield stresses,

$$\epsilon = \sqrt{\frac{235}{\sigma_y}} \tag{3.27}$$

with σ_y in N/mm^2. For the material used in the present study, σ_y = 314 N/mm^2, and so the limit b/t ratio is 45. That is, the limit value of the width-thickness ratio parameter R is about 0.9. Obviously, this is to ensure the local buckling of thin cross section parts to be prevented. In other words, the attainment of the material strength is assumed for all parts of the section in the ultimate limit state.

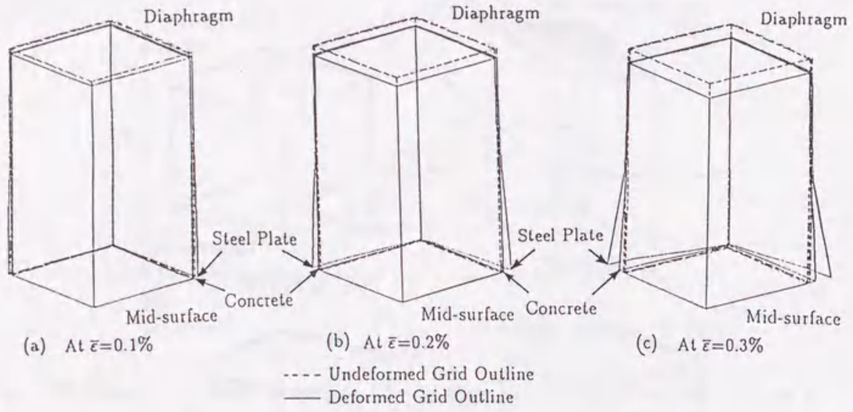

Fig. 3.12 3-D Deformed Geometry Plots for Concrete-Filled Steel Column: $\alpha = 2.0$

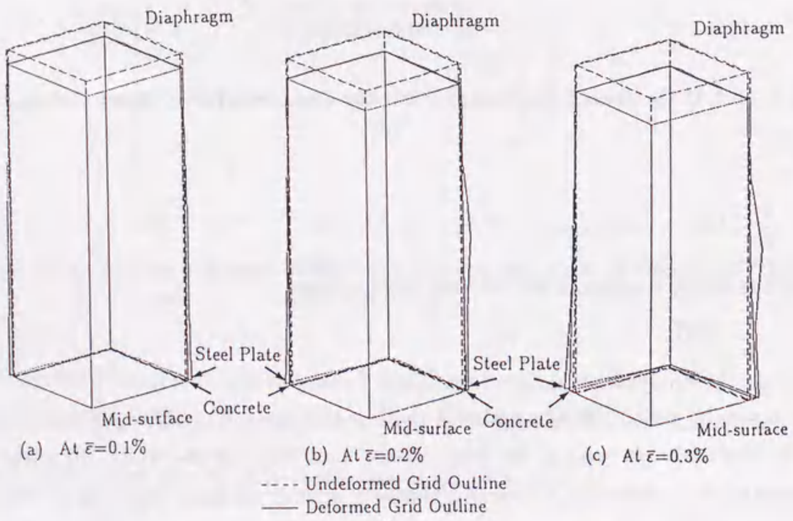

Fig. 3.13 3-D Deformed Geometry Plots for Concrete-Filled Steel Column: $\alpha = 3.0$

Table 3.3 Input Data for Concrete-Filled Stub-Column Analysis in Figure 3.14

Property or Parameter		Value
(a) Steel		
Young's modulus	$E(GPa)$	206
Yield stress	$\sigma_y(MPa)$	314
Poisson's ratio	ν	0.3
Plate thickness	$t(mm)$	20
Aspect ratio	α=a/b	2.0
Width-thickness ratio parameter	R	0.7, 0.9, 1.2 and 1.4
Residual stress	σ_{rc}/σ_y	0.3
Initial plate deflection	δ_{max}/b	1/500
(b) Concrete		
Compressive strength	$f_c(MPa)$	23.5
Elastic modulus	$E_c(GPa)$	24.5
Poisson's ratio	μ	0.18

To investigate the effect of the width-thickness ratio parameter on the strength of the concrete-filled stub-column, elasto-plastic finite element analyses have been conducted on four concrete-filled columns with different values of the width-thickness ratio parameters. The input data are summarized in **Table 3.3**. The width-thickness ratios, b/t, corresponding to R = 0.7, 0.9, 1.2 and 1.4, are 34, 44, 58 and 68, respectively. Obviously, two of them are below or near the limit value given in Eurocode 4 (1990), and two exceed this limit value.

The computed curves for these concrete-filled columns are shown in **Fig. 3.14**, with the computed load, P/P_y, the contribution from the component plates, σ_b/σ_y, as well as the contribution from the component concrete, σ_c/f_c, taken as the ordinate in **Figs. 3.14(a)**, **(b)** and **(c)** respectively, and the average strain as the abscissa. The quantities σ_b and σ_c are obtained as:

$$\sigma_b = \frac{\sum F_{si}}{A_s}, \qquad \sigma_c = \frac{\sum F_{ci}}{A_c} \tag{3.28}$$

in which F_{si} is the reaction force of the steel plate element node at the loaded surface, and F_{ci} is the reaction force of the concrete element node at the loaded surface. The following may be noted from these figures:

(1) The linear behavior in the regime of elasticity in **Fig. 3.14(a)** shows a little deviation among these four concrete-filled columns. In the loading condition adopted

here, both the component plates and component concrete are loaded simultaneously. Therefore, the shortenings of two materials are identical. The relation between the total load and the average strain can be easily derived as follows:

$$P = (E_s A_s + E_c A_c)\bar{\varepsilon} \tag{3.29}$$

Dividing by the squash load P_y in both sides of above equation yields

$$\frac{P}{P_y} = \frac{E_s A_s + E_c A_c}{\sigma_y A_s + f_{ck} A_c}\bar{\varepsilon} \tag{3.30}$$

As can be seen from the above equation, The initial stiffness of the $P/P_y - \bar{\varepsilon}$ curves depends also on the cross sectional areas of two materials, A_s and A_c, as well as the material properties. Since the cross sectional areas of two materials, A_s and A_c are different in these four concrete-filled columns, the linear behavior is thus different.

(2) The ultimate load, P_u/P_y, are almost the same, although the post-peak behavior is different in these concrete-filled columns. The post-peak strength decreases as the width-thickness ratio parameter R increases.

(3) The contribution from the component plates decrease as the the width-thickness ratio parameter R increases. It should be noted that no local bucklings occur in the cases of $R = 0.7$ and 0.9, while local buckling occurs in the cases of $R = 1.2$ and 1.4. This important phenomenon is consistent with the afore-mentioned Eurocode 4 (1990). Moreover, the contribution from the component plates are nearly the same and closer to 1.0 when the width-thickness ratio parameter R is less than 0.9.

(4) The maximum strengths of the component concrete are almost the same. It may be said that the increase in the strength of concrete due to the confinement of steel box could not be expected.

Case (3): Effects of the Initial Geometrical Imperfections

As analyzed previously, the initial plate deflections can be assumed to be in the form as given in **Eqs. (3.2)** and **(3.3)**. The fabrication tolerance specified by Japan Road Association (*JRA 90* 1990) is $b/150$ (b = plate width). On the other hand, the average value of the maximum plate deflections upon the measurement is $b/500$ (Fukomoto 1987). The maximum initial imperfections used in previous analyses were around $b/500$. To investigate the effects of the initial geometrical imperfections, both

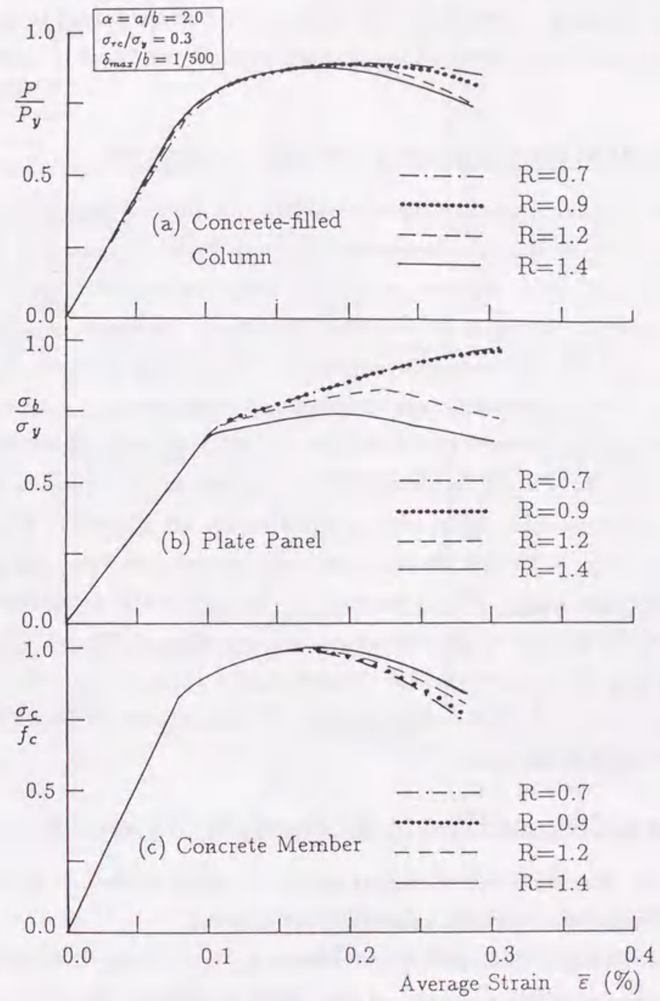

Fig. 3.14 Computed Load-Average Strain Curves: Effect of Width-Thickness Rataio Parameter R

$b/500$ and $b/150$ are assumed to be the maximum plate deflection in the cases of R = 0.9 and R = 1.4. The input data are summarized in **Table 3.4**. The computed load-average strain ($P/P_y - \bar{\varepsilon}$) curves are shown in **Fig. 3.15**. As observed in both the case of $R = 0.9$ [**Fig. 3.15(a)**] and the case of R=1.4 [**Fig. 3.15(b)**], the effects of initial geometrical imperfections on the ultimate strength are found to be relatively small.

Case (4): Effects of the Compressive Strength of Concrete

As the filled-in concrete used in composite columns, the nominal compressive strength of concrete proposed by Hanshin Expressway Highway Public Cooperation (1986) is $23.5MPa$ ($= 240\ kgf/cm^2$) . However, it is to be desired that higher strength concrete is used to increase the capacity of the concrete-filled column. In Eurocode 4 (1990), no limit value is specified for the compressive strength of the filled-in concrete. Therefore, studies on the effects of the compressive strength of concrete seem to be necessary. The compressive strengths used are: $23.5MPa$ ($= 240\ kgf/cm^2$), $29.4MPa$($= 300\ kgf/cm^2$) and $39.2MPa$($= 400\ kgf/cm^2$). The input data are summarized in **Table 3.5**, and the computed load versus average strain curves are plotted in **Fig. 3.16**. It can be seen in **Fig. 3.16** that the initial stiffness becomes less when the compressive strength becomes larger. This is because the ordinate is the nondimensionlized load P/P_y, and the abscissa is the average strain $\bar{\varepsilon}$ [see **Eq. (3.30)** for the relation between P/P_y and $\bar{\varepsilon}$]. Nevertheless, the ultimate loads, P_u/P_y, are not much different. Of course, it should be noted that the ultimate loads P_u are increased when the compressive strength is increased.

3.5 Design of Concrete-Filled Stub-Columns in Compression

Based on the aforementioned numerical studies, a design method is proposed for the strength of short concrete-filled columns in compression.

The ultimate strength of concrete-filled columns, P_u, is supposed to be obtained by a combined method of ultimate strength of steel plates and filled-in concrete as follows:

$$P_u = \sigma_b A_s + \beta f_{cd} A_c \tag{3.31}$$

in which, A_s and A_c are the areas of the steel member and the concrete member, respectively, f_{cd} is the design strength of concrete, β is the empirical reduction strength

Table 3.4 Input Data for Concrete-Filled Stub-Column Analysis in Figure 3.15

Property or Parameter		Value
(a) Steel		
Young's modulus	$E(GPa)$	206
Yield stress	$\sigma_y(MPa)$	314
Poisson's ratio	ν	0.3
Plate thickness	$t(mm)$	20
Aspect ratio	α=a/b	1.0
Width-thickness ratio parameter	R	0.9 and 1.4
Residual stress	σ_{rc}/σ_y	0.3
Initial plate deflection	δ_{max}/b	1/500 and 1/150
(b) Concrete		
Compressive strength	$f_c(MPa)$	23.5
Elastic modulus	$E_c(GPa)$	24.5
Poisson's ratio	μ	0.18

Table 3.5 Input Data for Concrete-Filled Stub-Column Analysis in Figure 3.16

Property or Parameter		Value
(a) Steel		
Young's modulus	$E(GPa)$	206
Yield stress	$\sigma_y(MPa)$	314
Poisson's ratio	ν	0.3
Plate thickness	$t(mm)$	20
Aspect ratio	α=a/b	1.0
Width-thickness ratio parameter	R	0.9
Residual stress	σ_{rc}/σ_y	0.3
Initial plate deflection	δ_{max}/b	1/500
(b) Concrete		
Compressive strength	$f_c(MPa)$	23.5, 29.4 and 39.2
Elastic modulus	$E_c(GPa)$	24.5, 27.4 and 31.4
Poisson's ratio	μ	0.18

with the value of 0.7 and σ_b is the local buckling strength of steel plates. To predict the local buckling strength of the steel plates, the following formula is proposed on the basis of previous parametric analysis:

$$\frac{\sigma_b}{\sigma_y} = \frac{1.2}{R} - \frac{0.3}{R^2} \leq 1.0 \tag{3.32}$$

where, R is the width-thickness ratio parameter [**Eq. (2.1)**] with $k = 4.0$. This equation is plotted in **Fig. 3.17** together with the computed strengths of the plate

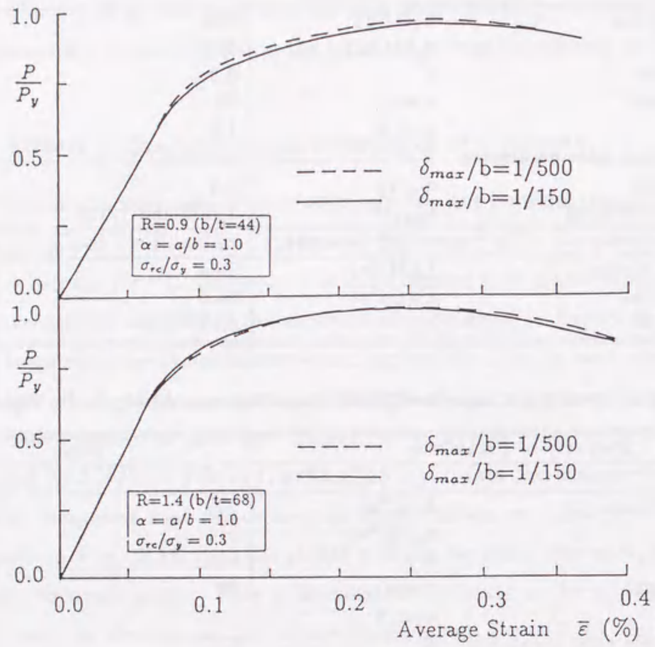

Fig. 3.15 Computed Load-Average Strain Curves: Effect of Initial Plate Deflection

panel in the concrete-filled columns analyzed previously. In **Fig. 3.17**, the empirical formula (Usami 1989), for the strength of compressed plates with simply supports, is also plotted. The design method proposed in Eurocode 4 (1990) is available only for those concrete-filled columns with small plate width-thickness ratio parameters so that no local plate buckling would occur. The proposed above equation, however, can be used to account for the effect of the plate local buckling. It is noted that the proposed equation is identical to the Eurocode 4 (1990) when the width-thickness ratio is within the limit specified in the code.

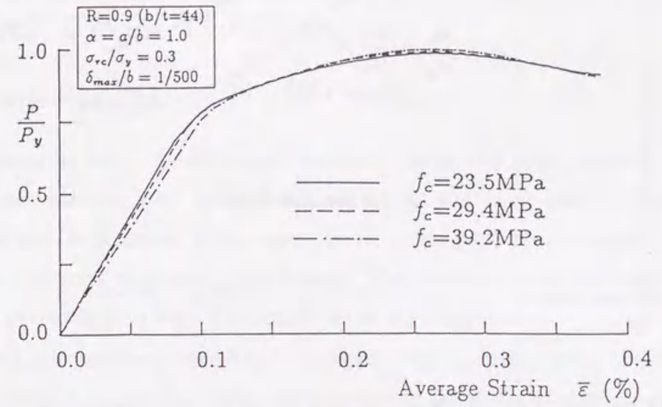

Fig. 3.16 Computed Load-Average Strain Curves: Effect of Concrete Compressive Strength

3.6 Summary

From the analysis on concrete-filled thin-walled stub-columns of box shape, the following important conclusions may be drawn.

(1) An elasto-plastic model of concrete is observed to satisfactorily predict for the stress-strain characteristic of concrete subjected to uniaxial and biaxial compressive loading.

(2) The ultimate strengths of concrete-filled columns obtained from the analysis generally agree well with the experimental results.

(3) An empirical reduction factor proposed in chapter 2, $\beta = 0.7$, for the cylindrical compressive strength of concrete, is found to be adequate for the ordinary filled-in concrete; $\beta = 0.85$ may be more rational for the high-performance filled-in concrete.

(4) The lowest ultimate strength of concrete-filled columns is obtained when the plate aspect ratio, α, is about 2.0.

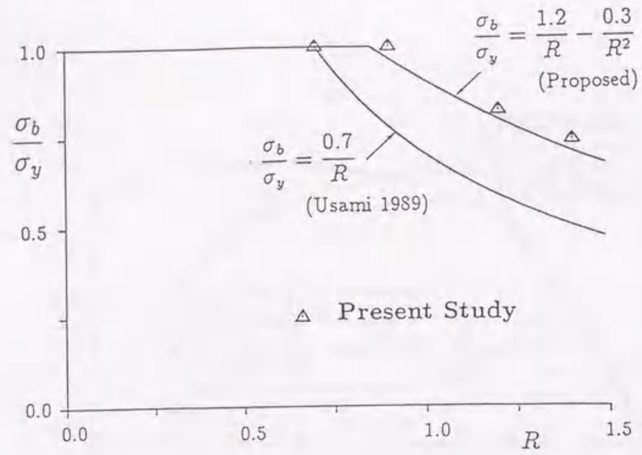

Fig. 3.17 Proposed Design Formula for Local Buckling Strength of Plate Member in Concrete-Filled Steel Box Columns

(5) Local plate buckling would occur when the width-thickness ratio parameter, R, is larger than about 0.9.

(6) The effects of initial geometrical imperfections of plate panels on the ultimate strength are relatively small.

(7) The nondimensionalized ultimate loads, P_u/P_y, are not sensitive to the concrete strength, though the ultimate strengths, P_u, of concrete-filled columns are increased when the concrete strength is increased.

(8) Design formulas [**Eqs. (3.31) and (3.32)**] are proposed to account for the effects of local plate buckling on the strength of concrete-filled columns.

4 DUCTILITY AND ENERGY-ABSORPTION CAPACITY OF PARTIALLY CONCRETE-FILLED STEEL BOX COLUMNS UNDER CYCLIC LOADING

4.1 General Remarks

Use of steel in bridge piers is now becoming more and more popular, especially in urban areas, because steel bridge piers are lighter and their construction period is shorter than that fo concrete bridge piers. Steel bridge piers are normally constructed as cantilever columns or planar rigid frames. The common cross sectional shapes of steel bridge piers are thin-walled box sections or pipe sections.

In general, structures or structural members such as bridge piers are designed to develop a certain amount of inelastic deformation in the event of a severe earthquake. However, they must be able to withstand the strong earthquakes without collapse. In designing a structure, therefore, ductility is one of the most important considerations. In Chapter 2, it has been shown that the use of steel sections with filled-in concrete has led to the improvement of the ductile behavior of compression members. In practical designs, thin-walled steel bridge piers are partially filled with the concrete in many cases, since it is important to reduce the dead weight of the structure for designing the foundations. Experimental work on the inelastic cyclic behavior of steel bridge piers has been conducted in recent years [e.g., Fukumoto and Kusama (1985), Watanabe et al. (1988, 1989, 1990) and Usami et al. (1991, 1992a, 1992b)]. However, very few experimental studies on the inelastic behavior of partial concrete-filled steel bridge piers under cyclic loading are available (Kawashima et al. 1992; Usami et al. 1992a, 1992b). Thus, further experimental investigations on the behavior of such columns under severe earthquakes are necessary in order to develop a reliable earthquake-resistant design method for partial concrete-filled steel piers with thin-walled box sections.

The present study is initiated with a purpose of developing a thin-walled steel bridge pier possessing higher ductility than normally designed one. For this purpose, four steel box column specimens and seven partial concrete-filled steel box columns were tested under constant compressive axial load and cyclic lateral loads. The test results are discussed in the light of improvement of ductility and energy-absorption capacity of steel bridge piers.

4.2 Outline of Experiment

4.2.1 Experimental Program and Test Specimen

In examining earthquake-resistant capability of steel bridge piers, the following parameters must be considered (Usami et al. 1992b): (1) cross-sectional shape, (2) steel grade, (3) structural configuration, (4) welding method of the flange-web connection, (5) width-thickness ratio, (6) slenderness ratio, (7) stiffener rigidity, (8) axial load, (9) lateral load history, and so on. Those parameters are also the main parameters considered in practical designs (Nakai et al. 1982).

In this study, a total of eleven unstiffened and stiffened box columns made of SS400 steel (nominal yield stress σ_y = 235 MPa) are designed as cantilever-type columns simulating fixed conditions in the footings and free at the top as in a common practice for designing bridges piers. A schematic illustration of test specimens is shown in **Fig. 4.1** and ranges of various parameters of the test specimens are listed in **Table 4.1**. Specimen designations starting with a UU refer to unstiffened columns (depth-to-breadth ratio $d/b = 3/4$), and those starting with a SS refer to stiffened columns ($d/b = 2/3$). The notation used in **Table 4.1** is as follows:

$$R_f = \frac{b}{t}\sqrt{\frac{12(1-\nu^2)}{\pi^2 k}}\sqrt{\frac{\sigma_y}{E}} \tag{4.1}$$

$$\overline{\lambda} = \frac{Kh}{r}\frac{1}{\pi}\sqrt{\frac{\sigma_y}{E}} \tag{4.2}$$

in which R_f = width-thickness ratio parameter of the flange plate; $\overline{\lambda}$ = slenderness ratio parameter of the column; b = flange width; t = plate thickness; σ_y = yield stress; E = Young's modulus; ν = Poisson's ratio; k = buckling coefficient of a plate [i.e., k=4.0 for a simply supported plate without stiffener and 36.0 for a simply supported plate with two longitudinal stiffeners]; h = column height (distance between the lowest diaphragm to the point of the application of horizontal load, see **Fig. 4.1**); K = effective length factor (K = 2.0 for a fixed-free column); r = radius of gyration of steel section; γ_l = relative flexural rigidity of one stiffener; and γ_l^* = optimum value of γ_l obtained from linear buckling theory ("DIN 4114" 1953).

The column specimens were designed in accordance with the JRA 80 specification ("JRA 80" 1980), in which plate buckling of compression flange plates is prevented by

Table 4.1 Parameters of Test Specimens

Specimen	R_f	$\overline{\lambda}$	$\frac{l_c}{h}$	N	$\frac{P}{P_y}$	γ_l/γ_l^*
UU0	0.70	0.40	—	3	0	—
UU1	0.70	0.40	—	3	0.2	—
UU2	0.70	0.40	0.3	3	0.2	—
UU3	0.70	0.40	0.5	3	0.2	—
UU4	0.70	0.40	0.5	5	0.2	—
UU5	0.70	0.60	0.3	3	0.2	—
UU6	0.90	0.40	—	3	0.2	—
UU7	0.90	0.40	0.3	3	0.2	—
SS1	0.45	0.50	—	3	0.2	3.0
SS8	0.45	0.50	0.3	3	0.2	1.0
SS9	0.45	0.50	0.5	3	0.2	1.0

Notes: R_f = Width-Thickness Ratio Parameter of Flange Plate [**Eq. (4.1)**];
$\overline{\lambda}$ = Slenderness Ratio Parameter of Column [**Eq. (4.2)**];
h = Column Height; l_c = Length of Filled Concrete;
N = Number of Loading Cycles; P = Applied Axial Load;
P_y = Squash Load of Steel Section.

limiting the width-thickness ratio as $R_f \leq 0.7$ for a simply supported plate and 0.5 for a simply supported plate with longitudinal stiffeners. This specification is similar to the Canadian CSA S6 M89 84a specification, the American AASHTO 89 specification and the Belgium NBN B51002 88 specification (Beedle 1991). The main selected parameters were the flange plate width-thickness ratio (R_f), column slenderness ratio ($\overline{\lambda}$), and length of filled concrete (l_c). The values of R_f and $\overline{\lambda}$ were determined to be in the range of practical designs (Nakai et al. 1982). In the case of the unstiffened column, the width-thickness ratio parameter, R_f, was taken to be 0.7 or 0.9, and the slenderness ratio parameter, $\overline{\lambda}$, was taken to be 0.4 except for one specimen UU5 ($\overline{\lambda}$ = 0.6). In the case of the stiffened column, the width-thickness ratio parameter and slenderness ratio parameter were kept constant (i.e., $R_f = 0.45$, $\overline{\lambda} = 0.5$). In areas without strong-motion earthquakes, the width-thickness ratios of plates may be beyond this range. However, past earthquake performance of steel bridges indicates that steel columns with extra-large plate width-thickness ratios are susceptible to damage from earthquakes, and modern earthquake resistant design requires that columns be designed to provide sufficient energy absorption capacity. Therefore, it is necessary to choose

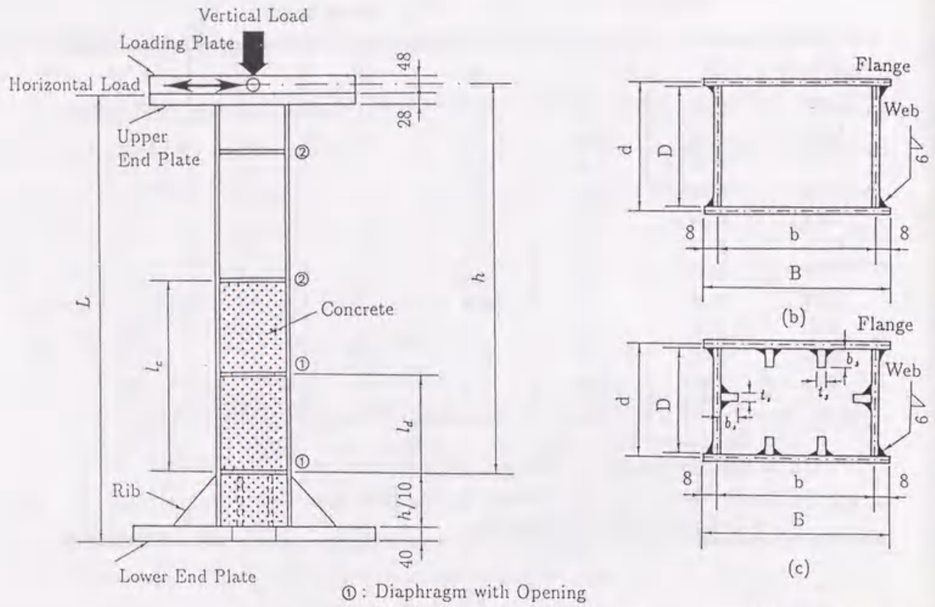

Fig. 4.1 Test Specimens

the plate width-thickness ratio within a moderate range when planning a earthquake resistant design of steel bridge piers. The length of filled concrete, l_c, was taken to be 0.3 or 0.5 times of the column height. Concrete was poured from the lower end plate up to the specified length where a diaphragm without opening was equipped. For this purpose, an opening was made on the lower end plate as well as on some of the intermediate diaphragms, as shown in **Fig. 4.1**. Because concrete is located between the diaphragm and lower end plate, concrete is supposed to be in a fully confined state. The parameter N in **Table 4.1** is the number of cycles of loading at each displacement level (see **Fig. 4.3**). At the top of the test specimen, an end plate of 28 mm in thickness (i.e., upper end plate in **Fig. 4.1**) was welded to bolt the loading plate, and at the base an end plate of 40 mm in thickness (i.e., lower end plate in **Fig. 4.1**) was also welded for anchoring the test specimen to the column base (see **Fig. 4.2**). A 6

Table 4.2 Measured Dimensions of Unstiffened Specimens

Specimen	B (mm)	D (mm)	t (mm)	L (mm)	h (mm)	l_d (mm)	l_c (mm)	$\overline{\lambda}$	R_f	R_w
UU0	170	110	4.51	854	762	306	—	0.362	0.664	0.430
UU1	169	111	4.51	854	762	306	—	0.362	0.664	0.430
UU2	170	111	4.51	854	762	229	229	0.362	0.664	0.430
UU3	170	111	4.51	854	762	381	381	0.362	0.664	0.430
UU4	170	111	4.51	854	762	381	381	0.362	0.664	0.430
UU5	170	110	4.51	1354	1216	365	365	0.577	0.664	0.430
UU6	214	145	4.51	1154	1035	394	—	0.381	0.854	0.575
UU7	214	145	4.51	1154	1035	311	311	0.381	0.854	0.575

Notes: B = Width of Flange Plates; D = Width of Web Plates;
L = Total Length of Specimen; R_w = Width-Thickness Ratio Parameters.

Table 4.3 Measured Dimensions of Stiffened Specimens

Specimen	B (mm)	D (mm)	b_s (mm)	t_s (mm)	γ_l/γ_l^*	l_c (mm)	$\overline{\lambda}$	R_f	R_w
SS1	312	193	44.0	4.36	3.23	—	0.490	0.430	0.427
SS8	311	192	44.0	4.36	1.16	501	0.490	0.429	0.424
SS9	311	192	38.0	4.39	0.98	836	0.487	0.430	0.424

Notes: t = Plate Thickness = 4.51 mm; L = Total Length of Specimen = 1854 mm;
h = Column Height = 1671 mm.

mm fillet weld was used for the flange-web junctions throughout. The applied axial load was 20% of the squash load, P_y, of test specimens (excluding concrete) except for one specimen (UU0, $P/P_y = 0.0$). **Tables 4.2** and **4.3** list the measured dimensions of the unstiffened specimens and stiffened specimens, respectively.

4.2.2 Test Setup

Fig. 4.2 shows the test setup. A detailed description and schematic view of the test setup are shown elsewhere (Usami et al. 1992b). The lower end plate of a test specimen was bolted to the column base, which was anchored to the test floor. The horizontal lateral load and the vertical axial compressive load were applied by an MTS servo controlled hydraulic actuator (capacity = 343 KN, maximum stroke = ± 125mm) and a hydraulic jack (capacity 686 KN), respectively. The horizontal load was applied

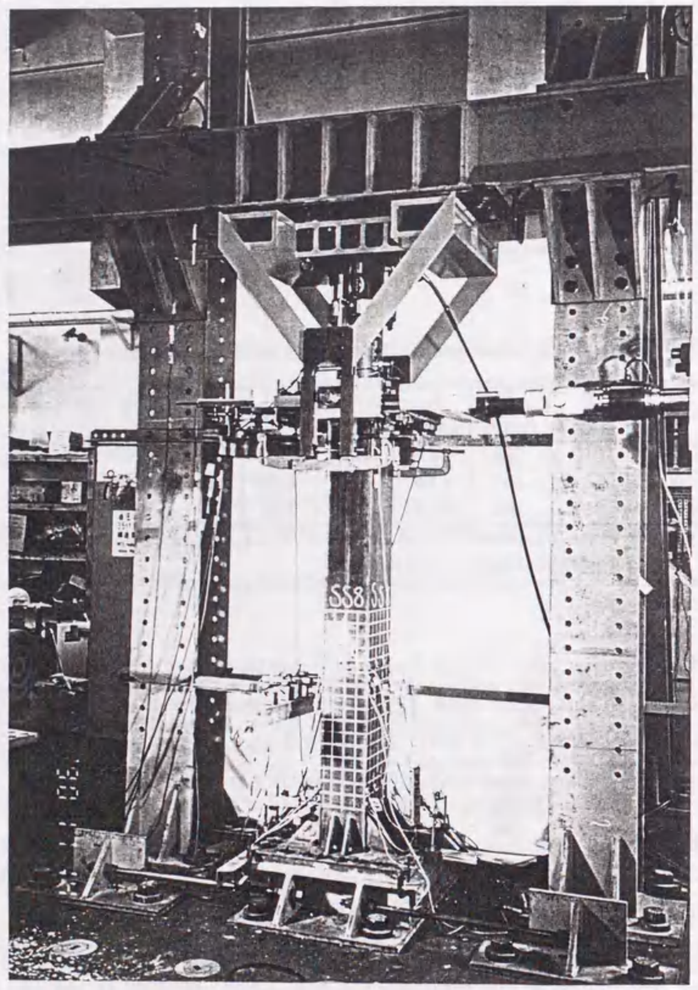

Fig. 4.2 Test Setup

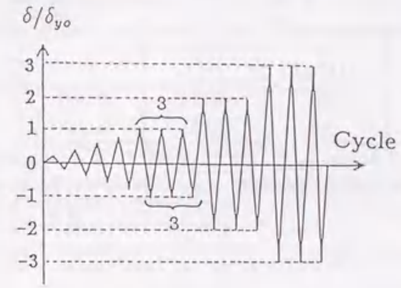

Fig. 4.3 Displacement History

to the centroid of the test specimen through a pair of steel bars which are fixed to the loading plate, so that up and down movement of the horizontal actuator is minimized. The vertical jack is installed inside the triangle frame which is suspended from two linear guides through four flat bearings. As the top of the test specimen displaces laterally, the triangle frame moves horizontally along the guide boards so that the jack always exerts a vertical load to the test specimen.

Horizontal displacements of a test specimen were measured with displacement transducers located at the top of the test specimen, the lowest diaphragm and other places. Vertical column displacements were also monitored by measuring the movement of the head of the vertical hydraulic jack.

4.2.3 Load Sequence

Each specimen excluding one specimen (UU0) was subjected to a prescribed horizontal displacement history under a constant axial load $P/P_y = 0.2$. The horizontal displacement history consists of sequences of fully reversed displacement cycles as shown in **Fig. 4.3**, namely, the peak displacements were increased stepwise after three successive cycles at each displacement level. For specimen UU4, the number of loading cycles, N, was taken to be 5 in order to examine its influence on the seismic response of the column. The notation used in **Fig. 4.3** is as follows:

$$H_{yo} = \frac{M_y}{h} \tag{4.3}$$

Table 4.4 Material Properties of Steel

Series	E (GPa)	σ_y (MPa)	ε_y (%)	ν	E_{st} (GPa)	ε_{st} (%)
Panel	197	266	0.134	0.269	9.40	1.53
Stiffener	198	298	0.151	0.258	8.47	2.33

Notes: E = Young's Modulus; σ_y = Yield Stress; ε_y = Yield Strain; ν = Poisson's Ratio; E_{st} = Strain-hardening Modulus; ε_{st} = Strain at Onset of Strain-hardening.

Table 4.5 Material Properties of Concrete

Days	E_c (GPa)	μ_c	f_c (MPa)	Test Column
46	28.2	0.157	39.8	SS8
48	28.3	0.157	40.0	SS9
59	28.7	0.157	40.8	UU5
61	28.8	0.157	41.0	UU7
75	29.3	0.157	42.1	UU2
77	29.4	0.157	42.2	UU3
80	29.5	0.157	42.5	UU4

Notes: E_c = Young's Modulus; μ_c =Poisson's Ratio;
f_c = Uniaxial Compressive Cylinder (10 cm diameter × 20 cm height) Strength.

$$\delta_{yo} = \frac{H_{yo}h^3}{3EI} \tag{4.4}$$

in which M_y = yield moment of steel section; and I = moment of inertia of steel section.

4.3 Experimental Results and Discussions

4.3.1 Material Properties

The steel used was mild steel of grade SS400 (nominal yield stress σ_y = 235 MPa), and the nominal thickness of each test specimen was 4.5 mm. The material properties are shown in **Table 4.4**, which were determined from the tension tests on three coupons in each series.

The concrete used had a water/cement ratio of 55.2% (by weight). The mechanical properties of concrete were determined from the compression tests on three cylinders (100 mm in diameter and 200 mm in length) in each series. Concrete cylinder tests

were carried out on the same day as column tests. The measured average values of concrete are given in **Table 4.5**.

4.3.2 Collapse Modes

For the test specimens without concrete infill in either the unstiffened case or the stiffened case, local plate buckling was first observed in the flange plates of the column base immediately after the peak horizontal load, and then extended to the web plates. Once local buckling occurred, the plates were not fully straighten out during reversed loading, buckling deformations progressively grew, and eventually the specimen lost its lateral resistance after either vertical cracking in the weld material of flange-web junctions or fracture in the plate material became considerable. In those test specimens, local buckling deformations were localized only in their base panels. Cracking or fracture appeared when the horizontal displacement was around two to three times of the displacement, δ_m, at the maximum horizontal load.

For the test specimens partially filled with concrete, in the case of l_c = 0.3h, slight local buckling deformations were first observed in the column base flange plate and then in the panel just above a diaphragm below which concrete was filled in. After that, the buckling waves progressively grew and most of the lateral deformation took place in the part where no concrete was filled in as depicted in **Fig. 4.4**(a). However, local buckling of test specimen UU5 occurred in its base panels only. It should be noted that the specimen UU5 had a larger slenderness ratio ($\overline{\lambda}$ = 0.6) than UU2 ($\overline{\lambda}$ = 0.4). On the other hand, in the case of l_c=0.5h, local buckling occurred in its base panel only [see **Fig. 4.4**(b)]. Once the flange plates were removed after failure by gas-cutting, it was observed that concrete behind the portions of plates that buckled was seriously crushed, while no damage was observed in the other parts. Shown in **Fig. 4.5** are typical failure appearances of filled-in concrete after taking the cracked concrete out of tested columns.

4.3.3 Horizontal Load versus Horizontal Displacement Hysteretic Curves

Since measured horizontal displacements of a test specimen are supposed to include rigid-body rotation of its base, the following correction is made for measured horizontal displacements:

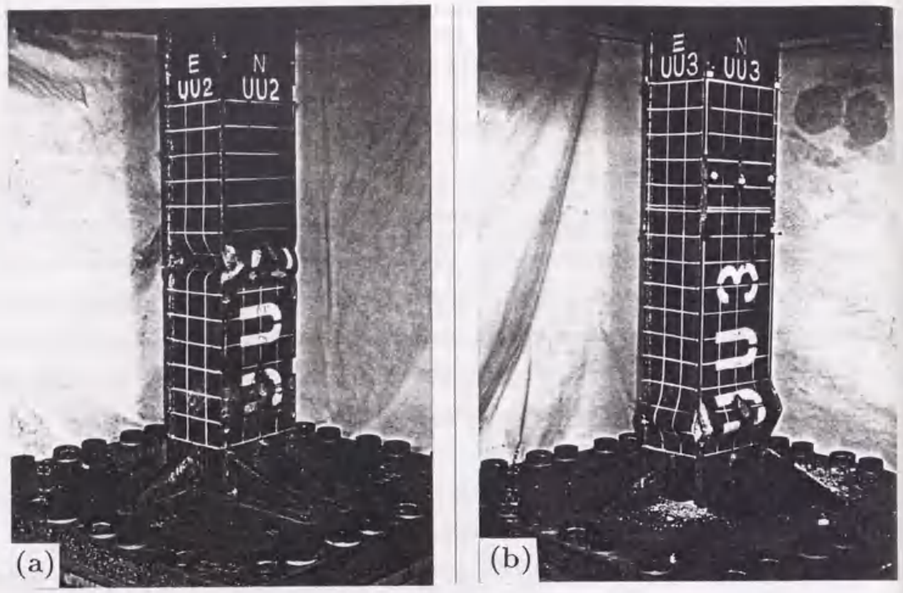

Fig. 4.4 Concrete-Filled Test Specimens after Failure: (a) UU2; (b) UU3

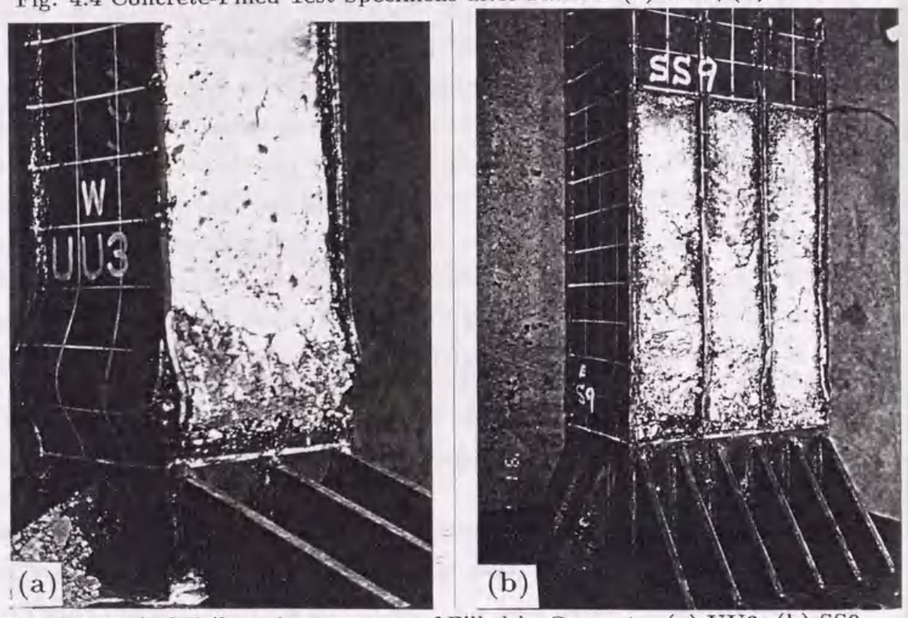

Fig. 4.5 Typical Failure Appearances of Filled-in Concrete: (a) UU3; (b) SS9

$$\delta = \delta_T - (h + \frac{h}{10}) \tan\theta \tag{4.5}$$

where δ = corrected horizontal displacement (mm); δ_T = horizontal displacement measured at the top of column; $\tan\theta = \delta_B/(h/10)$; and δ_B = horizontal displacement measured at location of the lowest diaphragm. Note that $(h + h/10)$ is the height of a test specimen from the surface of the base end plate (see **Fig. 4.1**) and that θ is an approximate expression for rigid-body rotation of the column base. Thus, the second term of right-hand side of **Eq. (4.5)** is an approximate expression for the rigid-body displacement at the top of column. This treatment is rather crude, however, as shown later (**Fig. 4.7**), the initial load-displacement curves are in good agreement with the theoretical ones in most of the test specimens.

Nondimensionalized horizontal load versus horizontal displacement hysteretic curves for some of test specimens are shown in **Fig. 4.6**. The load and the displacement are respectively nondimensionalized by H_{yo} and δ_{yo}. The test of SS9 specimen was terminated before its lateral resistance decreased considerably because of the limitation of stroke of the horizontal jack ($\pm$ 125 mm). Shown in **Fig. 4.7** are envelope curves of the horizontal load-displacement hysteretic curves. From the figures the following important facts are observed:

(1) Comparison between UU0 ($P/P_y = 0.0$) and UU1 ($P/P_y = 0.2$) shows that strength degradation after the peak loads is much affected by the compressive axial load, though the difference of the maximum lateral strengths is not too much [see **Fig. 4.7(a)**].

(2) Comparison among UU1 (without concrete infill), UU2 ($l_c = 0.3h$), and UU3 ($l_c = 0.5h$) shows that the strength and ductility capacity are obviously improved by the filled-in concrete. Especially, the ductility behavior in test specimen UU3 is much more stable because only slight local buckling occurred in the column base panels until the lateral deformation, δ/δ_{yo}, is about 10. After that, however, local buckling deformation was gradually increased due to cracking in the filled-in concrete, and finally cracks in the weld were observed. On the other hand, the test specimen UU2 shows a moderate ductility; but the post-peak strength is decreased owing to large local buckling deformation in the panels above the concrete-filled part [see **Fig. 4.7(b)**].

(3) Comparing UU3 ($N = 3$) and UU4 ($N = 5$), the column behavior is almost the same when the loading cycles are $N = 3$ and $N = 5$ [see **Fig. 4.7(b)**].

(4) Comparing steel columns UU1 ($R_f = 0.7$) and UU6 ($R_f = 0.9$), both of the maxi-

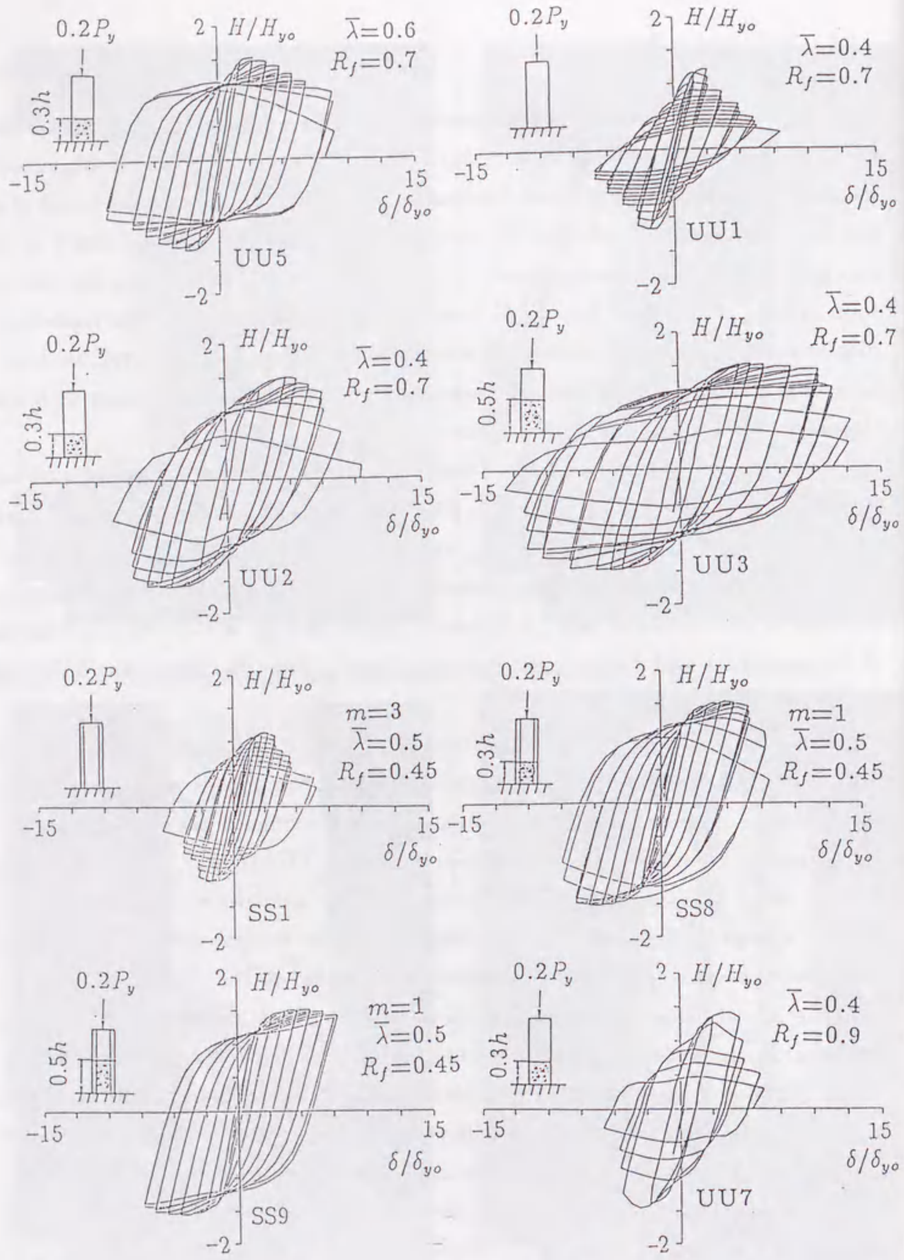

Fig. 4.6 Horizontal Load-Horizontal Displacement Hysteretic Curves

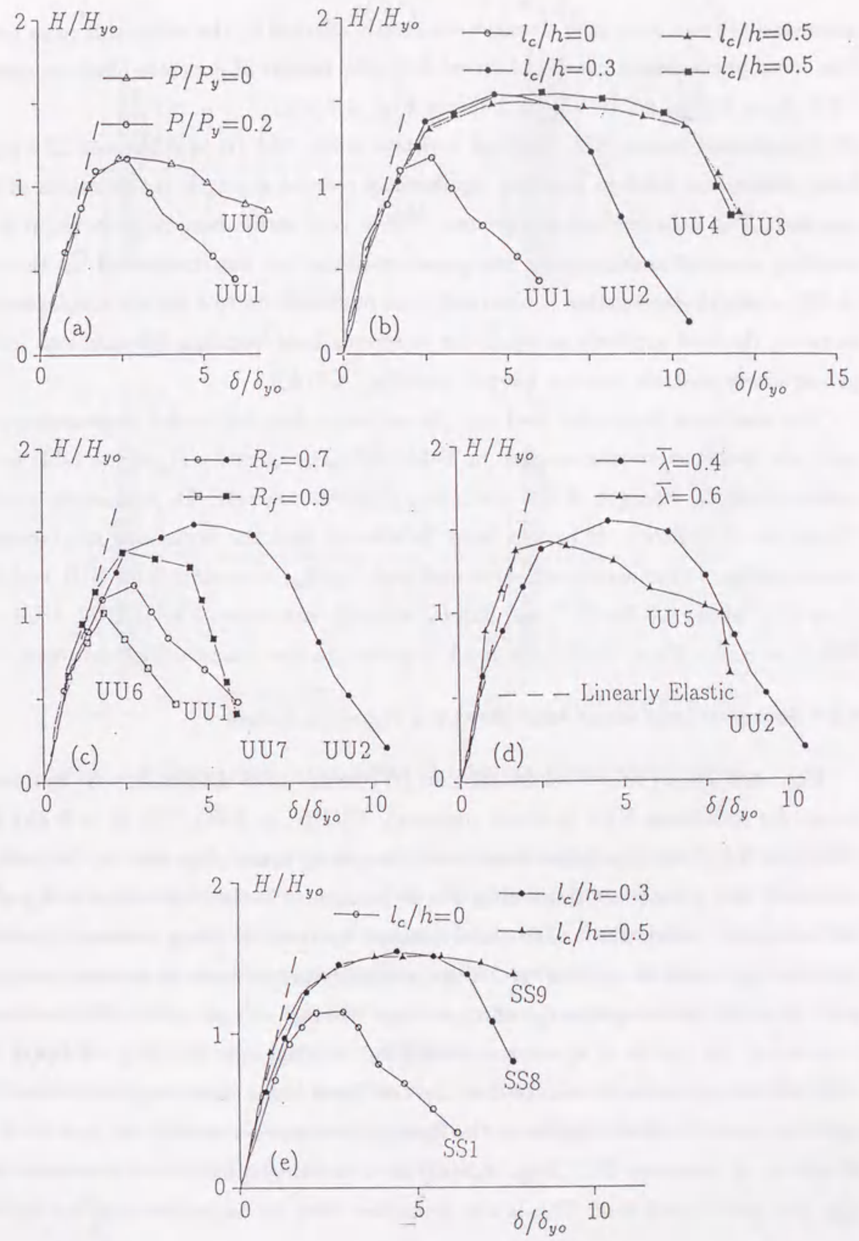

Fig. 4.7 Envelope of Horizontal Load-Horizontal Displacement Curves

mum strength and post-peak strength are greatly affected by the width-thickness ratio. The same phenomenon can be observed from the results of concrete-filled specimens UU2 ($R_f = 0.7$) and UU7 ($R_f = 0.9$) [see **Fig. 4.7(c)**].

(5) Comparison among SS1 (without concrete infill), SS8 ($l_c = 0.3h$) and SS9 ($l_c = 0.5h$) shows that filled-in concrete significantly reduces strength deterioration of the member. The behavior of test specimen SS9 is very stable because only slight local buckling occurred in the column base panels until the test was terminated. In the case of SS8, strength degradation is observed to be moderate up to a certain displacement; however, the load suddenly dropped due to serious local buckling deformations in the panels where concrete was not filled-in [see **Fig. 4.7(d)**].

The maximum horizontal load and the corresponding horizontal displacement for each test specimen are summarized in **Table 4.6**. The quantity H_y in the table is the predicted lateral strength of test specimens (without concrete) for monotonic loading (Usami et al. 1992b). It is seen from **Table 4.6** that the horizontal displacement corresponding to the maximum horizontal load, δ_m/δ_{yo}, is about 2.5 for UU1 and SS1 ($l_c = 0.0$), about 4.8 for UU2 and SS8 ($l_c = 0.3h$), and about 5.4 for UU3, UU4 and SS9 ($l_c = 0.5h$). Thus, ductility is much improved in the concrete-filled columns.

4.3.4 Horizontal Load versus Axial Shortening Hysteretic Curves

Fig. 4.8(a)-(d) shows horizontal load (H) versus axial shortening (Δ) hysteretic curves for specimens UU1 (without concrete), UU2 ($l_c = 0.3$h), SS8 ($l_c = 0.3$h) and SS9 ($l_c = 0.5$h). At the initial stage axial shortening takes place due to the vertical load only and subsequent shortening due to horizontal loads. Axial shortening after the maximum horizontal load is mainly caused by local buckling, material yielding, local damage (such as cracking) etc. Thus, the magnitude of axial shortening may be a good index for assessing damage of a member (Watanabe et al. 1989). This is clearly observed in the results of specimens UU2 [**Fig. 4.8(b)**] and SS8 [**Fig. 4.8(c)**]; the axial shortening suddenly increased at the last three loops when local plate buckling deformations became noticeable on the flange plates where concrete was not filled in. Moreover, in specimen UU1 [**Fig. 4.8(a)**] local buckling is found to be initiated just after the peak lateral load. This is also coincident with the experimental observations.

4.3.5 Ductility Factor and Energy Absorption Capacity

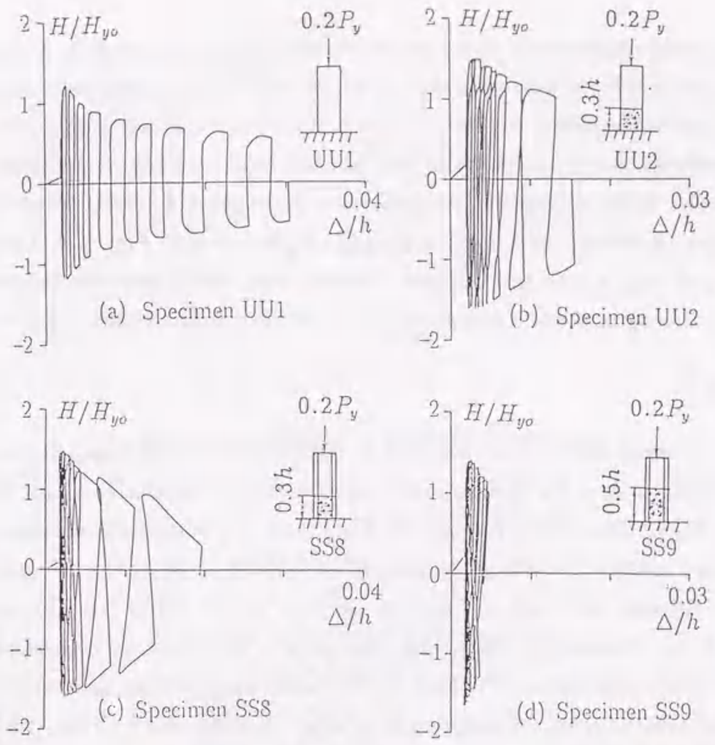

Fig. 4.8 Horizontal Load-Axial Shortening Hysteretic Curves

Ductility and energy-absorption capacity are important considerations in aseismic design. The design strength of a structure can be substantially reduced if the structure is able to provide a good deformation capacity beyond the elastic limit. Furthermore, energy dissipation through hysteretic damping can reduce the amplitude of seismic response thereby reducing the ductility demand on the structure. These quantities are now defined and evaluated for the test specimens.

There are many ways to define ductility of a structure. One way is to define ductility as the ratio of the displacement corresponding to the maximum lateral load, δ_m, to the displacement at which first yield or local buckling occurs:

$$\mu_m = \frac{\delta_m}{\delta_y} \tag{4.6}$$

where δ_y = the horizontal displacement corresponding to first yield or local buckling

(i.e., horizontal displacement at the top of column corresponding to H_y). Although this definition of ductility is physically clear, the load-deflection characteristics are not fully incorporated in the index. Another definition of ductility is to introduce an equivalent elastic-perfectly plastic model taking into account local buckling effect (Usami et. al. 1991, 1992b). In the concept of the model, the collapse point of a member is defined as a point where the lateral resistance is reduced to H_y as shown in **Fig. 4.9**. The collapse thus defined may not be real collapse of a specimen, but is intended to represent a particular damage state of a specimen. Then, ductility in this model is defined by

$$\mu = \frac{\delta_u}{\delta_y} \tag{4.7}$$

where δ_u = lateral displacement obtained by replacing the experimental hysteretic loop corresponding to $H = H_y$ by means of an equivalent elastic-perfectly plastic hysteretic loop (see **Figs. 10** and **11**). As shown in **Fig. 4.10** , experimentally obtained energy-absorption capacity of one loop A_u (area of the shaded zone) at the collapse point is generally different from that of the elastic-perfectly plastic model (i.e., A_0) because of local buckling, Bauschinger effect, and other effects. Therefore, an equivalent elastic-perfectly plastic hysteretic curve that has the same energy-absorption capacity A_u as the actual hysteretic loop is introduced as shown in **Fig. 4.11**. Then, the relation between A_u and the "equivalent" displacement δ_u is given by

$$A_u = 4H_y(\delta_u - \delta_y) \tag{4.8}$$

and A_0 is of the form:

$$A_0 = 4H_y(\delta' - \delta_y) \tag{4.9}$$

so that

$$\mu = \frac{\delta_u}{\delta_y} = \frac{A_u}{A_0}\left(\frac{\delta'}{\delta_y} - 1\right) + 1 = \frac{A_u}{A_0}\left(\frac{\frac{\delta'}{\delta_{yo}}}{\frac{\delta_y}{\delta_{yo}}} - 1\right) + 1 \tag{4.10}$$

in which $\delta_y/\delta_{yo} = H_y/H_{yo}$. The values of δ'/δ_{yo} and A_u/A_0 are listed in **Table 4.6**, together with the calculated values of two ductility factors μ_m and μ.

It has been pointed out (Ohno et al. 1984) that the inelastic performance of a structure is highly sensitive to the displacement history, and that the ductility index thus defined may be different if the structure is subject to a different displacement

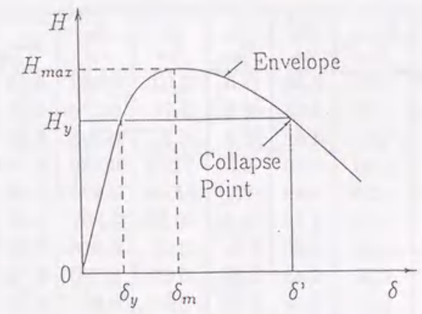

Fig. 4.9 Definition of Collapse Point

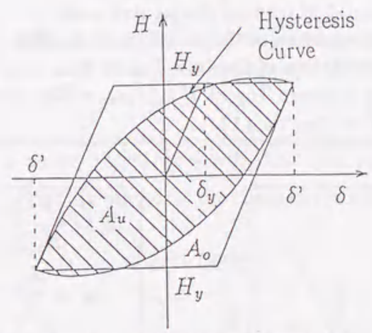

Fig. 4.10 Comparison of Energy-Absorption Capacity

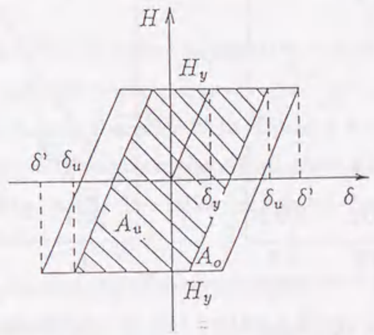

Fig. 4.11 Replacement of Energy-Absorption Capacity by Elastic-Perfectly Plastic Hysterestic Curve

Table 4.6 Ductility and Energy-Absorption Capacity

Specimen	H_{yo} (kN)	δ_{yo} (mm)	$\frac{H_{max}}{H_{yo}}$	$\frac{\delta_m}{\delta_{yo}}$	$\frac{H_y}{H_{yo}}$	$\frac{\delta'}{\delta_{yo}}$	$\frac{A_u}{A_o}$	μ_m	μ	$\hat{E}$
UU0	35.7	4.33	1.18	2.56	1.0	5.23	0.633	2.58	3.68	111
UU1	35.7	4.33	1.17	2.69	0.8	3.78	0.720	3.36	3.68	77
UU2	35.7	4.33	1.54	4.62	0.8	8.37	0.903	5.78	9.54	536
UU3	35.7	4.33	1.50	5.39	0.8	12.02	0.820	6.74	12.50	1088
UU4	35.7	4.33	1.55	5.63	0.8	11.54	0.825	8.29	12.90	1237
UU5	22.3	11.08	1.43	2.78	0.8	10.50	0.897	3.48	8.10	505
UU6	43.6	6.25	0.99	1.80	0.64	3.19	0.586	1.80	3.35	72
UU7	43.6	6.25	1.38	2.45	0.64	5.60	0.780	2.45	7.05	225
SS1	60.0	12.70	1.14	2.36	0.80	3.92	0.681	2.95	3.66	122
SS8	60.0	12.70	1.53	4.92	0.80	7.73	1.234	6.15	11.70	506
SS9	60.0	12.80	1.53	5.05	0.80	9.72	1.251	6.31	14.95	1040

Notes: H_{yo} = Calculated Yield Load[**Eq. (4.3)**]; H_y = Predicted Ultimate Strength;
H_{max} = Experimental Maximum Horizontal Load;
δ_{yo} = Calculated Deflection of Column Top at H_{yo}[**Eq. (4.4)**];
δ_y = Calculated Deflection of Column Top at H_y;
δ_m = Deflection of Column Top at H_{max}; μ_m = **Eq. (4.6)**;
μ = **Eq. (4.9)**; $\hat{E}$ = **Eq. (4.11)**.

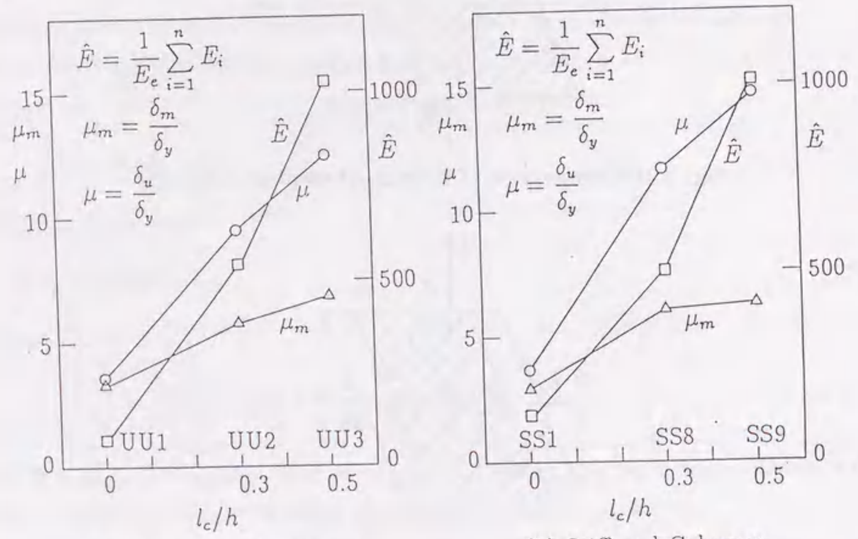

(a) Unstiffened Columns (b) Stiffened Columns

Fig. 4.12 Effect of l_c (Length of Filled Concrete) on Ductility and Energy-Absorption Capacity: (a) Unstiffened Columns; (b) Stiffened Columns

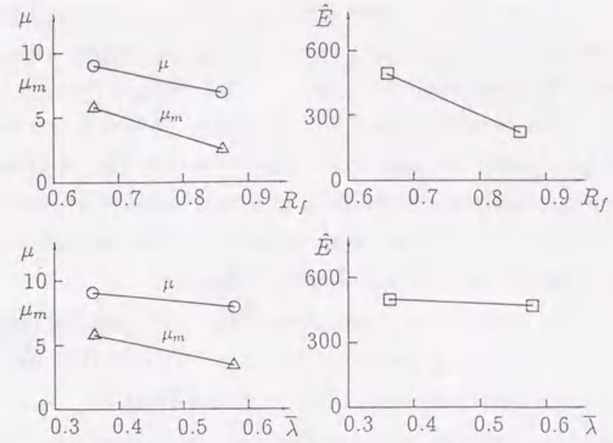

Fig. 4.13 Effect of R_f (Width-Thickness Ratio) and $\overline{\lambda}$ (Slenderness Ratio) on Ductility and Energy-Absorption Capacity

history. In view of that, a more objective measure of the inelastic performance of a test specimen is desirable. For this purpose, normalized cumulative energy absorption, $\hat{E}$, is defined as

$$\hat{E} = \frac{1}{E_e}\sum_{i=1}^{n} E_i \tag{4.11}$$

$$E_e = \frac{1}{2} H_y \delta_y \tag{4.12}$$

in which E_i = energy-absorption in cycle i of a test; n = cycle number after which the peak lateral resistance is reduced to H_y.

The values of the parameter $\hat{E}$ are listed in **Table 4.6**. On the other hand, the values of μ_m, μ and $\hat{E}$ are plotted against the ratio l_c/h in **Fig. 4.12**, and against the parameters R_f and $\overline{\lambda}$ in **Fig. 4.13**. The following can be observed from the table and figures:

(1) The concrete-filled specimens significantly increase both ductility and energy absorption capacity, e.g., comparing with SS1 (without filled-in concrete), specimen SS8 ($l_c/h = 0.3$) doubles the ductility and makes the energy-absorption capacity more than 4 times. The ductility and energy-absorption capacity are increased as the length of

filled concrete l_c is increased. This is because that inward local plate buckling displacements are prevented by filled-in concrete, local buckling deformations are delayed in their initiation and also moderated considerably, which leads to increase in ductility and in energy-absorption capacity remarkably. Moreover, the unstiffened columns and stiffened columns have nearly the same tendency, as shown in **Fig. 4.12(a)** and **(b)**. Thus, it could be concluded that the ductility of a thin-walled steel box column can be increased by filling the steel section with concrete, so that the column is able to undergo very large inelastic deformations during earthquake.

(2) Because of the P-Δ effect, it is apparent from **Fig. 4.13** that the longer column has smaller ductility. Comparing specimen UU2 ($\overline{\lambda} = 0.4$) with UU5 ($\overline{\lambda} = 0.6$), the reduction is found to be about 40% in μ_m, 15% in μ, and 6% in $\hat{E}$.

(3) Because of the local buckling, the ductility and energy-absorption capacity are reduced as the plate width-thickness parameter R_f is increased. It is noted that the ductility and energy-absorption capacity of specimen UU7 ($R_f = 0.9$) were only half as large as those of specimen UU2 ($R_f = 0.7$), although their plate width-thickness parameters were not much different.

4.4 Summary

A total of eleven unstiffened and stiffened steel box column specimens were tested under constant axial compression and cyclic lateral loads with varying displacement amplitude. The experimental results of seven steel box columns, partially filled with concrete up to 0.3 or 0.5 times of the column height, showed a very effective earthquake resistant capacity of such composite columns. The concrete-filled specimens significantly increased both ductility and energy-absorption capacity, e.g., comparing with specimen SS1 (without concrete infill), ductility and energy-absorption capacity of specimen SS8 ($l_c/h = 0.3$) increased two times and four times, respectively. This is because that inward local plate buckling displacements are prevented by filled-in concrete, local buckling deformations are delayed in their initiation and also moderated considerably, which leads to increase in ductility and in energy-absorption capacity remarkably. However, the longer columns and the larger plate width-thickness ratio columns had smaller ductility and energy-absorption capacity.

To make the earthquake resistant behavior of such composite columns more clear,

a further investigation is required. For example, the effects of the parameters R_f and $\overline{\lambda}$ on the strength, ductility and energy-absorption capacity of the column have to be studied in a more wide range.

5 FURTHER STUDY ON DUCTILITY AND ENERGY ABSORPTION CAPACITY OF CONCRETE-FILLED STEEL BOX COLUMNS UNDER CYCLIC LOADING

5.1 General Remarks

In Chapter 4, experimental results of the elasto-plastic behavior of concrete-filled steel box columns under combined constant axial force and cyclic lateral loads were presented. The specimens tested were of relatively large slenderness ratios ($\overline{\lambda} \geq 0.40$). In order to develop a reasonable design method for this kind of concrete-filled steel box columns, a further study is necessary to investigate various structural performances such as strength, deformation and failure characteristics in the case of comparatively shorter columns. Moreover, the experimental observations of a column with large plate width-thickness ratio showed that the improvement of ductility is very small when the length of filled-in concrete is taken to be $0.3h$ (h is column height). For this purpose, a total of twelve concrete-filled steel box column specimens modelling steel bridge piers are designed and tested under the same loading condition as before. Among the twelve columns, two columns are designed without a diaphragm over the concrete part for investigating the effect of the diaphragm on the column behavior.

5.2 Outline of Experiment

5.2.1 Test Specimen

In this work, seven unstiffened box columns and five stiffened box columns were designed as cantilever-type columns. As indicated previously, this work is aimed at laying emphasis on the columns with relatively small slenderness ratios. Thus, the slenderness ratio parameter, $\overline{\lambda}$, was taken to be 0.25 for most columns. The values of various parameters of the test specimens are listed in **Table 5.1**. Specimen designations starting with a UC refer to unstiffened concrete-filled columns (depth-to-breadth ratio $d/b = 3/4$), and those starting with a SC refer to stiffened concrete-filled columns ($d/b = 2/3$). In each specimen, the three ordered numerals following the UC or SC are related to values of plate width-thickness ratio parameter R_f, slenderness ratio parameter $\overline{\lambda}$ and length of filled-in concrete l_c, respectively. The number of cycles of

Table 5.1 Parameters of Test Specimens

No.	Specimen	R_f	$\overline{\lambda}$	l_c	N
1	UC70-40-3[0]	0.70	0.40	0.3h	0
2	UC70-25-3[0]	0.70	0.25	0.3h	0
3	UC70-25-3[3]	0.70	0.25	0.3h	3
4	UC70-25-5[3]	0.70	0.25	0.5h	3
5	UC70-25-3[3]D	0.70	0.25	0.3h	3
6	UC70-25-5[3]D	0.70	0.25	0.5h	3
7	UC90-40-5[3]	0.90	0.40	0.5h	3
8	SC45-25-3[0]	0.45	0.25	0.3h	0
9	SC45-25-3[3]	0.45	0.25	0.3h	3
10	SC45-25-5[3]	0.45	0.25	0.5h	3
11	SC60-35-3[3]	0.60	0.35	0.3h	3
12	SC60-35-5[3]	0.60	0.35	0.5h	3

Notes: R_f = Width-Thickness Ratio Parameter; $\overline{\lambda}$ = Slenderness Ratio Parameter; l_c = Length of Filled Concrete; N = Number of Loading Cycles.

loading, N, at each displacement level, is put within square brackets. In addition, the last character D in two columns means that a diaphragm is not provided over the filled concrete. The detailed explanations of the parameters used in **Table 5.1** are the same as in Chapter 4, and are not repeated here.

The parameters of interest were the flange plate width-thickness ratio (R_f), column slenderness ratio ($\overline{\lambda}$), and length of filled concrete (l_c). The values of R_f and $\overline{\lambda}$ are within the range of practical designs. In the case of the unstiffened column, the width-thickness ratio parameter, R_f, was taken to be 0.7 or 0.9, and the slenderness ratio parameter, $\overline{\lambda}$, was taken to be 0.25 or 0.4. In the case of the stiffened column, the value of the width-thickness ratio parameter (R_f) was 0.45 and 0.60, and the value of the slenderness ratio parameter ($\overline{\lambda}$) was 0.25 and 0.35. The length of filled concrete, l_c, was taken to be 0.3 or 0.5 times of the column height. Except for two columns without a diaphragm over the filled-in concrete, concrete was poured from the lower end plate up to the specified length where a diaphragm without opening was provided. For this purpose, an opening was made on the lower end plate as well as on some of the intermediate diaphragms, as shown in **Fig. 5.1**. In contrast, concrete was poured from the upper end plate for two specimens UC70-25-3[3]D and UC70-25-5[3]D. Just

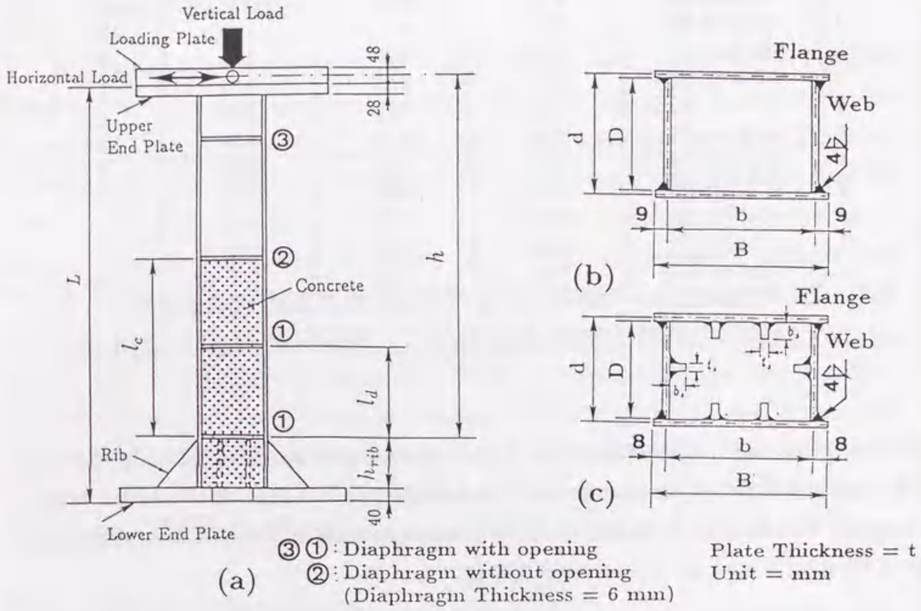

Note: Diaphragm ② is not provided for specimens UC70-25-3[3]D and UC70-25-5[3]D

Fig. 5.1 Test Specimens

like the test specimens presented in the last chapter, at the top of the specimen, an end plate 28 mm thick was welded to bolt the loading plate, and at the base, an end plate 40 mm thick was welded for anchoring the test specimen to the column base. For the flange-web junctions, a full penetration butt weld with V groove was first carried out followed by a fillet weld with 4 mm leg length. The applied axial load was 20% of the squash load, P_y, of test specimens (excluding concrete). **Tables 5.2** and **5.3** list the measured dimensions of the unstiffened and stiffened test specimens, and **Table 5.4** gives the calculated values of cross section constants.

Table 5.2 Measured Dimensions of Unstiffened Test Specimens

Specimen	B (mm)	D (mm)	L (mm)	h (mm)	h_{rib} (mm)	l_c (mm)	$\overline{\lambda}$	R_f
UC70-40-3[0]	235	156	1354	1216	122	365	0.429	0.750
UC70-25-3[0]	235	157	953	788	150	236	0.276	0.750
UC70-25-3[3]	235	157	952	788	150	236	0.276	0.750
UC70-25-5[3]	235	157	954	788	150	394	0.276	0.750
UC70-25-3[3]D	235	156	952	788	150	236	0.278	0.750
UC70-25-5[3]D	235	157	952	788	150	394	0.277	0.750
UC90-40-5[3]	296	202	1753	1578	160	789	0.434	0.961

Notes: B = Width of Flange Plates; D = Width of Web Plates;
t = Thickness of Plate = 5.87 mm; L = Total Length of Specimen;
h_{rib} = Height of Triangular Ribs; l_d = Distance between Diaphragms.

Table 5.3 Measured Dimensions of Stiffened Test Specimens

Specimen	B (mm)	D (mm)	b_s (mm)	γ/γ^*	L (mm)	h (mm)	h_{rib} (mm)	l_c (mm)	$\overline{\lambda}$	R_f
SC45-25-3[0]	317	196	23	1.17	952	838	100	251	0.245	0.479
SC45-25-3[3]	318	196	23	1.18	953	838	100	251	0.244	0.480
SC45-25-5[3]	317	196	34	1.22	952	838	100	419	0.249	0.479
SC60-35-3[3]	418	264	34	1.24	1854	1671	167	501	0.366	0.641
SC60-35-5[3]	418	264	34	1.24	1853	1671	167	836	0.367	0.639

Notes: b_s = Width of Stiffener; t_s = Thickness of Stiffener = 5.87 mm;
t = Thickness of Plate = 4.27 mm;
γ = Relative Flexural Rigidity; γ^* = Optimum Relative Flexural Rigidity.

5.2.2 Load Sequence

Each specimen was subjected to a prescribed horizontal displacement history under a constant axial load $P/P_y = 0.2$. The horizontal displacement history consists of sequence of fully reversed displacement cycles as shown in **Fig. 5.2**, that is, the peak displacements were increased stepwise after three successive cycles at each displacement level. The displacement increment adopted was $2\delta_{yo}$, where δ_{yo} is obtained from **Eq. (4.4)**.

5.3 Experimental Results and Discussions

5.3.1 Material Properties

Table 5.4 Constants for Steel Cross Section

Specimen	A_s (mm^2)	I (mm^4) ($\times 10^6$)	r (mm)	W (mm^3) ($\times 10^4$)	P_y (KN)	M_y (KN · mm)
UC70-40-3[0]	4591	21.86	69.0	26.0	1413	80083
UC70-25-3[0]	4603	22.16	69.4	26.2	1416	80689
UC70-25-3[3]	4603	22.16	69.4	26.2	1416	80689
UC70-25-5[3]	4603	22.16	69.4	26.2	1416	80689
UC70-25-3[3]D	4591	21.86	69.0	26.0	1413	80083
UC70-25-5[3]D	4603	22.16	69.4	26.2	1416	80689
UC90-40-5[3]	5847	45.72	88.4	42.7	1799	131475
SC45-25-3[0]	5200	36.78	84.1	35.9	1666	115002
SC45-25-3[3]	5207	36.87	84.1	36.0	1669	115271
SC45-25-5[3]	5586	38.04	82.5	37.1	1790	118936
SC60-35-3[3]	7030	88.36	112.1	64.7	2253	207437
SC60-35-5[3]	7022	87.64	111.7	64.4	2253	206504

Notes: A_s = Cross-sectional Area; I = Moment of Inertia ; r = Radius of Gyration; W = Section Modulus; P_y = Squash Load; M_y = Yield Moment.

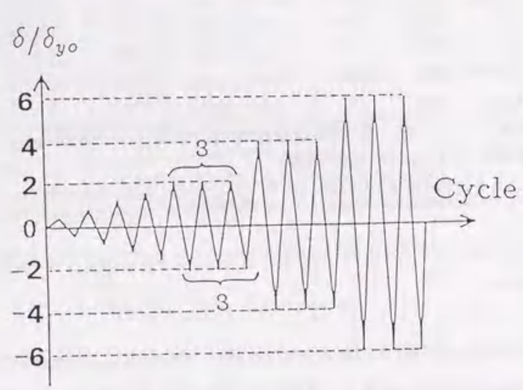

Fig. 5.2 Displacement History

The steel used was mild steel of grade SS400 (nominal yield stress $\sigma_y = 235$ MPa). The nominal thickness of flange and web plates was 6.0 mm for unstiffened columns, 4.5 mm for stiffened columns, while the stiffener thickness was 6.0 mm. The material properties are shown in **Table 5.5**, and were determined from the tension tests on three coupons in each series.

Table 5.5 Material Properties of Steel

Series	E (GPa)	σ_y (MPa)	ε_y (%)	ν	E_{st} (GPa)	ε_{st} (%)	σ_u (MPa)	δ_{el} (%)
t=6.0 mm	211	308	0.146	0.270	5.83	2.01	454	37
t=4.5 mm	216	320	0.148	0.283	4.68	2.34	483	36

Notes: E = Young's Modulus; σ_y = Yield Stress; ε_y = Yield Strain; ν = Poisson's Ratio; E_{st} = Strain-hardening Modulus; ε_{st} = Strain at Onset of Strain-hardening; σ_u = Tensile Strength; δ_{el} = Elongation.

Table 5.6 Material Properties of Concrete

Days	E_c (GPa)	μ_c	f_c (MPa)
14	25.9	0.163	32.4
28	24.2	0.158	36.4
44	26.4	0.174	39.1

Notes: E_c = Young's Modulus; μ_c =Poisson's Ratio; f_c = Uniaxial Compressive Cylinder Strength.

The water/cement ratio of concrete used was 57.0% (by weight). To determine the mechanical properties of concrete, compression tests were carried out on three cylinders (100 mm in diameter and 200 mm in length) in each series. Concrete cylinder tests were carried out on the same day as column tests. The measured average values for concrete are given in **Table 5.6**.

5.3.2 Collapse Modes

In the previous chapter, it was shown that the failure characteristics of the column are very useful in understanding its load-deformation behavior. Of course, the observations during the experiment can also give some important information for developing a ultimate design method. Therefore, in this section, phenomena observed during the tests of specimens, especially those whose slenderness ratios are relatively small ($\overline{\lambda} = 0.25$), will be described in detail.

The conditions of four column specimens after the tests are shown in **Fig. 5.3**. In each photograph, the double line shows the position of a diaphragm below which the concrete was filled.

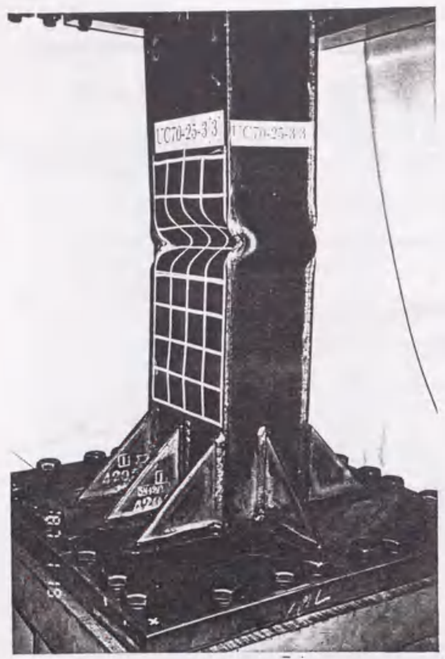

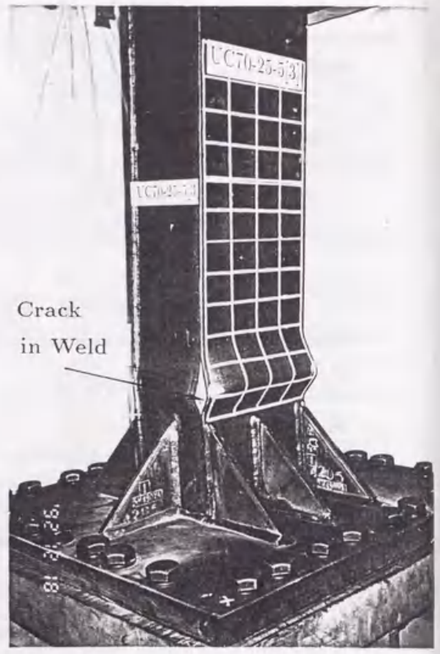

(a) UC70-25-3[3] (b) UC70-25-5[3]

Fig. 5.3 Specimens after Test (to be continued)

In case of $l_c/h = 0.3$, the hollow steel section just above the diaphragm buckled severely as shown in **Fig. 5.3(a)** and **(c)**. This observation indicates that although the filled-in concrete participated in dissipating energy during the later loading stages, the flange and web plates of the hollow steel section underwent significant inelastic action. It is noted that this buckling also caused a large deterioration in post-buckling strength as will be seen in a later section. It should also be pointed out that buckling occurred initially on the flange plates near the column base, but it hardly grew as the loading was continued. Moreover, these facts are consistent with those observed in the previous tests. For the stiffened specimen SC45-25-3[3], initial buckling shapes of flange plates were one and half sine waves with nodes at the stiffeners and corners, but it became progressively a inward half-sine wave as can be seen in the photograph.

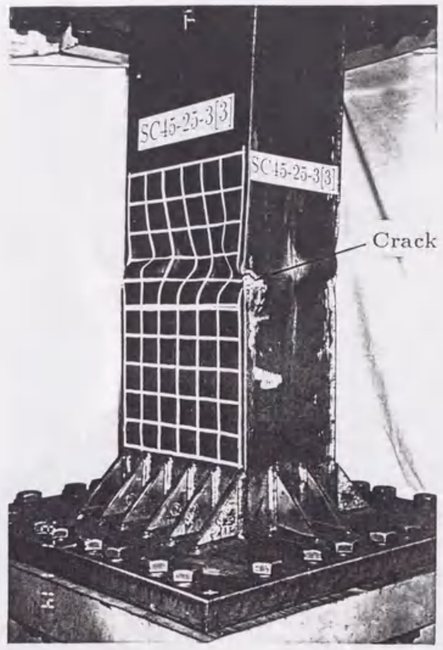

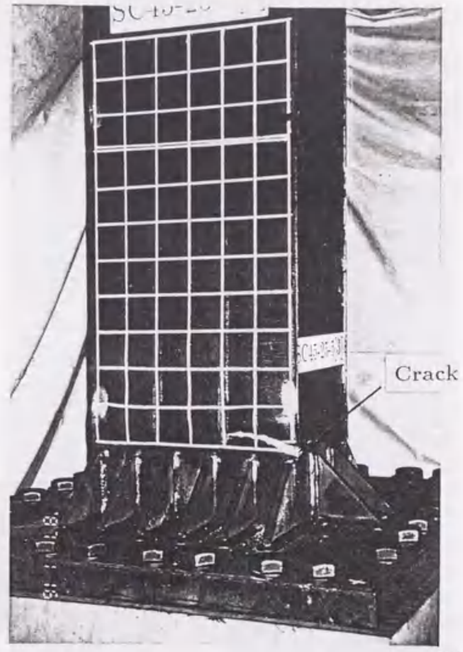

(c) SC45-25-3[3] (d) SC45-25-5[3]

Fig. 5.3 Specimens after Test (continued)

This is because the longitudinal stiffeners lost the stiffening-effect due to the buckling. As noted in **Fig. 5.3(c)**, a crack vertical to the weld was first observed at one of four flange-web junctions when the load-carrying capacity of the specimen was reduced to about 60% of the ultimate strength, in other words, at about $H/H_{yo} = 1.0$. Then cracks formed at two or three junctions else as displacement history was increased.

In the case of $l_c/h = 0.5$, buckling occurred only in the flange and web plates at the column base. It was observed that the plates slightly buckled outward before the cracks in weld or material took place. As discussed in the last chapter, this is because the filled-in concrete prevented the buckling of plates toward the interior direction. As viewed from the energy-absorption, the filled-in concrete's participation in dissipating energy during the loading was better than in the case of $l_c/h = 0.3$. Because both

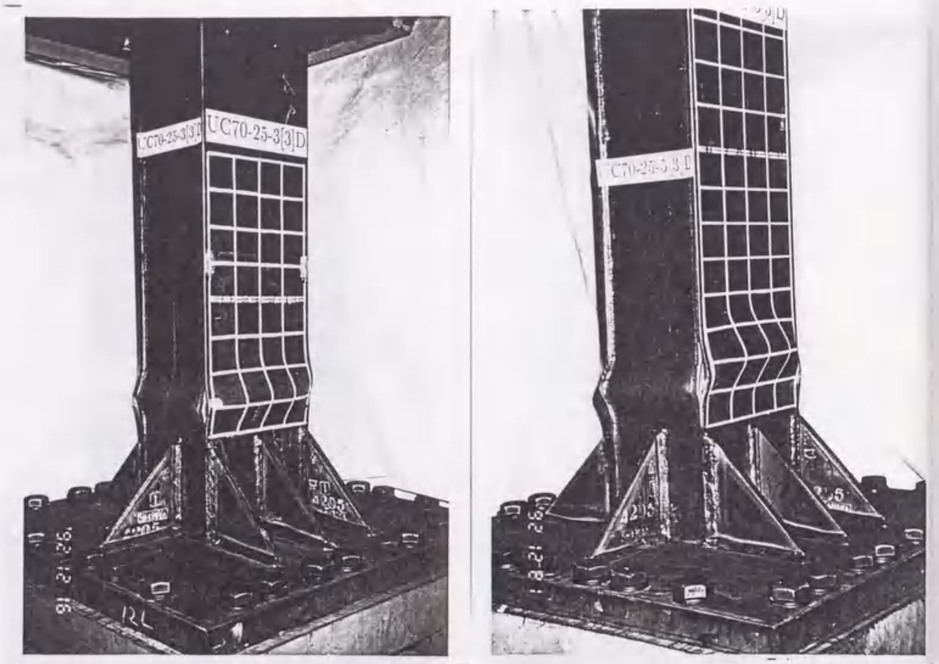

(a) UC70-25-3[3]D (b) UC70-25-5[3]D

Fig. 5.4 Specimens without a Diaphragm over Concrete after Test

the steel plates and filled-in concrete effectively participated in inelastic action, these columns showed excellent earthquake-resistant performances.

During the test of the unstiffened specimen UC70-25-5[3], a crack vertical to the weld was first observed at one of the corners of the column base when the load-carrying capacity was approximately H_{yo}. This was immediately followed by another crack which occurred in the weld as shown in **Fig. 5.3(b)**. The deterioration in the strength occurred as a consequence of severe cracking in the weld and filled-in concrete. In the final loading stage, the crushed concrete flowed out through the cracks.

For the stiffened specimen SC45-25-5[3], at approximately $H/H_{yo} = 1.6$ after the peak, namely at 88% of the maximum load, a crack vertical to the weld was initiated at one corner of the column base, and immediately followed by another crack at adjacent

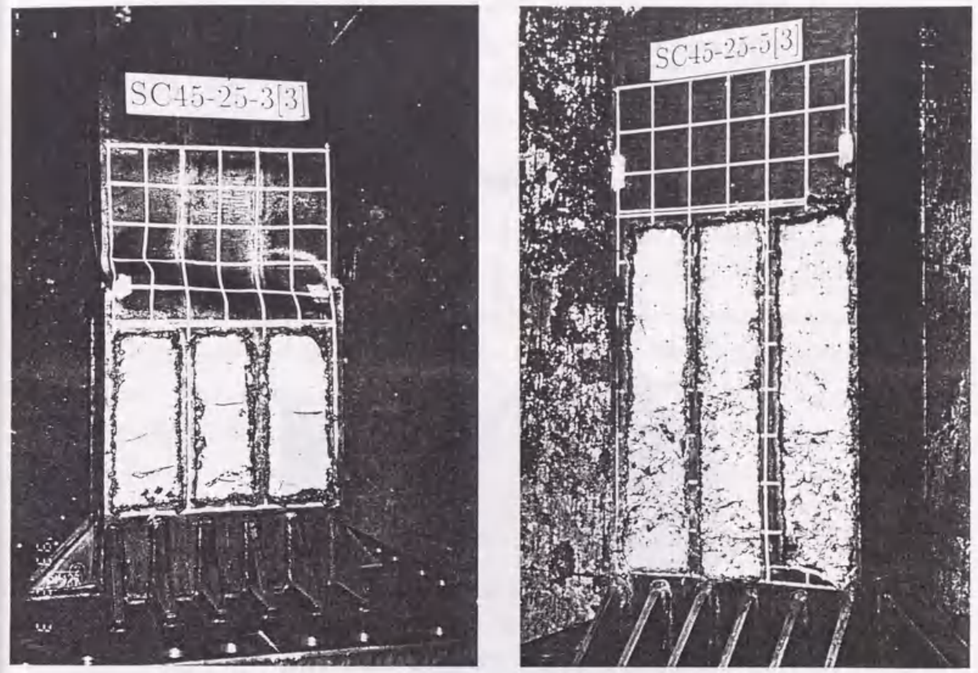

(a) SC45-25-3[3] (b) SC45-25-5[3]

Fig. 5.5 Filled-in Concrete after Test

corner. As the loading cycle was continued, cracks grew progressively. The test of this specimen was terminated when the cracks were as large as 1/3 of the flange width. The occurrence of this kind of crack at the tip of the weld surrounding the triangular rib might have resulted from low-cycle fatigue. Therefore, special attention must be paid to the welding of triangular ribs in practical constructions.

A diaphragm was not designed over the filled-in concrete in specimens UC70-25-3[3]D and UC70-25-5[3]D. Buckling of plates was observed at the column base regardless of the length of the filled-in concrete (see **Fig. 5.4**). Similar to the specimens with a diaphragm over the concrete, initial buckling occurred at the column base, just before the maximum load. This crack, however, grew progressively when cyclic loading was continued because the load was not increased sufficiently to form buckling at the hollow

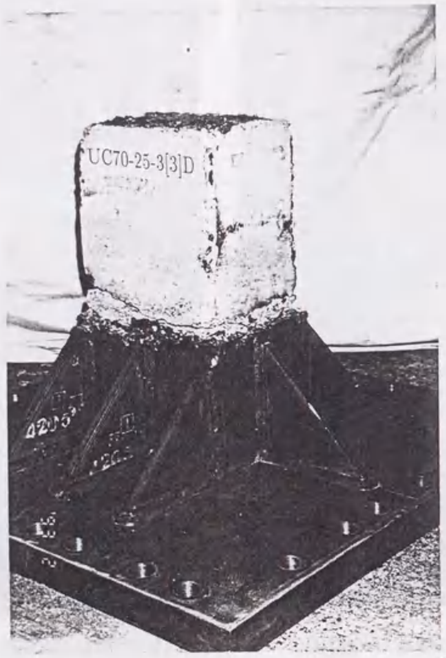

Fig. 5.6 Filled-in Concrete in Specimen UC70-25-3[3]D after Test

steel section above the concrete-filled part. Obviously, the contribution of the filled-in concrete to the ultimate load was small since the load was transmitted to the concrete only through the flange and web plates. As shown later, ductility capacities of two specimens were less than their corresponding specimens equipped with a diaphragm over the filled-in concrete. It could thus be said that the use of the diaphragm is effective in improving the earthquake-resistant behavior of the column.

Fig. 5.5 shows the conditions of the filled-in concrete of two specimens SC45-25-3[3] and SC45-25-5[3] after tests. As can be seen from the photographs, even though some cracks, which are marked with black lines for clarity, were observed on the surface of the concrete in specimen SC45-25-3[3], the concrete block was still sound without

any severe damage. The same failure appearance was observed in unstiffened specimen UC70-25-3[3]. For the specimens of $l_c = 0.5$h, for example specimen SC45-25-5[3], the concrete behind the portions of plates that buckled was seriously crushed. Shown in **Fig. 5.5(b)** is the condition after the crushed concrete was taken out. The depths of damage in concrete were varying. The maximum depth was about 4 centimeter near the corner where a crack in plate occurred. It was noted that this crack deeply penetrated the concrete. Additionally, it is important to note that directions of cracks observed were almost vertical to the column axis in each specimen.

Fig. 5.6 is a photograph showing the condition of the filled-in concrete of specimen UC70-25-3[3]D. As is seen from the figure, the concrete prism was completely cut at the column base, while no damage was observed elsewhere. This is because the concrete is pushed only by the flange plate due to the lateral loading, and so is easy to upturn from the base. Finally, the concrete was completely dislodged at the base due to the reversed cyclic lateral loading.

Usually, reinforced concrete columns subjected to combined axial force and lateral loading show shear failures. However, concrete-filled steel box columns tested had flexural cracks, which were vertical to the column axis, rather than diagonal. For examples, cracks observed on the surface of the filled-in concrete in specimen UC70-25-3[3] were vertical cracks, as was the critical crack in specimen UC70-25-3[3]D. As a result, these columns failed in flexure.

5.3.3 Horizontal Load versus Horizontal Displacement Hysteretic Curves

As was done in the previous chapter, to take into account the effect of rigid-body rotation of the base, the following correction is made for measured horizontal displacements:

$$\delta = \delta_T - (h + h_{rib}) \tan\theta \tag{5.1}$$

where δ = corrected horizontal displacement (mm); δ_T = horizontal displacement measured at the top of column; $\tan\theta = \delta_B / h_{rib}$; and δ_B = horizontal displacement measured at location of the lowest diaphragm. Note that $(h + h_{rib})$ is the height of a test specimen from the surface of the base end plate (see **Fig. 5.1**), where the value of h_{rib} for each specimen is given in **Tables 5.2** and **5.3**.

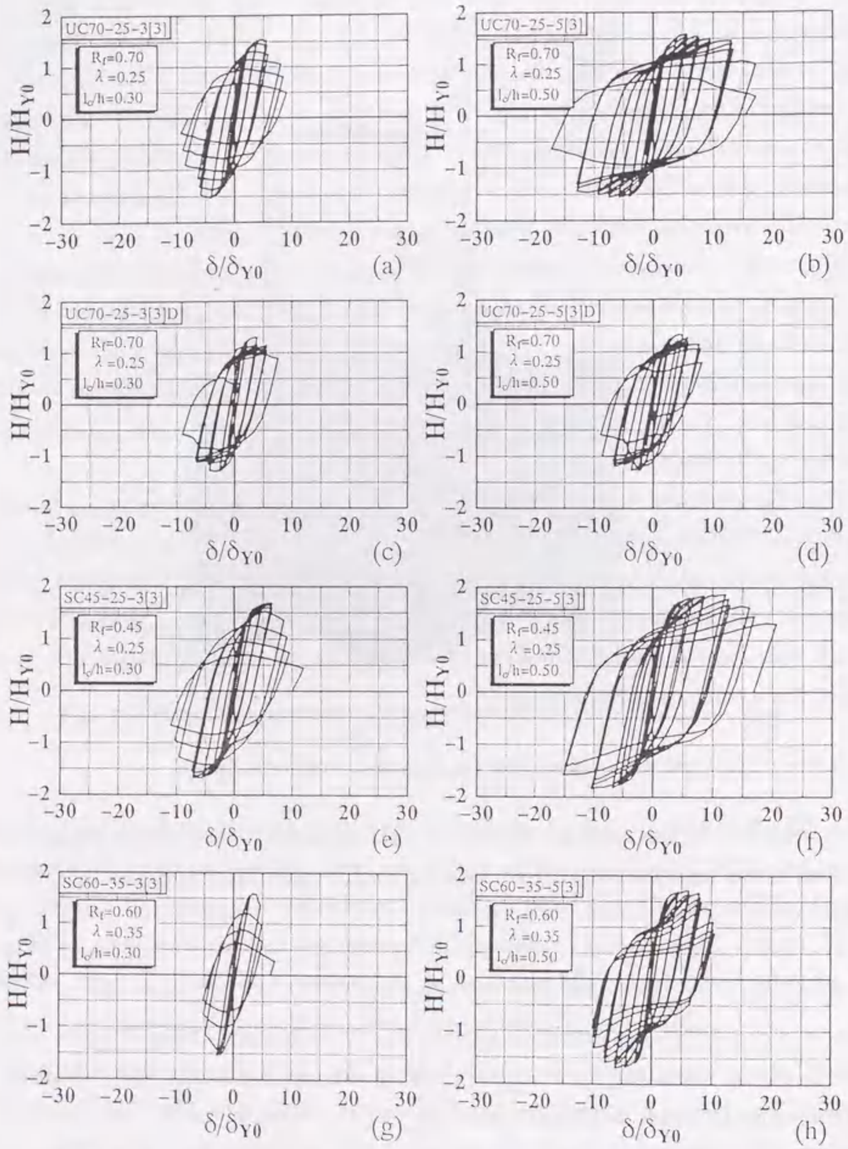

Fig. 5.7 Horizontal Load-Horizontal Displacement Hysteretic Curves

Nondimensionalized horizontal load versus horizontal displacement hysteretic curves for eight test specimens are shown in **Fig. 5.7**. The load and the displacement are respectively nondimensionalized by H_{yo} and δ_{yo} which are given in **Table 5.7**. Plots (a) to (d) are for unstiffened specimens, and (e) to (h) for stiffened specimens. The presence or absence of a diaphragm over concrete can be clearly identified from (a) and (c), or (b) and (d). It can be found in plots (e)-(h), that effects of width-thickness ratio and slenderness ratio are significant. Moreover, comparisons of the left four plots with the right four plots indicate that specimens of $l_c = 0.5h$ showed better hysteretic properties than those of $l_c = 0.3h$ except for the case when the diaphragm was not provided over the filled-in concrete.

Fig. 5.8 shows envelope curves for the horizontal load-displacement hysteretic curves. For comparison, experimental results of some specimens reported in Chapter 4 and in Takemoto's master thesis (1993) are included in the figure. From the figures the following important facts are observed.

(1) Effect of the filled-in concrete length

In the case of $R_f = 0.70$ and $\overline{\lambda} = 0.25$, comparisons of unstiffened concrete-filled specimens UC70-25-3[3] and UC70-25-5[3] with unstiffened steel specimen U70-25[3] show that the maximum loads were increased by about 37% and 40% when the concrete was filled up to the $0.30h$ and $0.50h$ respectively. Displacements corresponding to the maximum load were 1.76 and 2.54 times of the displacement of steel specimen (see **Fig. 5.8(a)**).

In the case of $R_f = 0.90$ and $\overline{\lambda} = 0.40$, it was observed from **Fig. 5.8(c)** that compared with steel specimen, the maximum loads of concrete-filled specimens were increased by about 40% in both $l_c = 0.3h$ and $l_c = 0.5h$, and their displacements at the peak were increased by about 20%.

By comparison with stiffened steel specimen S45-25[3], as shown in **Fig. 5.8(b)**, it was found that when the length of the filled-in concrete was taken to be $0.3h$ and $0.5h$, the maximum loads were increased by about 38% and 52%, respectively. On the other hand, the displacements obtained in the cases of $l_c = 0.3h$ and $l_c = 0.5h$ were as large as 167% and 277% of that of steel specimen, respectively.

Comparison of the load-deformation curves of specimen SC60-35-3[3] ($l_c = 0.3h$) and specimen SC60-35-5[3] ($l_c = 0.5h$) are given in **Fig. 5.8(d)**. Although the maximum

load in the case of $l_c = 0.5h$, was slightly larger than that in the case of $l_c = 0.3h$, the displacement corresponding to the maximum load for the former was 2.19 times of that for the latter.

As a result, it can be concluded that in the presence of a diaphragm provided over the filled-in concrete, both the ultimate strength and deformation capacity are obviously improved by the filled-in concrete. The increase in ductility is larger when the width-thickness ratio and slenderness ratio are small. In the case of $l_c = 0.3h$, a deterioration in strength was observed because local buckling occurred in the panels of the hollow steel section just above the filled-in concrete. On the other hand, specimens of $l_c = 0.5h$ showed prominent deformation characteristics in undergoing the inelastic action due to slight buckling in the panels at the column base. Nevertheless, it is worth noting that crack resulting from the low-cycle fatigue may occur at the corner near the weld surrounding the triangular ribs. Onset of cracking is indicated with a large dot.

(2) Effect of the Width-Thickness Ratio

As an example, the comparison of two unstiffened specimens, namely UC90-40-5[3] ($R_f = 0.9$) and UU3 ($R_f = 0.7$) is shown in **Fig. 5.8(e)**. The maximum load of the latter was about 10% higher than that of the former, while the displacement at the maximum load was 2.48 times of the former. Therefore, even if the filled-in concrete length is taken to be $0.5h$, the ductility capacity is significantly reduced as the value of width-thickness ratio parameter is increased from 0.7 to 0.9.

(3) Effect of the Number of Loading Cycles

Comparing the results of cyclic tests with 3 cycles at each displacement level ($n = 3$) and monotonic tests ($n = 0$) shows that the maximum load and corresponding displacement are nearly the same, but deterioration in the post-buckling strength is conspicuous in the case of the former. But in **Fig. 5.8(f)**, the peak load for UU2 is slightly higher than that of UC70-40-3[0]. This discrepancy can be attributed to the difference in compressive strength of the filled-in concrete. In the case of UU2 the compressive strength of concrete was found to be 42.2 MPa; whereas for UC70-40-3[0], it was 32.1 MPa.

(4) Effect of the Existence of a diaphragm over the Filled-in Concrete

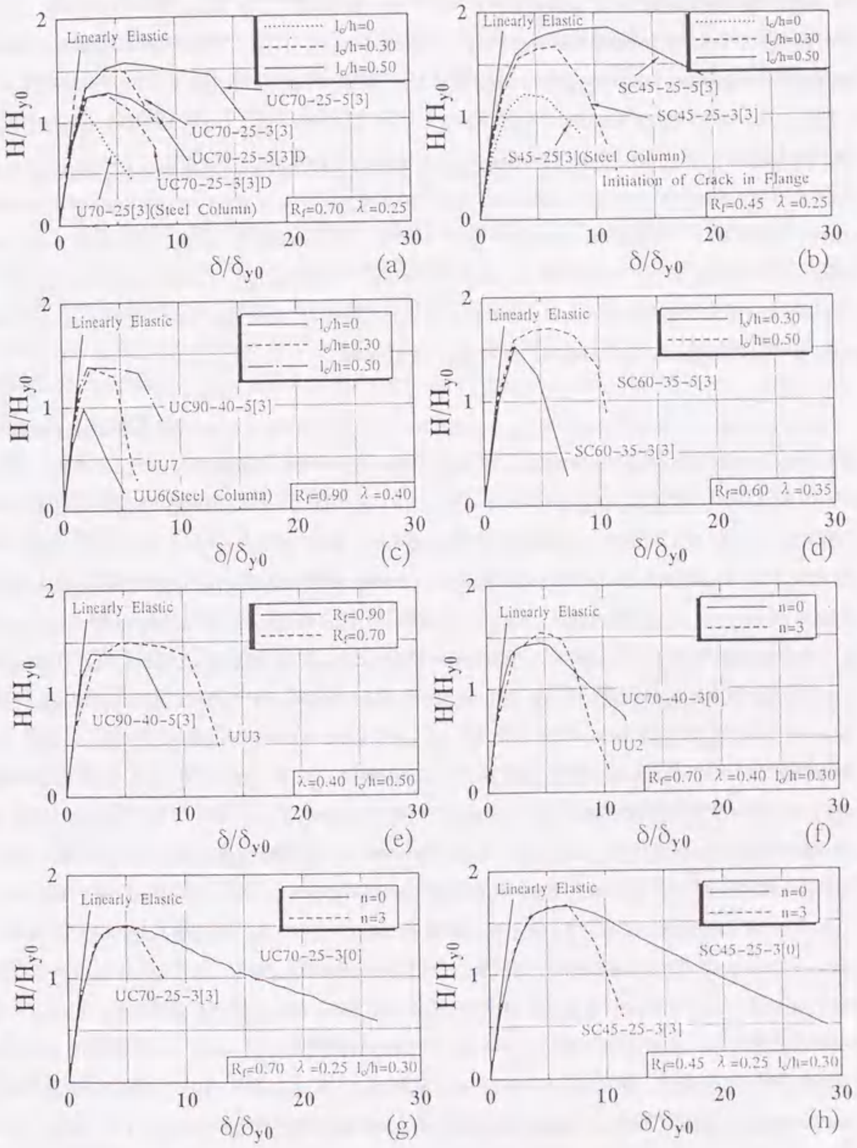

Fig. 5.8 Envelope of Horizontal Load-Horizontal Displacement Curves

The load-deformation envelope curves of two specimens without a diaphragm over the filled-in concrete are also shown in **Fig, 5.8(a)**. As can be seen, the load-deformation behavior was not sensitive to the length of the filled-in concrete before the maximum load was reached, and after the peak, the specimen UC70-25-5[3]D of $l_c = 0.5h$ behaved better than the specimen UC70-25-3[3]D of $l_c = 0.3h$. Compared with the steel specimen U70-25[3], the maximum loads of two concrete-filled specimens were increased by approximately 15%, and displacements at the maximum load point were almost doubled. This can be attributed to the confinement of the filled-in concrete which prevented local buckling of plates inside. Accordingly, some improvement of ductility capacity of the steel section due to the filled-in concrete can be expected even when a diaphragm is not present over the concrete.

To investigate the influence of the presence of a diaphragm over the filled-in concrete on the column behavior, comparative tests have been conducted for two cases: (1) $l_c = 0.3h$ (UC70-25-3[3]D and UC70-25-3[3]); (2) $l_c = 0.5h$ (UC70-25-5[3]D and UC70-25-5[3]). In the first case, although the maximum load of specimen UC70-25-3[3] was increased by approximately 20% due to the presence of the diaphragm, two specimens' displacements at the peak load point were almost the same. This is because,the severe plate buckling, which caused a remarkable degradation in the post-buckling strength, occurred in both specimens. In the second case, however, when a diaphragm was designed over the concrete, the maximum load and corresponding displacement are increased by approximate 22% and 30%, respectively. Especially, the post-buckling behavior of UC70-25-5[3] was very stable even when $\delta/\delta_{y0} = 10$. The explanation of this can also be made with reference to the failure mode. For specimen UC70-25-5[3]D, plate panels near the column base buckled seriously, while the filled-in concrete only cracked at the column base. As indicated previously, since no diaphragm was provided over the concrete, transmission of both axial force and lateral loads to the concrete was very limited, and so participation of the steel plates in undergoing inelastic action was predominant. In contrast, for specimen UC70-25-5[3], plate panels near the column base slightly buckled, and inside concrete seriously crushed. This implies that both the steel plates and filled-in concrete participated well in withstanding the axial force and cyclic lateral loads. Hence, this specimen showed a ductile behavior. It can thus be concluded that the use of a diaphragm over the filled-in concrete is very effective in

improving the strength and ductility capacity of the concrete-filled steel box column.

The maximum horizontal load and the corresponding horizontal displacement for each test specimen are summarized in **Table 5.7**. The quantity H_y in the table is the predicted lateral strength of test specimens (without concrete) for monotonic loading (Usami et al. 1992b).

5.3.4 Horizontal Load versus Axial Shortening Hysteretic Curves

As has been pointed out in Chapter 4, the magnitude of axial shortening can be considered as a good index for assessing damage of a member, since axial shortening after the maximum horizontal load is mainly caused by local buckling, material yielding, local damage (such as cracking) etc. Since the experimental phenomena for unstiffened specimens and stiffened specimens are similar, only unstiffened specimens will be discussed here.

Fig. 5.9 shows horizontal load (H) versus axial shortening (Δ) hysteretic curves for specimens UC70-25-3[3] ($l_c = 0.3$h), UC70-25-5[3] ($l_c = 0.5$h), UC70-25-3[3]D ($l_c = 0.3$h), and UC70-25-5[3]D ($l_c = 0.5$h). At the initial stage, axial shortening takes place due to the constant axial force only and subsequent shortening is due to horizontal loads. The axial shortening before the peak was very small in each case, and local buckling was found to be initiated near the peak lateral load. This is coincident with the experimental observations. In the case of specimen UC70-25-3[3] [see **Fig. 5.9(a)**], since local buckling progressively grew at the hollow steel section, axial shortening progressively increased. Sudden increase in the axial shortening at the last few loops was due to noticeable local buckling deformations on the flange plates where concrete was not filled in. For specimen UC70-25-5[3] (**Fig. 5.9(b)**), some increase in the axial shortening was observed, but it was not as large as in specimen UC70-25-3[3], because buckling occurred only at the column base and its deformation was very small. In the final loading stage, a large irregular shortening was observed since cracking in the weld took place and the filled-in concrete flowed out during the test. On the other hand, the horizontal load-axial shortening curves of two specimens UC70-25-3[3]D and UC70-25-5[3]D shown in **Fig. 5.9(c)** an **(d)** were almost identical due to the same failure modes. Compared with specimen UC70-25-3[3], axial shortening in specimen UC70-25-3[3]D was relatively small since plate panels only buckled outward due to the confinement of the filled-in concrete.

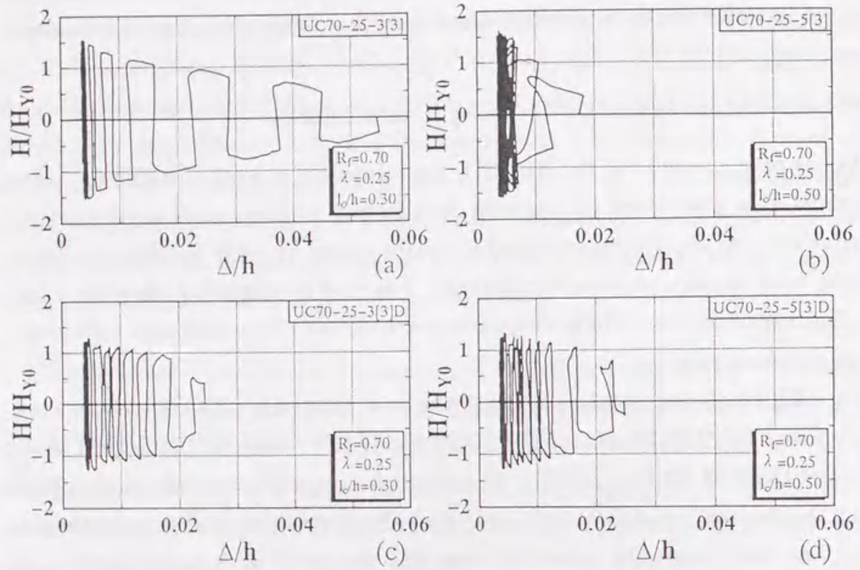

Fig. 5.9 Horizontal Load-Axial Shortening Hysteretic Curves

5.3.5 Ductility Factor and Energy Absorption Capacity

Ductility and energy-absorption capacity are important considerations in aseismic design. The design strength of a structure can be substantially reduced if the structure is able to provide a good deformation capacity beyond the elastic limit. Furthermore, energy dissipation through hysteretic damping can reduce the amplitude of seismic response and, thereby, lower the ductility demand on the structure. These quantities are now defined and evaluated for the test specimens.

In chapter 4, two ductility parameters for evaluating the deformation capacity of test specimens were used. One was defined as the ratio of the displacement corresponding to the maximum lateral load, δ_m, to the displacement at which first yield or local buckling occurs:

$$\mu_m = \frac{\delta_m}{\delta_y} \tag{5.2}$$

where δ_y = the horizontal displacement corresponding to first yield or local buckling (i.e., horizontal displacement at the top of column corresponding to H_y). Although this definition of ductility is physically clear, the load-deflection characteristics are not fully incorporated in the index. Moreover, in some cases, the degradation slope of the load-deformation curve is very gentle so that the peak point is difficult to locate. As in the last chapter, the value of the yield displacement, δ_y, can be theoretically calculated using a linear relation ($\delta_y/\delta_{yo} = H_y/H_{yo}$). However, it seems more appropriate to determine δ_y from the horizontal load-horizontal displacement envelope curve. The ratio of the experimental value to the theoretical value, which is denoted by $\delta_y)_{ex}/\delta_y)_{th}$, is given in **Table 5.7** for comparison. The later discussions will be made with respect to the experimental one.

Another ductility parameter μ, is given by

$$\mu = \frac{\delta_u}{\delta_y} \tag{5.3}$$

where δ_u = equivalent lateral displacement at the defined "collapse" point where the lateral resistance is reduced to H_y. That is, δ_u is related to the real lateral displacement at the "collapse" point by means of the equivalent elastic-perfectly plastic model presented in the last chapter. The characteristics of this model is that local buckling effect can be taken into account.

However, it has been shown that crack may occur at the column near the base due to low cycle fatigue when the slenderness ratio is small. For this reason, in some cases, the ductility parameter, μ, does not seem to be the realistic measure of the cyclic deformation capacity of the concrete-filled steel box columns.

On the basis of above discussions, it seems more reasonable that the failure point of the column be defined as a point where the load-carrying capacity is degraded to H_{95}, namely 95% of the maximum load. Hence, it is convenient to define this new parameter in the following way (**Fig. 5.10**).

$$\mu_{95} = \frac{\delta_{95}}{\delta_y} \tag{5.4}$$

where δ_{95} = lateral displacement obtained at $H = H_{95}$.

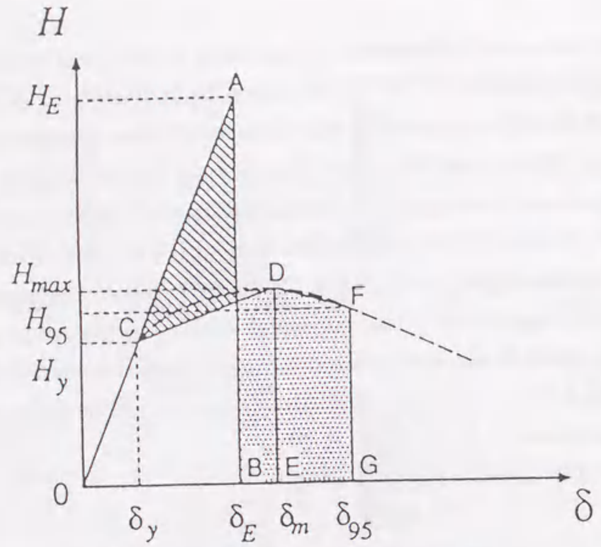

Fig. 5.10 Definition of Collapse Point

The values of the parameters μ_m and μ_{95} are listed in **Table 5.8**, and plots of μ_m and μ_{95} against the ratio l_c/h and parameter R_f are shown in **Fig. 5.11**. The following can be observed from the table and figures:

(1) Effect of the filled-in concrete length

When a diaphragm is present over the filled-in concrete, the ductility factor of the member is increased as the length of the filled-in concrete is increased, as shown in **Fig. 5.11(a)-(d)**. In other words, the ductility behavior of the steel box column can be largely improved by the filled-in concrete.

(2) Effect of the width-thickness ratio

It has been shown that ductility factors μ_m and μ_{95} were decreased as the width-thickness ratio parameter R_f was increased from 0.7 to 0.9 in the case of $l_c = 0.3h$. **Fig. 5.11(f)** shows the effect of R_f on the ductility for the case of $l_c = 0.5h$. It was observed that the ductility parameter μ_m is decreased as R_f is increased, but it is not so with the parameter μ_{95}.

Table 5.7 Strength and Deformation Capacity

Specimen	H_{yo} (KN)	δ_{yo} (mm)	$\frac{H_{max}}{H_{yo}}$	$\frac{\delta_m}{\delta_{yo}}$	$\frac{\delta_{95}}{\delta_{yo}}$	$\frac{H_y}{H_{yo}}$	$\delta_y)_{ex}/\delta_y)_{th}$
UC70-40-3[0]	65.9	8.57	1.44	4.40	5.62	0.76	1.40
UC70-25-3[0]	102.4	3.58	1.51	4.63	7.19	0.76	1.38
UC70-25-3[3]	102.4	3.58	1.54	3.92	6.01	0.76	1.40
UC70-25-5[3]	102.4	3.58	1.57	5.66	9.94	0.76	1.40
UC70-25-3[3]D	101.6	3.60	1.28	4.11	4.94	0.76	1.46
UC70-25-5[3]D	102.4	3.58	1.29	4.26	6.18	0.76	1.46
UC90-40-5[3]	83.3	11.33	1.39	2.17	6.54	0.55	1.00
SC45-25-3[0]	137.2	3.39	1.66	6.46	9.03	0.78	1.53
SC45-25-3[3]	137.6	3.39	1.68	6.77	7.30	0.78	1.60
SC45-25-5[3]	141.9	3.39	1.85	11.22	12.83	0.79	1.43
SC60-35-3[3]	124.2	10.14	1.57	2.80	3.25	0.71	1.44
SC60-35-5[3]	123.6	10.17	1.70	6.13	7.97	0.71	1.33
UU2	35.7	4.33	1.54	4.62	6.52	0.80	1.50
UU3	35.7	4.33	1.50	5.39	9.04	0.80	1.50
UU5	22.3	11.08	1.43	2.78	4.31	0.80	0.98
UU6	43.6	6.25	0.99	1.80	2.00	0.64	1.50
UU7	43.6	6.25	1.38	2.45	3.95	0.64	1.13
SS8	60.0	12.70	1.53	4.92	6.60	0.80	1.20
SS9	60.0	12.80	1.53	5.05	7.24	0.80	1.08

Notes: H_{yo} = Calculated Yield Load; δ_{yo} = Calculated Deflection of Column Top at H_{yo};
H_y = Predicted Lateral Strength of Test Specimens (without Concrete);
H_{max} = Maximum Lateral Load of Test Specimens;
δ_m = Deflection of Column Top at H_{max};
$\delta_y)_{ex}/\delta_y)_{th}$ = Ratio of the experimental yield displacement to theoretical yield displacement.

(3) Effect of the existence of a diaphragm over the filled-in concrete

When the diaphragm was not provided over the filled-in concrete, the increase in ductility was not noticeable in the case of $l_c = 0.3h$ and the case of $l_c = 0.5h$ (**Fig. 5.10(e)**). However, the ductility parameter μ_{95} of the specimen UC70-25-5[3]D was only half of the specimen UC70-25-5[3].

(4) Comparison of the two parameters μ_m and μ_{95}

In the case of the unstiffened specimen, some increase in the ductility parameter μ_m was reached when the length of the filled-in concrete was increased. The rate of increase was much more in the case of the stiffened specimen. On the other hand, the parameter μ_{95} was considerably increased when the length of the filled-in concrete was

Table 5.8 Ductility and Energy-Absorption Capacity

Specimen	δ_y	Ductility Factor		Energy-Absorption		Equivalent Seismic Coefficient	
	(mm)	μ_m	μ_{95}	$\hat{E}_{max}$	$\hat{E}_{95}$	RF_m	RF_{95}
UC70-40-3[0]	9.11	4.14	5.28	13	17	0.315	0.264
UC70-25-3[0]	3.75	4.41	6.86	14	23	0.299	0.220
UC70-25-3[3]	3.81	3.68	5.65	20	76	0.331	0.245
UC70-25-5[3]	3.81	5.32	9.34	99	328	0.265	0.181
UC70-25-3[3]D	3.99	3.72	4.47	23	46	0.347	0.306
UC70-25-5[3]D	3.96	3.85	5.59	30	99	0.339	0.263
UC90-40-5[3]	6.23	3.95	11.89	30	432	0.296	0.141
SC45-25-3[0]	4.05	5.40	7.55	21	30	0.260	0.206
SC45-25-3[3]	4.22	5.45	5.86	79	101	0.258	0.245
SC45-25-5[3]	3.84	9.91	11.34	282	371	0.180	0.163
SC60-35-3[3]	10.40	2.73	3.17	9	13	0.391	0.348
SC60-35-5[3]	9.63	6.47	8.42	107	238	0.226	0.187
UU2	5.19	3.85	5.43	41	139	0.327	0.256
UU3	5.19	4.49	7.53	77	227	0.301	0.212
UU5	8.65	3.57	5.52	26	132	0.350	0.259
UU6	6.00	1.87	2.08	4	20	0.558	0.509
UU7	4.50	3.40	5.48	10	68	0.341	0.240
SS8	12.19	5.13	6.88	158	260	0.277	0.226
SS9	11.04	5.85	8.40	163	378	0.257	0.201

increased in both the unstiffened specimen and the stiffened specimen. This is because the filled-in concrete prevented the strength degradation after the peak.

Evaluation equation of equivalent seismic coefficient given in the *JRA 90* code (1990) is as follows:

$$\frac{k}{k_e} = \frac{1}{\sqrt{2\mu - 1}} \tag{5.5}$$

Where

k_e : the seismic design coefficient of the elastic system,

k : the equivalent seismic coefficient of the inelastic system,

μ : the ductility factor of the inelastic system [Eq.(5.3)].

Equation (5.5) is based on the Newmark's energy principle for inelastic one-mass systems with elastic-perfectly plastic restoring-force characteristics. The above equation is obtained by establishing the equivalence of the energy between the elastic and the elastic-perfectly plastic system. Obviously, it is not necessarily pertinent to the

concrete-filled steel box columns, since neglecting the fact that the maximum load H_{max} is relatively larger than the yield strength H_y would lead to a very conservative evaluation. For this reason, an elasto-plastic skeleton curve is considered. In a case where "collapse" is defined as occurring at the maximum load point (i.e., $H = H_{max}$), the following equation can be obtained by equating the area under the elastic curve "OAB" with that under the inelastic curve "OCDE".

$$RF_m = \frac{1}{\sqrt{\mu_m(1+\alpha) - \alpha}} \tag{5.6}$$

where $\alpha = H_{max}/H_y$.

Likewise, when "collapse" is defined as occurring at a point where the load-carrying capacity is deteriorated to 95% of the maximum load (i.e., $H = H_{95}$), the following equation can be obtained by equating the area under the elastic curve "OAB" with that under the inelastic curve "OCDFG".

$$RF_{95} = \frac{1}{\sqrt{\mu_m(1-\beta) + \mu_{95}(\alpha+\beta) - \alpha}} \tag{5.7}$$

with $\beta = H_{95}/H_y = 0.95\alpha$. The computed values of the reduction factors RF_m and RF_{95} for the equivalent seismic coefficients are given in **Table 5.8**. It may be observed that values displayed in the last column of the table are less than 0.3 with two exceptions. This implies that for concrete-filled steel box columns the seismic design coefficient can be reduced as much as 70% in the inelastic design.

Similarly, normalized cumulative energy absorptions at the maximum load point and the point of 95% of the maximum load, which are denoted by $\hat{E}_m$ and $\hat{E}_{95}$, are used as more objective measures of the inelastic performance of test specimens. Both $\hat{E}_m$ and $\hat{E}_{95}$ are calculated using the following expressions:

$$\hat{E} = \frac{1}{E_e}\sum_{i=1}^{n} E_i \tag{5.8}$$

$$E_e = \frac{1}{2}H_y\delta_y \tag{5.9}$$

in which E_i = energy-absorption in cycle i of a test; n = cycle number at the failure (i.e., at H_{max} or H_{95}).

The values of the parameters $\hat{E}_m$ and $\hat{E}_{95}$ are also listed in **Table 5.8**. On the other hand, the values of $\hat{E}_m$ and $\hat{E}_{95}$ are plotted against the ratio l_c/h and parameter R_f in **Fig. 5.11**. The following can be observed from the table and figures:

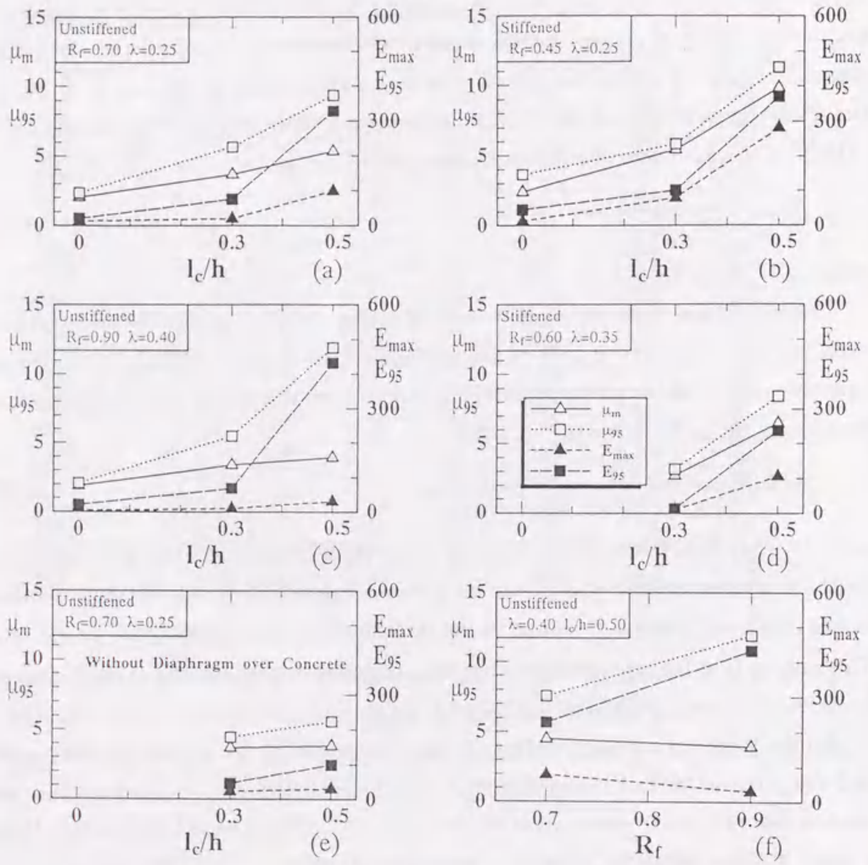

Fig. 5.11 Effect of l_c and R_f on Ductility and Energy-Absorption Capacity

(1) Effect of the filled-in concrete length

The concrete-filled specimens have significantly higher energy absorption capacity, e.g., comparing with U70-25[3] (without filled-in concrete), specimen UC70-25-3[3] ($l_c/h = 0.3$) increases the energy-absorption capacity by more than 3 times. The energy-absorption capacity is increased as the length of filled concrete l_c is increased. This is because the inward local plate buckling displacements are prevented by filled-in

concrete, local buckling deformations are delayed in their initiation and also moderated considerably, which leads to a remarkable increase in energy-absorption capacity. Moreover, the unstiffened columns and stiffened columns have nearly the same tendency, as shown in **Fig. 5.11(a)-(d)**. Thus, it could be concluded that the ductility of a thin-walled steel box column can be increased by filling the steel section with concrete, so that the column is able to undergo very large inelastic deformations during earthquake.

(2) Effect of the width-thickness ratio

Regarding the parameter $\hat{E}_m$, the energy-absorption capacity is reduced as the plate width-thickness parameter R_f is increased. But for $\hat{E}_{95}$, it is found that the specimen UC90-40-5[3] ($R_f = 0.9$) had larger energy-absorption capacity than the specimen UU3 ($R_f = 0.7$).

(3) Effect of the presence of a diaphragm over the filled-in concrete

It is apparent that when the length of the filled-in concrete is increased from $0.3h$ to $0.5h$, the increase is very limited in $\hat{E}_{max}$ and $\hat{E}_{95}$ in the absence of a diaphragm over the filled-in concrete. On the other hand, comparisons of the presence and absence of the diaphragm show that the energy increase is not remarkable in the case of $l_c = 0.3h$, while the energy absorption increases in both $\hat{E}_{max}$ and $\hat{E}_{95}$ by more than 200% in the case of $l_c = 0.5h$.

(4) Comparison of the two parameters $\hat{E}_{max}$ and $\hat{E}_{95}$

The values of the parameter $\hat{E}_{max}$ are much less than those of the parameter $\hat{E}_{95}$. In other words, the energy absorption capacity is much improved due to the filled-in concrete if "collapse" is defined as occurring at the point where the load is reduced to 95% of the maximum load. It is understood that excessive deterioration in post-buckling strength was prevented due to the contribution of the filled-in concrete.

5.4 Summary

Based on the results presented, the following conclusions are made:

(1) Concrete-filled steel box specimens under constant axial force and cyclic lateral loading showed generally prominent earthquake-resistance characteristics in undergoing the inelastic action.

(2) The diaphragm over the filled-in concrete was found to be very effective in improving the strength, ductility and energy absorption capacity of the column. In the seismic design of partially concrete-filled steel bridge piers of box sections, it appears beneficial to provide a diaphragm over the filled-in concrete.

(3) In the specimens with small slenderness ratios, crack vertical to the weld occurred at approximately $H = H_{yo}$ with the exception of specimen SC45-25-5[3], which had a crack near the column base early at 88% of the maximum load. It might have resulted from low cycle fatigue. Accordingly, special attention is necessary to be paid on the welding surrounding the triangular ribs in practical constructions.

(4) When "collapse" is defined as occurring at the maximum load point and at a point where the load-carrying capacity is reduced to 95% of the maximum load, the ductility and energy absorption capacity are much different. That is, the parameters μ_{95} and $\hat{E}_{95}$ are considerably larger than the parameters μ_m and $\hat{E}_{max}$. This is contributed to the presences of the filled-in concrete and the diaphragm over the concrete.

6 MOMENT-CURVATURE RELATIONS FOR STEEL COLUMN SEGMENTS AND CONCRETE-FILLED STEEL COLUMN SEGMENTS

6.1 General Remarks

In the previous chapters, experimental investigations of concrete-filled steel box columns are presented. It is found that this type of steel-concrete composite columns generally exhibit flexural failure. This means that, the load-deflection relationships of concrete-filled steel box columns may rationally be determined from the point of view of flexural failure theory. One of the approximate methods is to integrate the moment-curvature relations along the member length. Thus, before we undertake the analysis of the load-deflection behavior of the column, the moment-curvature relations of hollow steel box section and concrete-filled steel box section will be presented in this chapter.

In the beginning, researches on the elasto-plastic response of column segments subjected to compression combined with a uniaxial bending moment in the past are to be briefly reviewed. In 1976, Chen and Atsuta proposed a series of approximate formulas for the relation between moment and curvature for short beam-column segments of various cross-sectional shapes, in which the stress-strain relationship of the material was assumed to be elastic-perfectly plastic. However, this kind of simple approach is less satisfactory for thin-walled plated steel structures because the effect of local buckling was not included. To overcome this shortcoming, Lee et al. (1987) calculated the moment-curvature relations using a numerical method originally proposed by Little (1979). However, it was found that the M-P-Φ relations calculated by Little's method are inaccurate in some cases (Usami and Fukumoto, 1989). In order to obtain a rigorous moment-curvature relation, an elasto-plastic, large displacement finite element analysis was carried out by Usami and Fukumoto (1989). However, for arbitrary curvature and arbitrary axial force in the analysis of beam-column members or frame structures, corresponding moment and tangent stiffness have to be calculated by interpolation from discreted data of the M-P-Φ relations. Moreover, Miwa et al. (1993) proposed a set of formulas to describe the moment-curvature relations for thin-walled steel box column segments based on a nonlinear finite element analysis. However, the